4-2016

Hydrogen-Bonding Control of Solvatochromism and Non-Radiative Decay in the Fluorescence of 3-Aminofluoren-9-one Derivatives

Isaac Gregory Alty
College of William and Mary

Hydrogen-Bonding Control of Solvatochromism and Non-Radiative Decay in the Fluorescence of 3-Aminofluoren-9-one Derivatives

A thesis submitted in partial fulfillment of the requirement
for the degree of Bachelor of Science in Chemistry from
The College of William and Mary

by

Isaac Gregory Alty

Accepted for HONORS
(Honors, High Honors, Highest Honors)

Christopher J. Abelt, Chemistry, Director

Jonathan Scheerer, Chemistry

Kristin Wustholz, Chemistry

Vassiliki Panoussi, Classical Studies

Williamsburg, VA
April 19, 2016

Table of Contents

Background

The study of molecular sensors is a burgeoning area in the field of physical organic chemistry. Over the past few decades, many molecules have been discovered and synthesized whose unique physical and chemical characteristics allow them to serve as quantitative sensors of the properties of a microenvironment. These molecular sensors are often applied to biological systems, in order to further understand the specific binding properties of enzymes or the solvent characteristics of cellular compartments.

One molecule that has been of particular interest to our group in recent years is 6-propionyl-2-(dimethylamino)naphthalene (PRODAN). Originally synthesized by Weber and Farris in 1979 as a hydrophobic fluorescent probe of the enzyme bovine serum albumin, PRODAN has since received much attention from researchers because of its charge transfer excited state.[1]

Figure 1. Structures of PRODAN in its ground state (left) and excited state (right), showing charge separation across the naphthalene moiety in the excited state

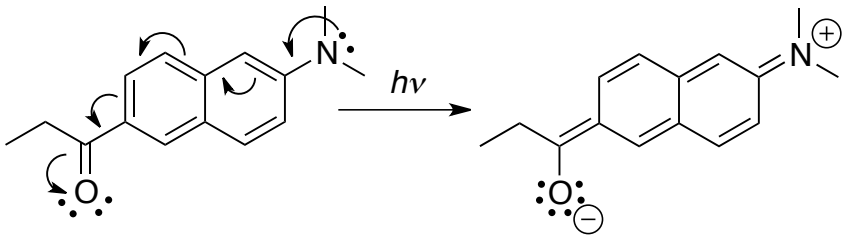

In the first singlet excited state, PRODAN's amino nitrogen takes on a positive charge when it donates a lone pair of electrons into the naphthalene ring system, and this lone pair is ultimately accepted by the carbonyl oxygen of the propionyl moiety, resulting in a negatively charged oxygen atom (Figure 1). This separation of charge across the naphthalene ring system gives rise to a number of fluorescence properties, including solvatochromism and effective quenching by protic solvents.[2]

Recently, our group has found that PRODAN derivatives are particularly sensitive sensors for protic solvents when the carbonyl group is twisted out of the plane of the naphthalene ring.[3] PRODAN derivatives are effective sensors of these protic solvents because they exhibit strong fluorescence quenching when alcohol groups hydrogen bond to the carbonyl oxygen. We have applied this finding to study the denaturation of human serum albumin in the presence of the common surfactant molecule sodium dodecylsulfate using PRODAN as a sensor. As the enzyme denatures, the carbonyl oxygen of PRODAN gradually becomes exposed to the solvation sphere of the enzyme, and its fluorescence is quenched.[4] Thus, our studies of PRODAN have shown it to be an effective molecular sensor not only of solvent dipolarity through solvatochromism, but also of low solvent acidity through hydrogen-bond quenching.

One question that currently remains unanswered about PRODAN's properties as a molecular sensor is that of the geometry of hydrogen bonding to the carbonyl oxygen in the charge-separated excited state. This is a difficult question to address on PRODAN, as its carbonyl oxygen is connected to the naphthalene ring system by one carbon-carbon single bond, and therefore it is free to rotate about this bond.

Figure 2. Comparison of the structures of PRODAN (left) and 3-aminofluoren-9-one (right) shows the high degree of rotation about single bonds near the carbonyl in PRODAN is more restricted in 3-aminofluoren-9-one by the rigid ring structure.

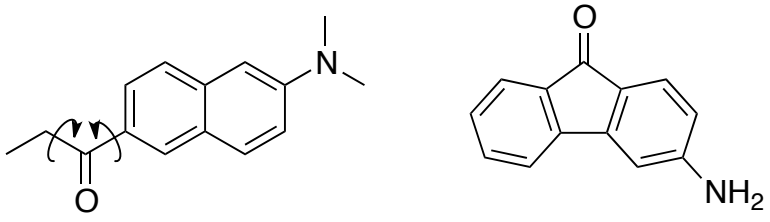

As such, any attempt to specifically hinder the formation of hydrogen bonds to this carbonyl oxygen would involve very complex substitution of the naphthalene ring and could potentially perturb the native fluorescent properties of PRODAN. Therefore, we turned to another well-

studied fluorescent molecule as a model compound for studying hydrogen-bonding geometry: 3-aminofluoren-9-one (Figure 2).

Introduction

Their unusually high quantum yield of fluorescence has garnered much attention for amino-substituted fluorenones, as they also have separation of charge across an aromatic ring system in their first singlet excited state. Of the various amino-substituted fluorenones, 3-aminofluoren-9-one has the greatest separation of charge in the excited state, with the amino group *para* to the carbonyl group across one of the six-membered rings (Figure 3).

Figure 3. Structures of 3-aminofluoren-9-one in its ground state (left) and excited state (right), showing charge separation across the fluoren-9-one ring system in the excited state

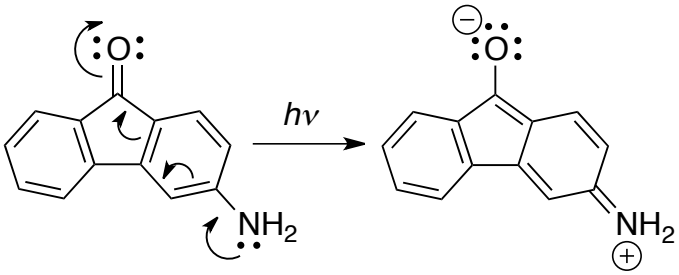

However, 3-aminofluoren-9-one's carbonyl group is locked in place by its integration into the planar aromatic ring system, thus eliminating the rotational degrees of freedom available to the carbonyl group of PRODAN. The aromatic ring system of fluoren-9-one also provides a useful scaffold for substitution to spatially constrain the number of hydrogen bonds available to the carbonyl oxygen (Figure 4).

Figure 4. Convenient sites for substitution of 3-aminofluoren-9-one to block formation of hydrogen bonds to the carbonyl oxygen, and possible derivatives with groups blocking one (middle) or both (right) in-plane hydrogen bonds.

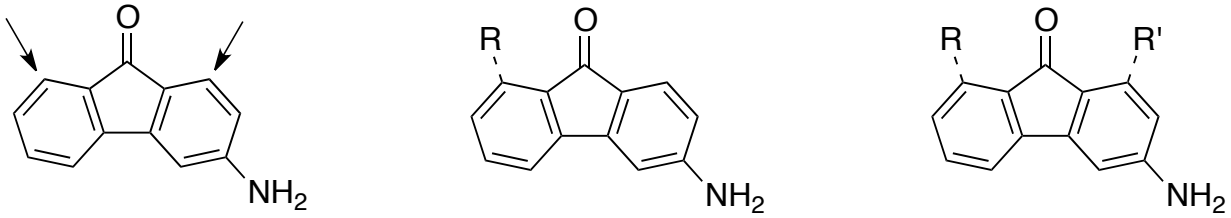

The reactivity of the two benzene moieties and the spatial proximity of substitution sites to the carbonyl make 3-aminofluoren-9-one an ideal candidate for derivitization in order to study hydrogen-bonding control of fluorescence quenching. This paper details the synthesis of 3-aminofluoren-9-one derivatives and examines their fluorescence properties in the presence of hydrogen-bond donating solvents.

In order to fully understand the fluorescence properties that make 3-aminofluoren-9-one a good model compound for the study of molecular sensing mechanisms, an explanation of the photophysics behind solvatochromism and fluorescence quenching is necessary.

Figure 5. Jabłoński Diagram illustrating electronic states (bold horizontal lines), vibrational states (thin horizontal lines) and electronic transitions possible for a molecule. Radiative processes (bold arrows) involve absorption (excitation) or emission (fluorescence, phosphorescence) of light. Non-radiative processes (dashed or wavy arrows), such as vibrational relaxation (V.R.), internal conversion (I.C.), and intersystem crossing (I.S.C.) occur with no absorption or emission of light. S_1 represents the first singlet excited state; T_1 the first triplet excited state. Dashed horizontal lines are high vibrational modes of the ground singlet state S_0.

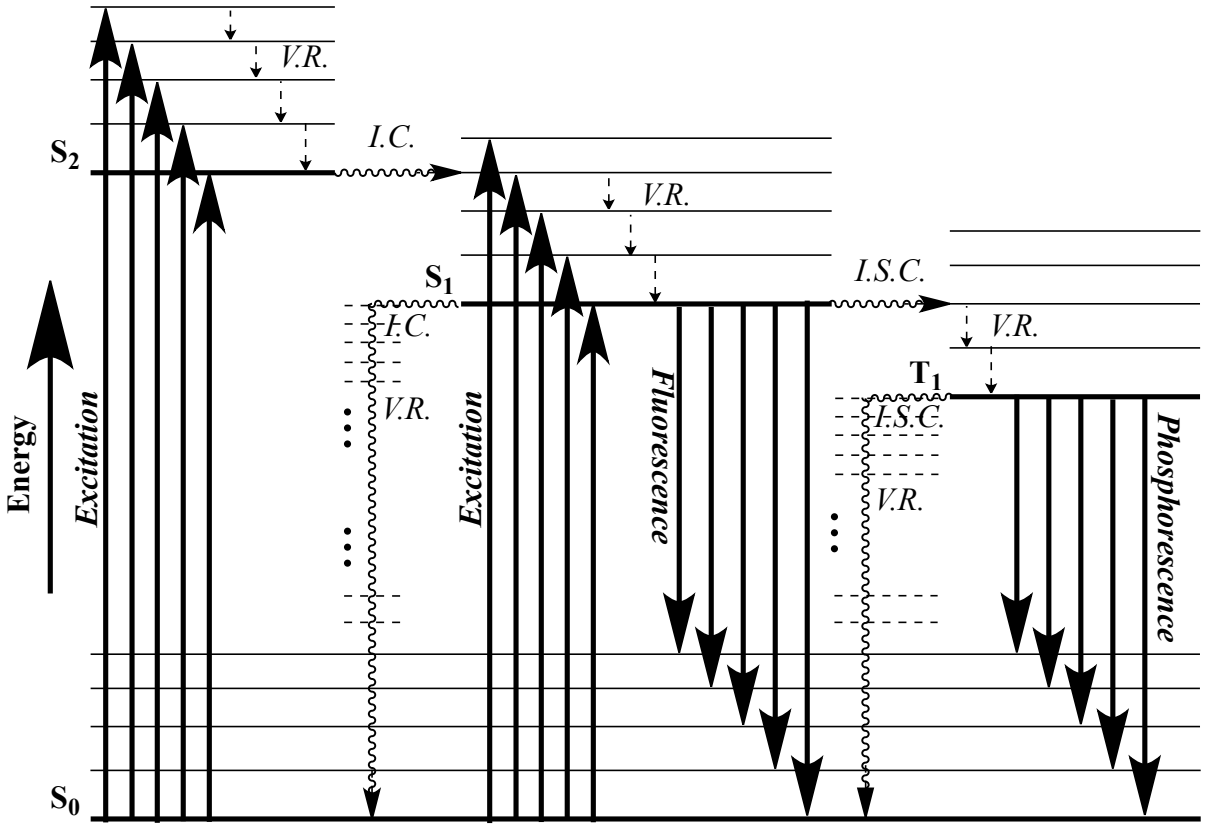

First and foremost, there are many modes of excited state deactivation (Figure 5), and their relative activity depends partly on the solvent composition. Also, although molecules have quantized electronic energy levels, these energy levels can be increased or decreased relative to the ground state in different solvent environments. Solvatochromism is generally observed as a bathochromic shift in fluorescence in the presence of solvents of increasing dipolarity. This behavior is common to many molecules that exhibit charge separation in a singlet excited state. Because the singlet excited state has greater dipolarity than the ground state in molecules like PRODAN and 3-aminofluoren-9-one, its energy is affected more by interaction with polar solvents than the less polar ground state, leading to an overall change in the energy gap between the two singlet states. This change in energy gap is best illustrated by a simplified version of the Jablonski diagram (Figure 6).

Figure 6. Simplified energy diagram showing only one deactivation process, fluorescence. Solvents are illustrated as ovals with charges. Coulombic attraction of partial charges stabilizes the charge-separated excited state in polar solvents, but not in nonpolar solvents. Thus the change in energy for fluorescence is greater in nonpolar solvents than in polar solvents.

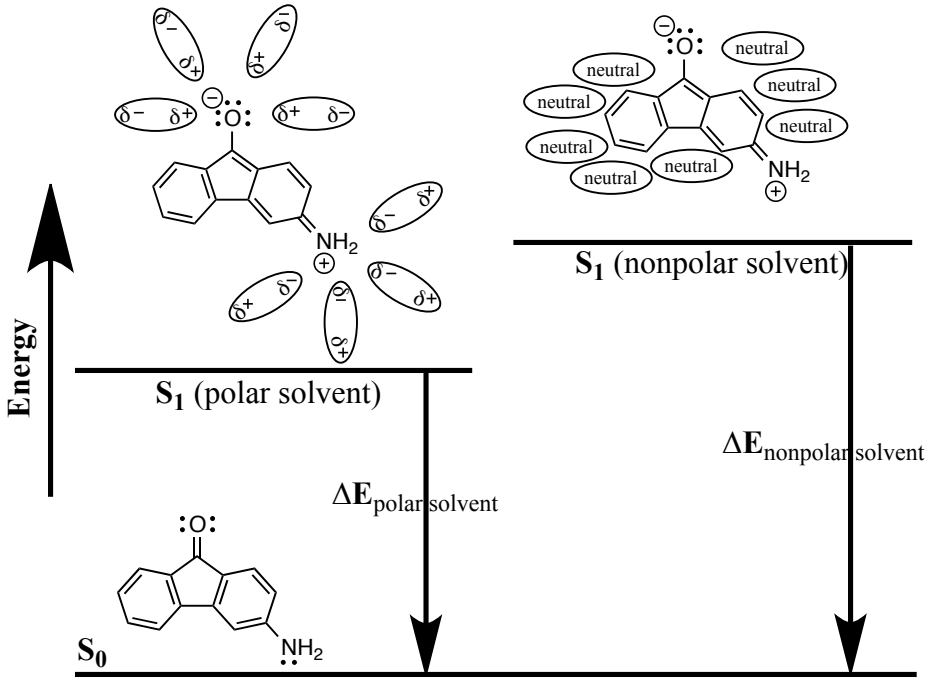

In solvents with high dipolarity, the energy gap between the ground state and the first singlet excited state is relatively small because the solvent molecules can stabilize the positive and negatively charged atoms of the fluorophore through Coulombic attraction. This favorable interaction between the partial charges on the solvent and the formal charges of the fluorophore results in more favorable solvation of the excited state, thus decreasing slightly the energy of the charge-separated excited state. On the other hand, solvents of low dipolarity cannot stabilize the positive and negative charges of the excited state except through van der Waals interactions. This leads to a larger energy gap between the two electronic states of the fluorophore as the excited state energy is increased slightly. Because the magnitude of the energy gap between the ground state and the first excited state of the same multiplicity is proportional to the frequency of light emitted in fluorescence, molecules with charge separation in their excited state will generally emit light of higher frequency in nonpolar solvents and light of lower frequency in more polar solvents.

Until recently, the molecular processes that contributed to solvatochromism were largely unknown to scientists.[5] Recent studies have shown that in addition to solvent dipolarity, solvent acidity can affect the solvatochromism of fluorophores and can lead to significant decreases in fluorescence intensity as a result of fluorescence quenching through hydrogen-bonding interactions between the solvent and the fluorophore. Because quenching is observed in the presence of protic solvents, it can be concluded that the formation of a hydrogen bond between the fluorophore and a solvent molecule can be sufficient to result in an energy transfer that returns the fluorophore to its ground state without the emission of a photon. For some fluorophores, this method of quenching can be treated similarly to a collisional quenching process. As such, Stern-Volmer plots showing the ratio of fluorescence intensity in the presence

of quencher to that in the absence of quencher as a function of quencher concentration generally show linear relationships for these molecules. However, other molecules exhibit different quenching behavior, including the derivatives of 3-aminofluoren-9-one, largely due to the combination of static and dynamic modes of quenching. For these molecules, Stern-Volmer relations deviate slightly from linearity and are modeled best by 2nd order polynomial functions (Figure 7).

Figure 7. Stern-Volmer relation for a 3-aminofluoren-9-one derivative, with a linear function of slope 7.4614 as a reference to show the deviation from linearity.

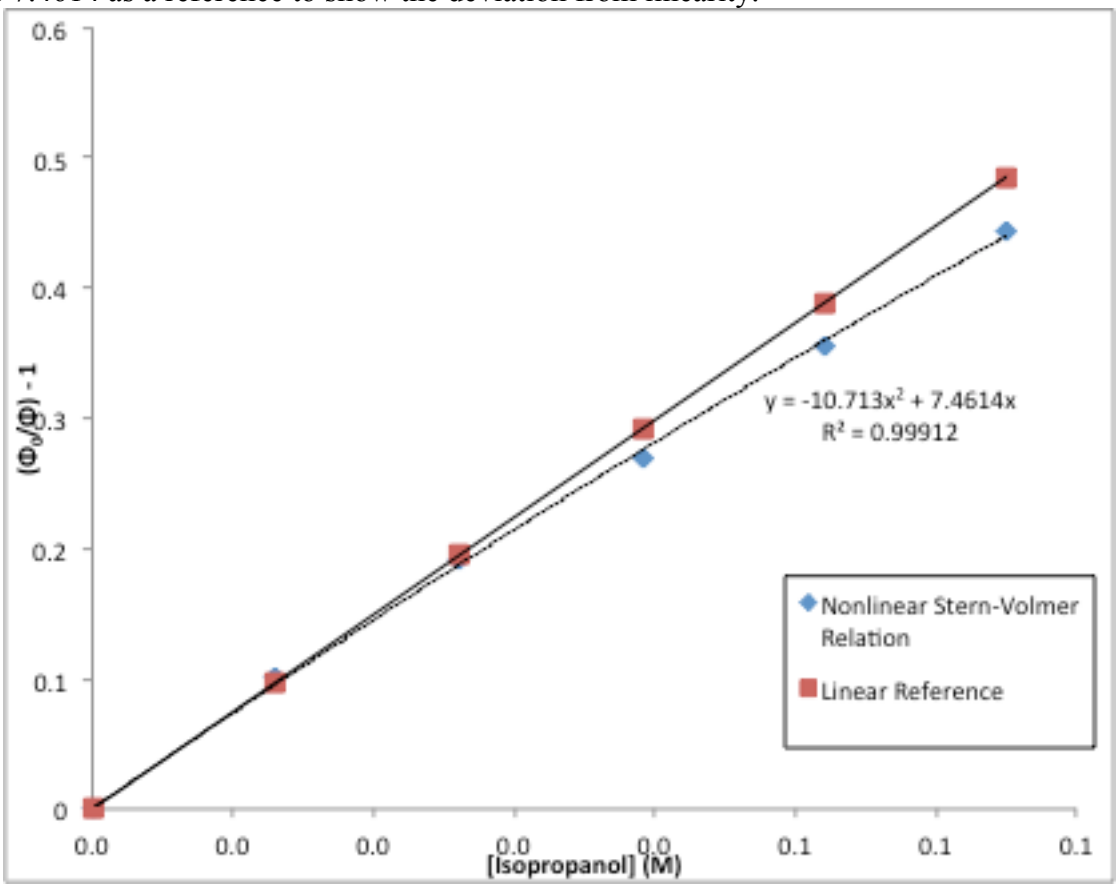

Comparison of these rates of hydrogen-bond quenching between different derivatives can elucidate the molecular processes underlying the photophysical behavior of 3-aminofluoren-9-one. By extension, these comparisons can inform the study of similar processes in molecules containing hydrogen-bond accepting groups such as carbonyls.

The fluorescence quenching of 3-aminofluoren-9-one and other amino-substituted fluoren-9-ones in the presence of alcohol solvents already had been studied rather extensively by the Inoue group at Tokyo Metropolitan University by the turn of the millennium. They determined that intermolecular hydrogen-bonding interactions strongly contributed to quenching of excited molecules in studies of aminoanthraquinones.[6] Because aminoanthraquinone derivatives contain two carbonyl groups (Figure 8), they also turned to aminofluoren-9-ones as a better class of model compounds that contain only one carbonyl group to accept hydrogen bonds from solvent molecules.

Figure 8. Two aminoanthraquinone derivatives investigated by the Inoue group prior to their studies of aminofluoren-9-ones, 1-aminoanthraquinone (left) and 2-aminoanthraquinone (right).

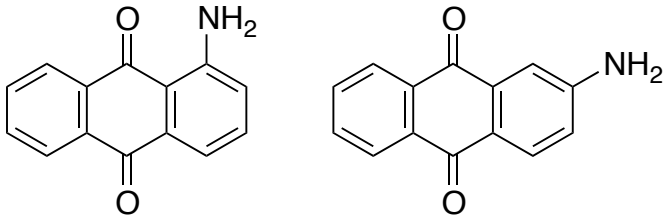

Through these studies, they determined that the hydrogen bond effectively promotes internal conversion of the fluorophore from a low vibrational mode of its excited electronic state to a high vibrational mode of the ground electronic state, and their conclusion was supported by a number of other studies.[7] By studying the solution photophysics of 3-aminofluoren-9-one and derivatives containing one or two methyl substituents on the amino nitrogen, the Inoue group produced a model for the radiationless deactivation of the 3-aminofluoren-9-one singlet excited state involving three possible hydrogen-bonding modes (Figure 9).[8]

Figure 9. Energy diagram adapted from Inoue et al. showing possible modes of non-radiative decay of excited-state aminofluorenones through hydrogen-bonding interactions with solvent molecules.[8] The orbital geometry of the negatively charged carbonyl oxygen gives rise to these perpendicular modes of hydrogen-bonding. In this scheme k_1 represents the rate constant for H-bond formation to the excited state carbonyl oxygen, and $\alpha + \beta = 1$.

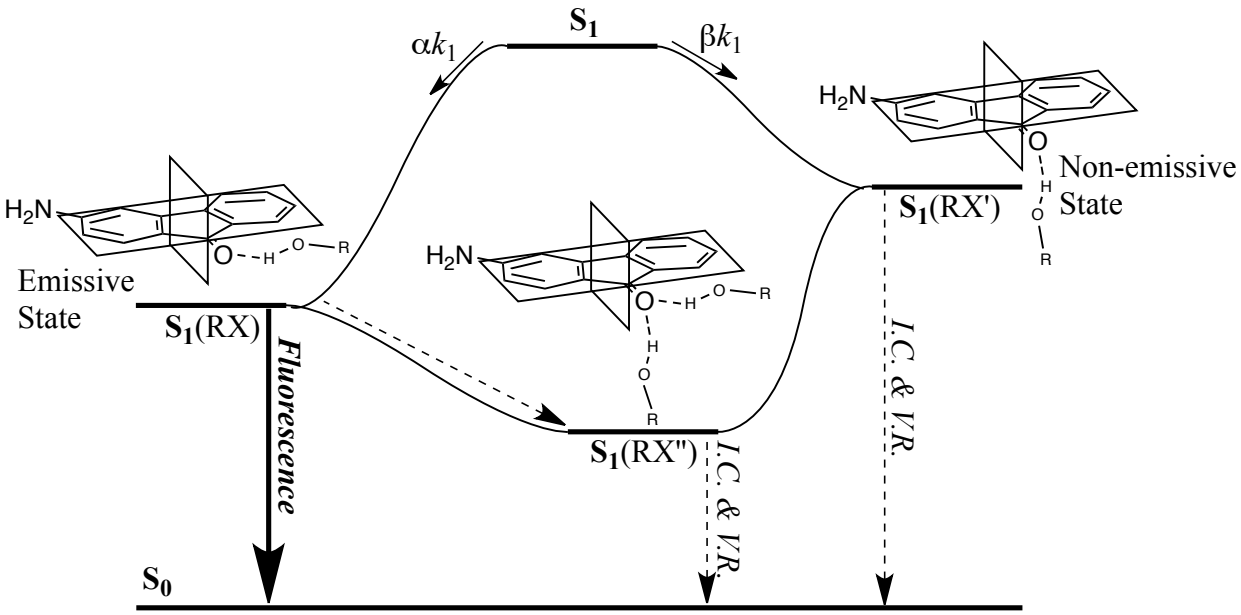

This model shows three possible hydrogen-bonding modes available to the carbonyl oxygen of an amino-substituted fluoren-9-one—a mode in which the hydrogen bond forms to a lone pair in an orbital in the plane of the aromatic ring system, a mode where the hydrogen bond forms perpendicular to the plane of the ring system, and a doubly hydrogen-bonded state with one in-plane and one out-of-plane hydrogen bond each. Of these three, the Inoue group concluded that the single in-plane bond is the only emissive state.

The aim of this study was to experimentally determine the validity of this model through the synthesis and testing of molecules that restrict the formation of one or more in-plane hydrogen bonds to the lone pairs of the carbonyl oxygen in 3-aminofluoren-9-one. In previous studies, the only derivatives of 3-aminofluoren-9-one used to test this model were the methylamino- and dimethylamino- derivatives of 3-aminofluoren-9-one (Figure 10).[9]

Figure 10. Methylamino- and dimethylamino- derivatives of 3-aminofluoren-9-one synthesized by the Inoue group.[9] These derivatives yielded little information on the geometry of H-bonds to the carbonyl oxygen.

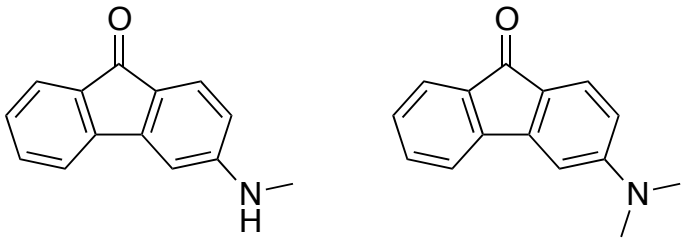

These derivatives can provide information about the twisting of the amino group with respect to the aromatic ring system, but they do not provide direct evidence to confirm the hydrogen-bond geometry about the carbonyl oxygen in the charge-separated excited state. In this study, we took advantage of the proximity of the aromatic ring system to the carbonyl and used it as a scaffold for the substitution of methyl groups *ortho* to the carbonyl to sterically block the formation of in-plane hydrogen bonds. As these methyl groups contain no bonds of significant dipolarity, they cannot form intramolecular hydrogen bonds to the carbonyl oxygen's lone pairs, as has been observed for the *ortho*-amino-substituted fluoren-9-one (Figure 11).

Figure 11. Intramolecular H-bond formed between amine and carbonyl oxygen in 1-aminofluoren-9-one. Our group has studied such intramolecular H-bonds in PRODAN.[10]

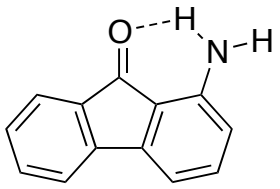

Furthermore, the methyl group is theoretically simple to incorporate into a synthesis of these 3-aminofluoren-9-ones, and it should not interfere (except through the blocking of hydrogen bonds) with the photophysics of the fluorophore. Finally, it is large enough to effectively block the in-plane hydrogen bond, but not bulky enough to also hinder the formation of the out-of-

plane bond. In addition to 3-aminofluoren-9-one, two derivatives were synthesized to selectively block one or both in-plane hydrogen bonds to the carbonyl oxygen (Figure 12).

Figure 12. 3-aminofluoren-9-one (**1**) and two derivatives synthesized for this study, 3-amino-6,8-dimethylfluoren-9-one (**2**) which blocks one in-plane H-bond, and 3-amino-1,8-dimethylfluoren-9-one (**3**) which blocks two in-plane H-bonds.

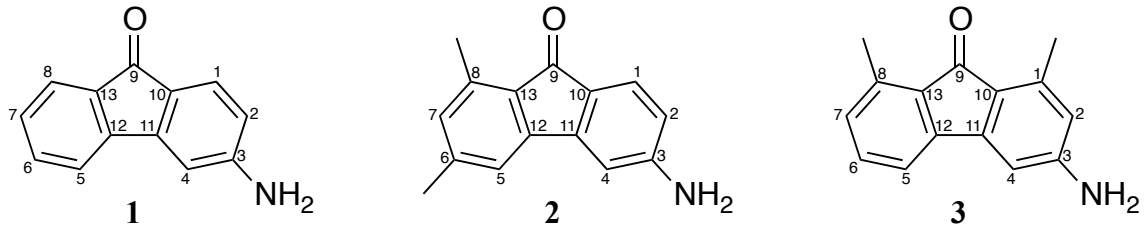

After their synthesis, these derivatives were analyzed by spectrofluorimetry in a binary solvent mixture consisting of toluene and increasing concentrations of various alcohol molecules. The fluorescence spectra of these molecules were analyzed to produce Stern-Volmer plots of the quenching rate, and these plots were compared to determine which modes of hydrogen bonding were active for each molecule as the concentration of quencher was increased. Comparison of quenching rates across these three derivatives, taking into account the number of hydrogen bonds blocked for each molecule, should provide insight into the emissivity of each hydrogen-bonding mode.

Methods

Synthesis of Derivatives

For more detailed information on the procedure used for each step in these synthetic pathways, consult Appendix B. ^{1}H NMR spectra for all intermediates and ^{13}C NMR spectra for final products are located in Appendix C. Starting materials and reagents were purchased from commercial suppliers, and the purity of all organic starting materials and reagents was assessed by ^{1}H NMR prior to their use.

3-aminofluoren-9-one (**1**)

The synthesis of 3-aminofluoren-9-one (**1**) was designed around a polyphosphoric acid intramolecular ring closing reaction to form the fluoren-9-one carbon skeleton of the final product (Figure 13). This method allows for greater specificity in substituting the fluoren-9-one moiety than direct substitution of fluoren-9-one. The precursor for the polyphosphoric acid ring closure is easily synthesized from 4-nitrotoluene.

Figure 13. Synthesis of 3-aminofluoren-9-one (**1**) in five steps from 4-nitrotoluene

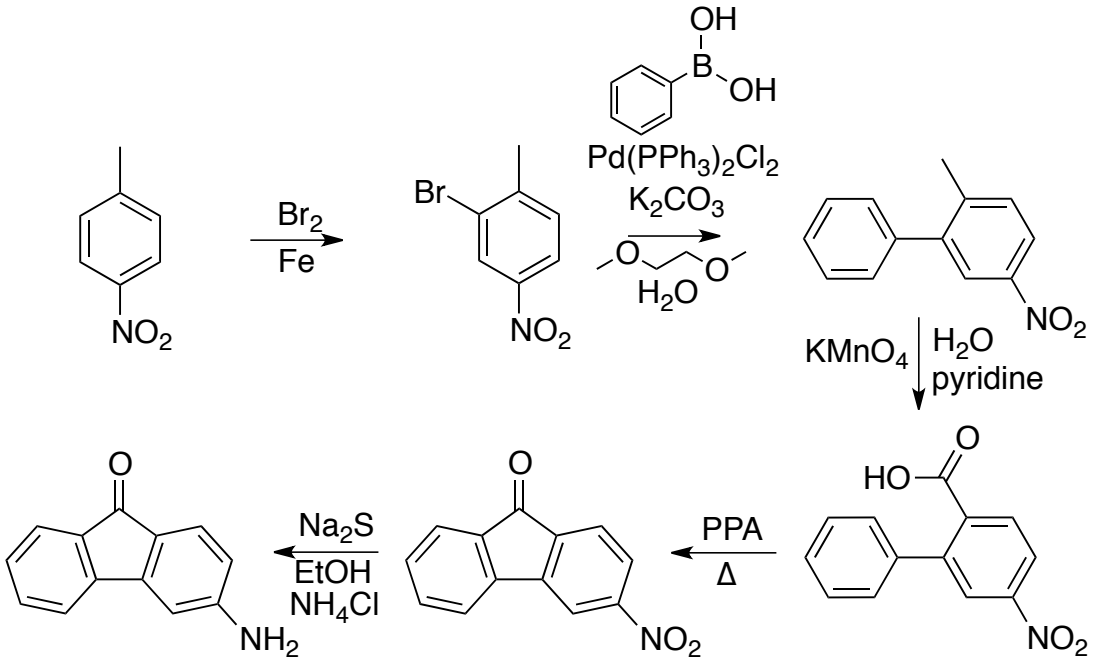

Commercially available 4-nitrotoluene was brominated to give 2-bromo-4-nitrotoluene at 66% yield, following a scaled-down version of the procedure of Bunnett & Rauhut.[11] The work-up to this bromination was modified from the original procedure to utilize solubility instead of phase transitions as a means of separating impurities from the product. A Suzuki coupling was then carried out on 2-bromo-4-nitrotoluene using phenylboronic acid to give 4-nitro-2-phenyltoluene at 90% yield following the procedure of Sams, Larsen & Mikkelsen.[12] This 4-nitro-2-phenyltoluene was then oxidized with hot, concentrated $KMnO_4$ to give 4-nitro-2-phenylbenzoic

acid at 53% yield following the procedure of Sebti & Hamilton.[13] This procedure was modified slightly: the reaction mixture was heated to boiling after the addition of $KMnO_4$ to reduce danger of explosions from adding $KMnO_4$ to an already boiling reaction mixture. The 4-nitro-2-phenylbenzoic acid was then heated in the presence of polyphosphoric acid to give 3-nitro-9-fluoren-9-one at 96% yield following the procedure of Iihama et al.[14] This 3-nitro-9-fluoren-9-one was reduced using sodium sulfide and ammonium chloride to give **1** at 54% yield following the procedure of Ray & Barrick.[15] The overall yield of this five-step synthetic pathway from 4-nitrotoluene was 16%. This synthesis of **1** involves few steps, relatively inexpensive reagents, and allows for placement of alkyl groups on the ring not containing the amino moiety if alkylated phenylboronic acids are used for the Suzuki coupling.

3-amino-6,8-dimethylfluoren-9-one (**2**)

Figure 14. Synthesis of 3-amino-6,8-dimethylfluoren-9-one (**2**) in five steps from 4-nitrotoluene

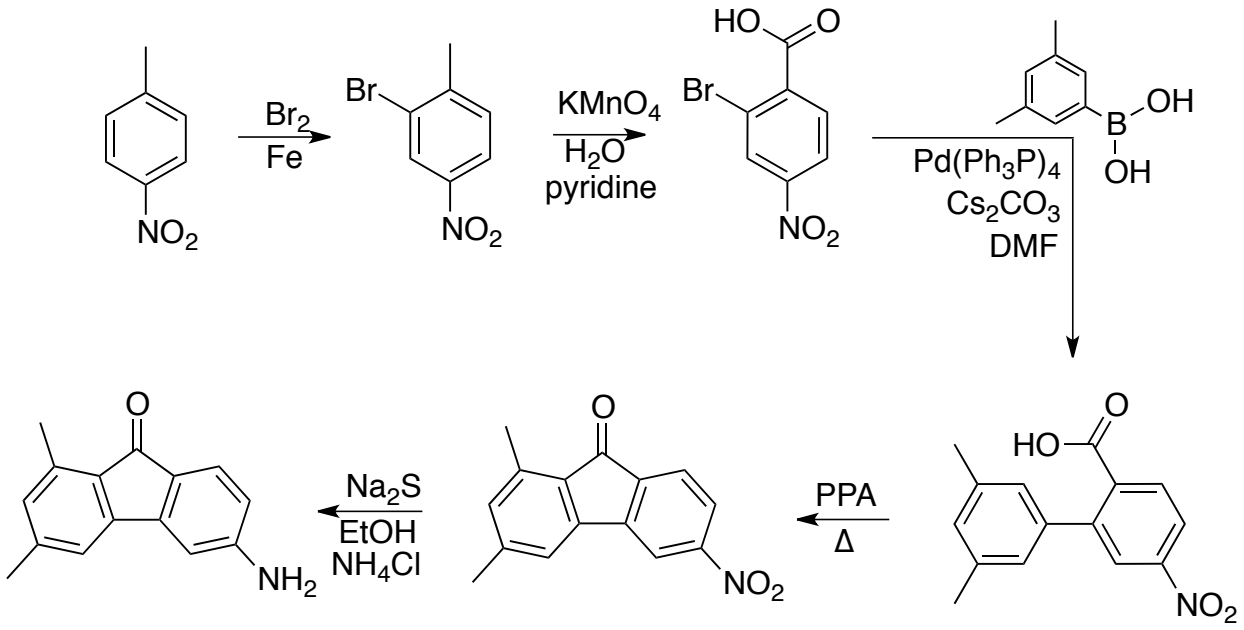

Using a similar synthetic pathway to that of **1**, 3-amino-6,8-dimethylfluoren-9-one (**2**) was synthesized (Figure 14). Commercially available 4-nitrotoluene was brominated to give 2-

bromo-4-nitrotoluene at 66% yield, following the same scaled-down and modified version of the procedure of Bunnett & Rauhut as was used to synthesize the precursor to **1**.[11] This 2-bromo-4-nitrotoluene was then oxidized with hot, concentrated $KMnO_4$ to give 2-bromo-4-nitrobenzoic acid at 53% yield following the procedure of Sebti & Hamilton.[13] A Suzuki coupling was then carried out on 2-bromo-4-nitrobenzoic acid using 3,5-dimethylphenylboronic acid to give 3',5'-dimethyl-5-nitro-[1,1'-biphenyl]-2-carboxylic acid at 31% yield following the procedure of Sebti & Hamilton.[13] This product was heated in the presence of polyphosphoric acid to give 1,3-dimethyl-6-nitrofluoren-9-one at 41% yield using stoichiometry similar to the procedure of Iihama et al.[14] This 1,3-dimethyl-6-nitrofluoren-9-one was then reduced by sodium sulfide in the presence of ammonium chloride to produce **2** at 20% yield using stoichiometry similar to the procedure of Ray & Barrick.[15] The overall yield of this five-step synthetic pathway from 4-nitrotoluene was 1%.

3-amino-1,8-dimethylfluoren-9-one (**3**)

Figure 15. Synthesis of 3-amino-1,8-dimethylfluoren-9-one in four steps from 3-bromo-5-nitrotoluene.

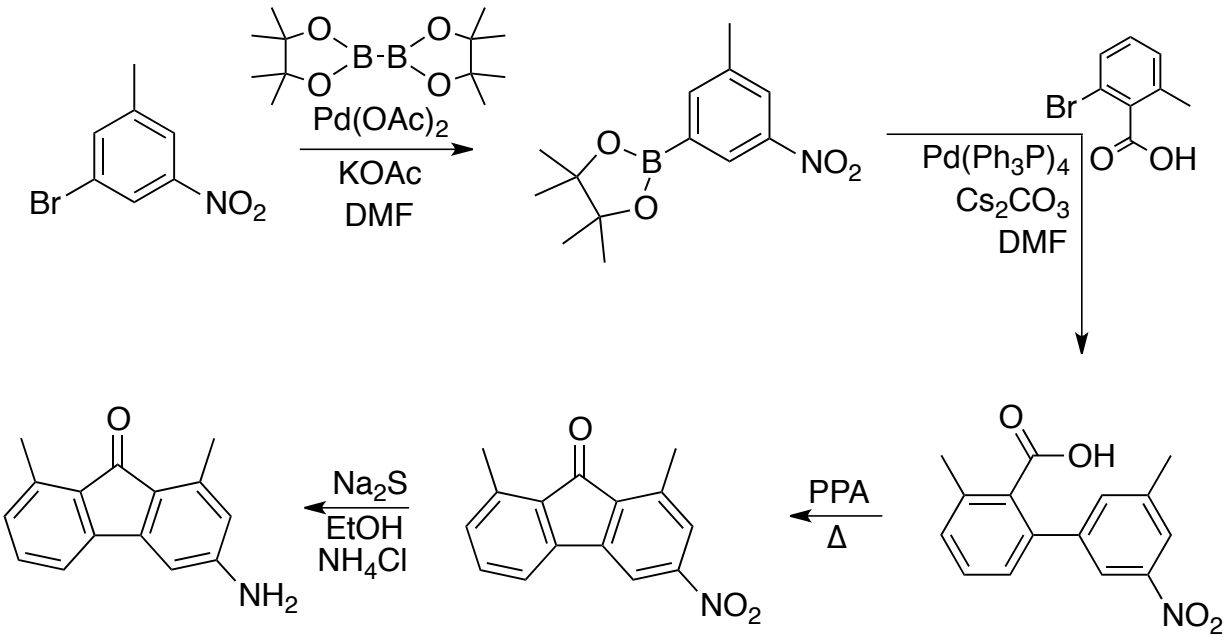

The synthesis of 3-amino-1,8-dimethylfluoren-9-one (**3**) was designed around the same intramolecular Friedel-Crafts acylation step, but the starting materials were rather difficult to produce, owing to their substituent regiochemistry and their substitution with groups that are strongly deactivating to electrophilic aromatic substitution. Therefore, the synthesis was started with commercially available 3-bromo-5-nitrotoluene (Figure 15) instead of the 4-nitrotoluene used in the syntheses of other 3-aminofluoren-9-one derivatives. This 3-bromo-5-nitrotoluene was reacted with bis(pinacolato)diboron in the presence of a catalytic amount of palladium(II) acetate to produce 4,4,5,5-tetramethyl-2-(3-methyl-5-nitrophenyl)-1,3,2-dioxaborolane at 44% yield. This product was reacted in a Suzuki coupling with 2-bromo-6-methylbenzoic acid in the presence of a catalytic amount of tetrakis(triphenylphosphine)palladium(0) to produce 3,3'-dimethyl-5'-nitro-[1,1'-biphenyl]-2-carboxylic acid at 52% yield using a modified version of the procedure of Sebti & Hamilton.[13] This product was heated in the presence of polyphosphoric acid to give 1,8-dimethyl-3-nitrofluoren-9-one at 40% yield using stoichiometry similar to the procedure of Iihama et al.[14] This 1,8-dimethyl-3-nitrofluoren-9-one was then reduced by sodium sulfide and ammonium chloride to produce **3** at 21% yield using stoichiometry similar to the procedure of Ray & Barrick.[15] The overall yield of this four-step synthetic pathway from 3-bromo-5-nitrotoluene was 2%.

General Methods

An Agilent DD2-400 or Varian Mercury VX-400 spectrometer was used to obtain ^{1}H NMR and ^{13}C NMR spectra. All ^{1}H NMR spectra were collected between 0 and 10 ppm. A Bruker Apex-Qe instrument was used to acquire high resolution ESI-MS spectra for novel compounds (**2**, **3**). All solvents used for fluorescence and absorption measurements were spectrophotometric grade. A fiber optic system with a 366 nm LED light source and an Ocean

Optics Maya CCD detector were used to collect fluorescence emission data. Samples were thermostated at 23°C. Absorption spectra were obtained from this same fiber optic system using a miniature deuterium/tungsten light source instead of the LED source.

Absorption Data

Two solutions of identical concentrations of fluorophore were made by diluting 20 μL of a stock solution of fluorophore (~5 mg /10 mL toluene) to 5 mL with the aprotic and protic solvents. Two series of data were acquired for each binary system. In the first set 2.0 mL of the aprotic solution was sequentially spiked with four aliquots of the protic solution, and the solution was stirred for thirty seconds before recording the intensity. In the second set, 2.0 mL of the alcohol solution was spiked with two aliquots of the aprotic solution. In this way the absorbances for a set of regularly-spaced binary mixtures (0, 10, 20, 40, 60, 80, 90, 100 mol %) were determined. For an example of these aliquot volumes and the subsequent mole fractions of both solvents in each solution, consult Table A1. The best-fit third-order polynomial to the plot of normalized absorption vs. mole fraction was used to calculate the relative molar absorptivities for the solutions used in the fluorescence studies below.

Fluorescence Data

Two solutions of identical concentrations of molecules **1**, **2**, or **3** in the aprotic and protic solvents were made by diluting 20 μL of a stock solution of molecules **1**, **2**, or **3** (~5 mg /10 mL toluene) to 5 mL. Two sets of emission data were acquired for each binary system. In the first set 2.0 mL of the toluene solution was sequentially spiked with nineteen to twenty-two aliquots of variable but increasing volume of the alcohol solution, and the solution was stirred for thirty seconds before recording the emission. In the second set, 2.0 mL of the alcohol solution was spiked with seven aliquots of variable but increasing volume of the aprotic solution. For an

example of these aliquot volumes and the subsequent mole fractions of both solvents in each solution, consult Table A2. The abscissa scale of the intensity *vs.* wavelength data was converted to wavenumbers before subsequent mathematical treatment. The electronic noise was subtracted from the raw emission intensity. The net intensity at each point was divided by the spectral response of the Hamamatsu S10420 CCD and multiplied by $\lambda^2/\lambda_{max}^2$ to account for the effect of the abscissa-scale conversion.[16]

Calculation of Spectral Values and Fractional Changes

Two sets of spectral values (Y) were determined from the fluorescence spectrum of each compound. These spectral values were the relative quantum yield (Q_{rel}), and the product of the center of mass and the relative quantum yield ($\tilde{\nu}_{CM} \bullet Q_{rel}$).[17] Equation (*1*) was used to convert the integrated emission intensities into relative quantum yields, so that the relative molar absorptivities (ε) and refractive indices (η) of the solvent mixtures were taken into account.

$$Q_{rel} = \frac{I_{adj}}{(I_{adj})_{max}} \quad \text{where} \quad I_{adj} = I_{int} \cdot \frac{\varepsilon_{max}}{\varepsilon} \cdot \frac{\eta^2}{\eta_{min}^2} \tag{1}$$

The refractive indices of toluene/methanol mixtures were available from the literature,[18] and the refractive indices of the toluene/isopropanol mixtures were calculated using the Gladestone-Dale equation from the excess molar volume data for known solvent compositions.[19] The emission center-of-mass values were calculated using Equation (*2*).

$$\tilde{\nu}_{CM} = \frac{\int I(\tilde{\nu}) \cdot \tilde{\nu}\, d\tilde{\nu}}{\int I(\tilde{\nu})\, d\tilde{\nu}} = \frac{\int I(\tilde{\nu}) \cdot \tilde{\nu}\, d\tilde{\nu}}{I_{int}} \tag{2}$$

Equation (*3*) was used to determine the fractional changes (Γ) in the spectral values (Y), where Y_1 is the spectral value for the excited fluorophore in the aprotic solvent and Y_2 is the spectral value for the excited fluorophore in the protic solvent.

$$\Gamma = \frac{Y_1 - Y}{Y_1 - Y_2} \tag{3}$$

Preferential Solvation Model

Equations (*4*) and (5) describe the two-step exchange solvation model formulated by Rosés & Bosch.[20-27] The equations show equilibria involving three solvated excited states (*F**): one is surrounded by only aprotic solvents, another by only protic solvents, and the third by a mixture of the aprotic and protic solvents. The equilibrium constant $f_{2/1}$ is for the process of double solvent exchange, and $f_{12/1}$ is for single solvent exchange.

$$F^*(\text{aprotic})_2 + \text{protic} \underset{}{\overset{f_{12/1}}{\rightleftharpoons}} F^*(\text{aprotic, protic}) + \text{aprotic} \qquad (4)$$

$$F^*(\text{aprotic})_2 + 2\ \text{protic} \underset{}{\overset{f_{2/1}}{\rightleftharpoons}} F^*(\text{protic})_2 + 2\ \text{aprotic} \qquad (5)$$

Equation (*6*) relates the change in spectral value (Γ) to the equilibrium constants and the mole fraction of protic solvent.

$$\Gamma = \frac{Y_1 - Y}{Y_1 - Y_2} = \frac{f_{2/1}x^2 + f_{12/1}r\,x(1-x)}{(1-x)^2 + f_{2/1}x^2 + f_{12/1}x(1-x)} \qquad (6)$$

Taking the difference between the two types of spectral values results in the elimination of the second order term in the numerator, as shown in Equation (*7*):

$$\Gamma_{\text{CM}\cdot\text{Q}} - \Gamma_{\text{Q}} = \frac{f_{12/1}\Delta r\,x(1-x)}{(1-x)^2 + f_{2/1}x^2 + f_{12/1}x(1-x)} \qquad \text{where } \Delta r = r_{\text{CM}\bullet\text{Q}} - r_{\text{Q}} \qquad (7)$$

Taking the first derivative of Equation (*7*) with respect to the mole fraction yields a quadratic term in the numerator of Equation (*8*).

$$\frac{d(\Gamma_{\text{CM}\cdot\text{Q}} - \Gamma_{\text{Q}})}{dx} = \frac{(x^2(1-f_{2/1}) - 2x + 1) \times (f_{12/1}\Delta r)}{((1-x)^2 + f_{2/1}x^2 + f_{12/1}x(1-x))^2} \qquad (8)$$

When this first derivative is equal to zero, the difference function Γ_{Q} - $\Gamma_{\text{CM}\bullet\text{Q}}$ has an extreme value, and this occurs when the quadratic term in the numerator of Equation (*8*) is equal to zero. The mole fraction where this local maximum occurs is determined by fitting six points on a plot

of Γ_Q - $\Gamma_{CM \bullet Q}$ *vs. x* to a third order polynomial function, taking the first derivative, setting it equal to zero, and solving for the mole fraction *x*. Equation (*9*) relates this mole fraction value to $f_{2/1}$.

$$f_{2/1} = \frac{1}{x^2} - \frac{2}{x} + 1 \qquad (9)$$

The remaining parameters in Equation (*6*) are determined using non-linear least-squares fitting of plots of both Γ_Q and $\Gamma_{CM \bullet Q}$ *vs.* mole fraction *x*.

Results

Absorbance Data

All three derivatives showed progressive changes in their absorption spectra, generally consisting of decreased absorbance with successive addition of aliquots of alcohol solvent and shifting of the spectrum towards longer wavelengths with successive addition of alcohol solvents (Figures A2, A4, A6, A8, A10, A12).

Fluorescence Data

Table 1. Observed and calculated parameters from the fluorescence spectra of compounds in various binary solvent mixtures

Molecule, Solvent	Q_0	$\tilde{\nu}_{CM0}$ (cm^{-1})	Q_{rel}	$\tilde{\nu}_{CM}$ (cm^{-1})	Q_{rel} (1H-bond)	$\tilde{\nu}_{CM\ (1H\text{-}bond)}$ (cm^{-1})	$f_{2/1}$	$f_{12/1}$
1, tol/EtOH	1.00	18900	0.05	16530	0.42	17680	9559	249.0
1, tol/*i*PrOH	1.00	18900	0.11	16660	0.40	17570	6475	196.3
2, tol/EtOH	1.00	19070	0.06	16550	0.58	17800	7922	168.2
2, tol/*i*PrOH	1.00	18990	0.18	17070	0.66	18230	10815	194.1
3, tol/EtOH	1.00	19240	0.10	17060	1.03	18200	3435	82.86
3, tol/*i*PrOH	0.98	19180	0.14	17090	1.01	18260	2272	83.24

3-Aminofluoren-9-one (**1**) *Fluorescence Data*

3-Aminofluoren-9-one (**1**) showed strong quenching of fluorescence in solvent mixtures containing either ethanol or isopropanol (Figure A1, A3). In a solution of pure toluene, the quantum yield of fluorescence for a 5.1μM solution of **1** was 1.00, but in a solution of pure ethanol, its fluorescence quantum yield relative to the toluene solution was only 0.05. In a solution of pure isopropanol, the fluorescence quantum yield relative to the toluene solution was 0.11. The quantum yield of the singly H-bonded species relative to the species with no H-bonds was determined to be 0.42 in mixtures of toluene and ethanol, and 0.40 in mixtures of toluene and isopropanol. The Stern-Volmer plot of **1** in toluene/ethanol mixtures (Figure A13) showed a non-linear relationship that was modeled best by a 2nd order polynomial function. This function was concave-down, and had a limiting slope of 13.41, which roughly corresponds to the Stern-Volmer constant k_{SV}. In toluene/isopropanol mixtures also, the Stern-Volmer plot for **1** (Figure A15) was concave-down with a less steep limiting slope of $k_{SV} \approx 9.4$.

Compound **1** also exhibited solvatochromic behavior in the form of red shifting with successive addition of ethanol or isopropanol to the toluene solution. For the toluene/ethanol mixture, the value of $\tilde{\nu}_{CM}$ shifted from 18900 cm^{-1} in pure toluene to 16530 cm^{-1} in pure ethanol, and for the toluene/isopropanol mixture, the value of $\tilde{\nu}_{CM}$ shifted from 18900 cm^{-1} in pure toluene to 16660 cm^{-1} in pure isopropanol. The value of $\tilde{\nu}_{CM}$ for the singly H-bonded species was calculated to be 17680 in toluene/ethanol mixtures and 17570 in toluene/isopropanol mixtures. Using the preferential solvation model of Rosés & Bosch, we determined the values of the solvent exchange equilibrium constants $f_{2/1}$ and $f_{12/1}$ for solvent mixtures of toluene/ethanol and toluene/isopropanol (Table 1). The high values of $f_{2/1}$ for both solvent mixtures indicate that

1 has a strong preference for alcohol solvents over nonpolar solvents, and this is also evident from the sharp deviation from linearity of the plot of Γ_{CM} and Γ_Q *vs. x* (Figures A14 & A16).

3-Amino-6,8-dimethylfluoren-9-one (**2**) *Fluorescence Data*

3-Amino-6,8-dimethylfluoren-9-one (**2**) also showed strong quenching of fluorescence in solvent mixtures containing either ethanol or isopropanol (Figure A5, A7). In a solution of pure toluene, the quantum yield of fluorescence for a 4.5μM solution of **2** was 1.00, but in a solution of pure ethanol, its fluorescence quantum yield relative to the toluene solution was only 0.06. In a solution of pure isopropanol, the fluorescence quantum yield relative to the toluene solution was 0.18. The quantum yield of the singly H-bonded species relative to the species with no H-bonds was determined to be 0.58 in mixtures of toluene and ethanol, and 0.66 in mixtures of toluene and isopropanol. The Stern-Volmer plot of **2** in toluene/ethanol mixtures (Figure A17) showed a non-linear relationship that was modeled best by a 2nd order polynomial function. This function was concave-down, and had a limiting slope of $k_{SV} \approx 7.74$. In toluene/isopropanol mixtures also, the Stern-Volmer plot for **2** (Figure A19) was concave-down with a similar limiting slope of $k_{SV} \approx 7.5$.

Compound **2** also exhibited solvatochromic behavior in the form of red shifting with successive addition of ethanol or isopropanol to the toluene solution. For the toluene/ethanol mixture, the value of $\tilde{\nu}_{CM}$ shifted from 19069 cm^{-1} in pure toluene to 16550 cm^{-1} in pure ethanol, and for the toluene/isopropanol mixture, the value of $\tilde{\nu}_{CM}$ shifted from 18990 cm^{-1} in pure toluene to 17070 cm^{-1} in pure isopropanol. The value of $\tilde{\nu}_{CM}$ for the singly H-bonded species was calculated to be 17800 in toluene/ethanol mixtures and 18230 in toluene/isopropanol mixtures. Using the preferential solvation model of Rosés & Bosch, we determined the values of the solvent exchange equilibrium constants $f_{2/1}$ and $f_{12/1}$ for solvent mixtures of toluene/ethanol

and toluene/isopropanol (Table 1). The high values of $f_{2/1}$ for both solvent mixtures indicate that like compound **1**, derivative **2** has a strong preference for alcohol solvents over nonpolar solvents, and this is also evident from the sharp deviation from linearity of the plot of Γ_{CM} and Γ_Q *vs. x* (Figures A18 & A20).

3-Amino-1,8-dimethylfluoren-9-one (**3**) *Fluorescence Data*

3-Amino-1,8-dimethylfluoren-9-one (**3**) behaved slightly differently than the other derivatives, but it still showed strong quenching in solvent mixtures containing either ethanol or isopropanol (Figure A9, A11). In a solution of pure toluene, the quantum yield of fluorescence for a 2.2μM solution of **3** was 1.00, but in a solution of pure ethanol, its fluorescence quantum yield relative to the toluene solution was only 0.10. In the toluene/isopropanol experiment, the quantum yield of fluorescence decreased from 0.98 in pure toluene to 0.14 in pure isopropanol. The quantum yield of the singly H-bonded species relative to the species with no H-bonds was determined to be 1.03 in mixtures of toluene and ethanol, and 1.01 in mixtures of toluene and isopropanol, a sharp difference from **1** and **2**. The Stern-Volmer plot of **3** in toluene/ethanol mixtures (Figure A21) showed a non-linear relationship that was modeled best by a 2nd order polynomial function. This function was very unusual in that it was concave-up instead of concave-down, and it had a limiting slope of $k_{SV} \approx 0.31$. However, in toluene/isopropanol mixtures, the Stern-Volmer plot for **3** (Figure A23) was concave-down with an only slightly greater limiting slope of $k_{SV} \approx 1.86$.

Compound **3** also exhibited solvatochromic behavior in the form of red shifting with successive addition of ethanol or isopropanol to the toluene solution. For the toluene/ethanol mixture, the value of $\tilde{\nu}_{CM}$ shifted from 19240 cm^{-1} in pure toluene to 17060 cm^{-1} in pure ethanol, and for the toluene/isopropanol mixture, the value of $\tilde{\nu}_{CM}$ shifted from 19180 cm^{-1} in pure

toluene to 17090 cm^{-1} in pure isopropanol. The value of $\tilde{\nu}_{CM}$ for the singly H-bonded species was calculated to be 18200 in toluene/ethanol mixtures and 18260 in toluene/isopropanol mixtures. Using the preferential solvation model of Rosés & Bosch, we determined the values of the solvent exchange equilibrium constants $f_{2/1}$ and $f_{12/1}$ for solvent mixtures of toluene/ethanol and toluene/isopropanol (Table 1). The high values of $f_{2/1}$ for both solvent mixtures indicate that like compound **1** and derivative **2**, derivative **3** has a strong preference for alcohol solvents over nonpolar solvents, and this is also evident from the sharp deviation from linearity of the plot of Γ_{CM} and Γ_Q *vs. x* (Figures A22 & A24). However, the values for $f_{12/1}$ for **3** are notably smaller than the corresponding values for **1** and **2**.

Discussion

Interpretation of Fluorescence Data

Table 2. Coefficients from the 2nd order polynomial lines of best fit to the Stern-Volmer plots of each compound in binary solvent mixtures. For 2nd order polynomials with forced *y*-intercepts of $y=0$, of the form $Ax^2 + Bx$, the magnitude of A corresponds to the degree of concavity, the sign of A corresponds to the direction (+ up, - down) of concavity of the function, and B corresponds to the limiting slope of the function, which is analogous to the Stern-Volmer constant k_{SV}.

Molecule, Solvent	A	B≈k_{SV}
1, tol/EtOH	-11.5	13.41
1, tol/*i*PrOH	-10	9.4
2, tol/EtOH	-4	7.74
2, tol/*i*PrOH	-11	7.5
3, tol/EtOH	12.2	0.31
3, tol/*i*PrOH	-0.32	1.86

These data are inconsistent with the predictions of the model proposed by the Inoue group. In order for the model to hold true, we would expect derivative **3**, which has both in-plane hydrogen bonds blocked, to exhibit the highest initial rate of quenching. This derivative

should quench immediately, because the first singlet excited state can only deactivate through formation of the out-of-plane hydrogen bond, which Inoue et al. described as a non-radiative process (*c.f.* Figure 9). We also would expect derivative **2** to exhibit slightly higher quenching than **1** because it has one of the two possible in-plane hydrogen bonds blocked by a methyl group, thus eliminating half of the microstates leading to an emissive hydrogen-bonded state.

Rather, we observed the opposite: derivative **3** showed a very low initial rate of quenching compared to **1** and **2** (Table 2), and derivative **2** had a slightly lower initial rate of quenching than **1**. Comparison of the calculated values for Q_{rel} for the singly H-bonded species (shown as $Q_{rel\,(1\text{H-bond})}$ in Table 1) reveals that the fluorescence quantum yield for the singly H-bonded species of derivative **3** is almost exactly the same as the fluorescence quantum yield for **3** without any hydrogen bonds to solvent molecules. Also, $Q_{rel\,(1\text{H-bond})}$ was consistently higher for **2** than for **1**, indicating that derivative **2** is more likely to decay through radiative pathways than is **1**. Also, comparison of the preferential solvation equilibrium constants $f_{2/1}$ and $f_{12/1}$ across the three derivatives reveals that the values of both of these constants for derivative **3** are less than half of the respective values for derivative **2** and **1**. While this may be due in part to the increased hydrophobicity of the molecule from the presence of two methyl groups, it could also indicate the reduced amount of interaction between the hydrogen bond donating alcohol groups of the solvent molecules and the carbonyl oxygen of **3**, compared to **2** and **1**.

The Stern-Volmer relation for **3** in toluene/ethanol mixtures was concave-up, and similarly for its initial Stern-Volmer relation in toluene/isopropanol, although the toluene/isopropanol plot eventually became concave-down at higher quencher concentrations. Both of these concave-up initial quenching relations indicate that the rate of quenching is slow at first and increases with higher concentrations of quencher. For **1** and derivative **2**, the initial rate

of quenching was high and decreased with higher concentrations of quencher. Although the lower rates of quenching observed for **3** seem to suggest that the out-of-plane hydrogen bond is the emissive state and the in-plane hydrogen bond is the non-emissive state for the 3-aminofluoren-9-one carbonyl oxygen in the singlet excited state (Figure 16), some aspects of the data are more elusive of clear interpretation.

Figure 16. Revised energy diagram showing possible modes of non-radiative decay of excited-state aminofluoren-9-ones through hydrogen-bonding interactions with solvent molecules. Here the emissive state corresponds to the single out-of-plane H-bond and the non-emissive state corresponds to the single in-plane H-bond. As in Figure 9, k_1 represents the rate constant for H-bond formation to the excited state carbonyl oxygen, and $\alpha + \beta = 1$.

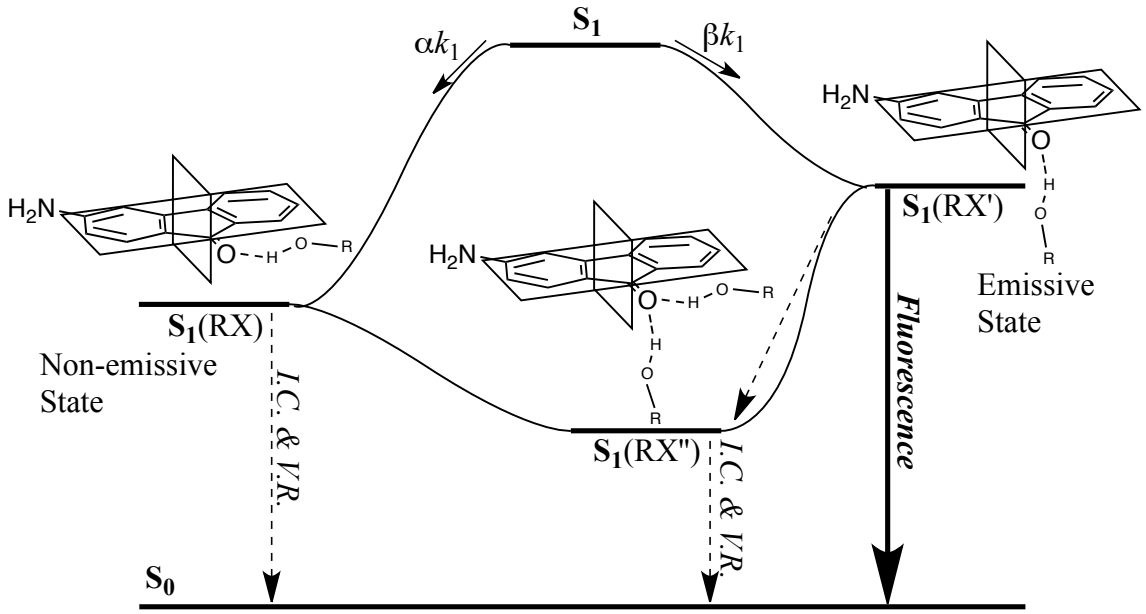

The fluorescence spectra of **3** in mixtures of toluene/ethanol and toluene/isopropanol both show that although **3** was resistant to quenching in low concentrations of alcohol, it eventually reached a critical concentration after which rapid quenching occurred. The mode of this quenching is not adequately explained by Figure 16, as all non-radiative decay pathways involve the formation of an in-plane hydrogen bond. One possible explanation for this quenching that involves hydrogen-bonding interactions is the formation of a second hydrogen bond to the lone pair in the orbital along the axis of the C–O bond (Figure 17).

Figure 17. Orbital geometry of the carbonyl oxyanion of the first singlet excited state of 3-aminofluoren-9-one showing a two H-bonds, one out-of-plane (to green *p*-orbital) and one to the C–O axis lone pair (blue *sp*-hybrid orbital). Orbital geometry adapted from Inoue et al.[8]

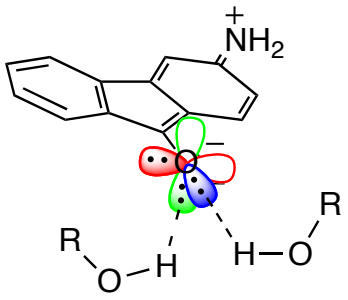

Though this H-bond is technically in-plane, it involves a different orbital than the other in-plane bonds, and thus the energetics of this interaction may differ significantly from the in-plane hydrogen bond to the lone pair in the orbital orthogonal to the C–O bond. This energetic difference may be great enough to render it inactive in most scenarios where bonds to the in-plane orbital orthogonal to the C–O bond are available.

One notable aspect of the fluorescence behavior of these aminofluoren-9-one derivatives is the similarity of the quenching behavior across alcohols of different solvent acidities. The data for the quenching behavior of each derivative is almost identical in toluene/ethanol and toluene/isopropanol mixtures, quite unlike the PRODAN derivatives previously studied by our group.[3] It is possible that if the lone pair in the orbital along the C–O bond axis provides a mode of H-bond quenching, then there may be a tradeoff between sterics and electronics that gives rise to this apparent unresponsiveness to solvent acidity. Generally, alcohols with low solvent acidity tend to have bulkier alkyl groups than those with high solvent acidity. Since the incoming H-bond to this lone pair is located opposite to the fluorene ring system, it is the least hindered H-bonding mode. Bulky alcohols with lower solvent acidity such as isopropanol, 2-octanol, and *tert*-butanol may experience steric hindrance from the ring system, making this H-bonding mode more likely to occur even though it is energetically less favorable than the formation of an in-

plane H-bond. In solvents with higher solvent acidity such as methanol and ethanol, this steric interaction does not occur, which results in decreased quenching from this H-bonding mode. This theory could be tested by further studies of the fluorescence of compounds **1** and **3** in binary solvent mixtures of toluene and alcohols of various solvent acidities.

Synthetic Obstacles

In the synthesis of **1**, an attempt to reduce the nitro group to an amine via palladium-catalyzed hydrogenation resulted in successful reduction of the nitro group, but this procedure also reduced the fluoren-9-one carbonyl to a mixture of alcohol and hydrocarbon. A subsequent attempt to protect the carbonyl as an ethylene glycol ketal resulted in no reaction upon palladium hydrogenation. Because of the susceptibility of the carbonyl to reduction under these conditions, we turned from metal catalysis to other redox chemistry to effect this reduction. We used sodium sulfide, which had previously been used to successfully reduce 3-nitrofluoren-9-one to 3-aminofluoren-9-one by Ray & Barrick.[15]

Prior to the development of the synthesis of **2**, we attempted to synthesize 3-amino-1-methylfluoren-9-one to block one of the two in-plane H-bonds available to the fluoren-9-one carbonyl oxygen. The synthesis of 3-amino-1-methylfluoren-9-one was designed around initial formation of the carbonyl bridge between the two six-carbon rings of the fluoren-9-one molecule, followed by closure of the five-membered ring via Pschorr cyclization (Figure 18). Commercially available 2-aminobenzoic acid was reacted with triphosgene in THF to give isatoic anhydride at 86% yield following the procedure of Dong et al.[28] This isatoic anhydride was then converted to a Weinreb amide using N,O-dimethylhydroxylamine to give 2-amino-*N*-methoxy-*N*-methylbenzamide at 66% yield following the procedure of Frye, Johnson, & Valvano.[29]

Figure 18. Attempted synthesis of 3-amino-1-methylfluorenone in five steps from 2-aminobenzoic acid.

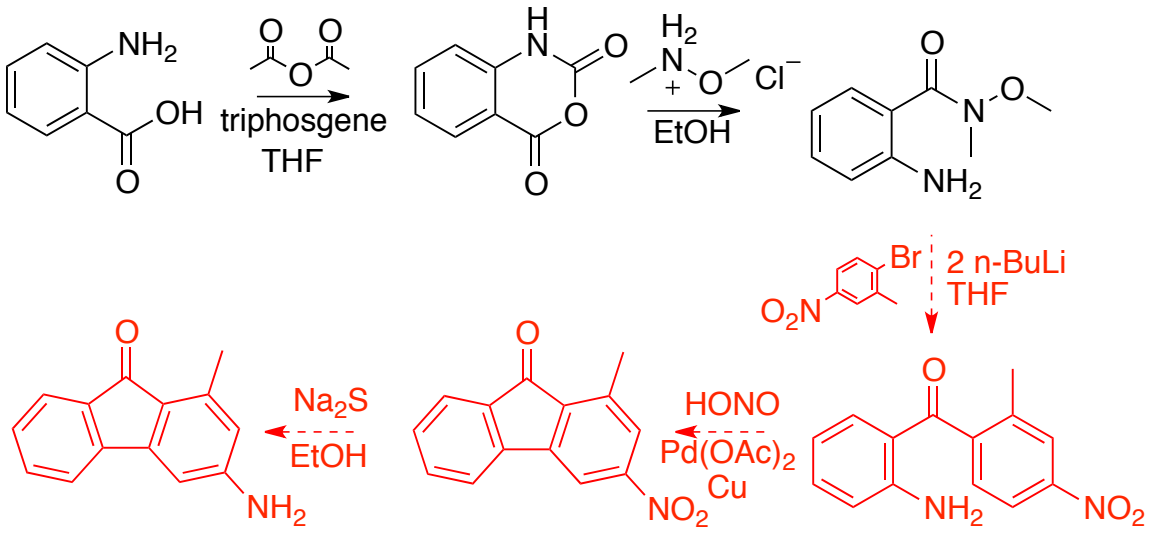

An attempt to add 2-bromo-5-nitrotoluene to the amide via an aryllithium reaction failed to produce any product, although ^{1}H NMR did show evidence of metal-halogen exchange. Thus, the most likely explanation for the failure of the reaction was low reactivity of the Weinreb amide due to the electron-donating amino substituent on the benzene ring. Attempts to add a methylsulfonate group to this amine were successful, but the aryllithium reaction still failed to produce any desired product. An attempt to add two methylsulfonate groups to the amine was also unsuccessful, so an alternate synthesis pathway was developed to produce an analogous 3-aminofluoren-9-one derivative that will exhibit similar hydrogen bonding and photophysical behavior to 3-amino-1-methylfluoren-9-one. That synthesis pathway, shown in Figure 14, successfully yielded **2**.

The synthesis of **3** was originally designed around a similar final set of steps to the synthesis of 3-amino-1-methyl-9-fluorenone (Figure 19). As such, this synthetic pathway was abandoned when it was discovered that the aryllithium addition of 2-bromo-5-nitrotoluene to an aminobenzyl Weinreb amide would not proceed to completion. Also, this synthesis required a

large number of steps to produce a starting material analogous to the 2-aminobenzoic acid used in the synthesis of 3-amino-1-methylfluoren-9-one. Despite these apparent drawbacks, the synthesis had been completed to the production of 2-methyl-6-nitrobenzoic acid before this discovery, and all steps to that point in the synthesis had succeeded in producing reasonable yields of intermediates.

Figure 19. Attempted synthesis of 3-amino-1,8-dimethylfluorenone (**3**) in ten steps from *o*-toluidine.

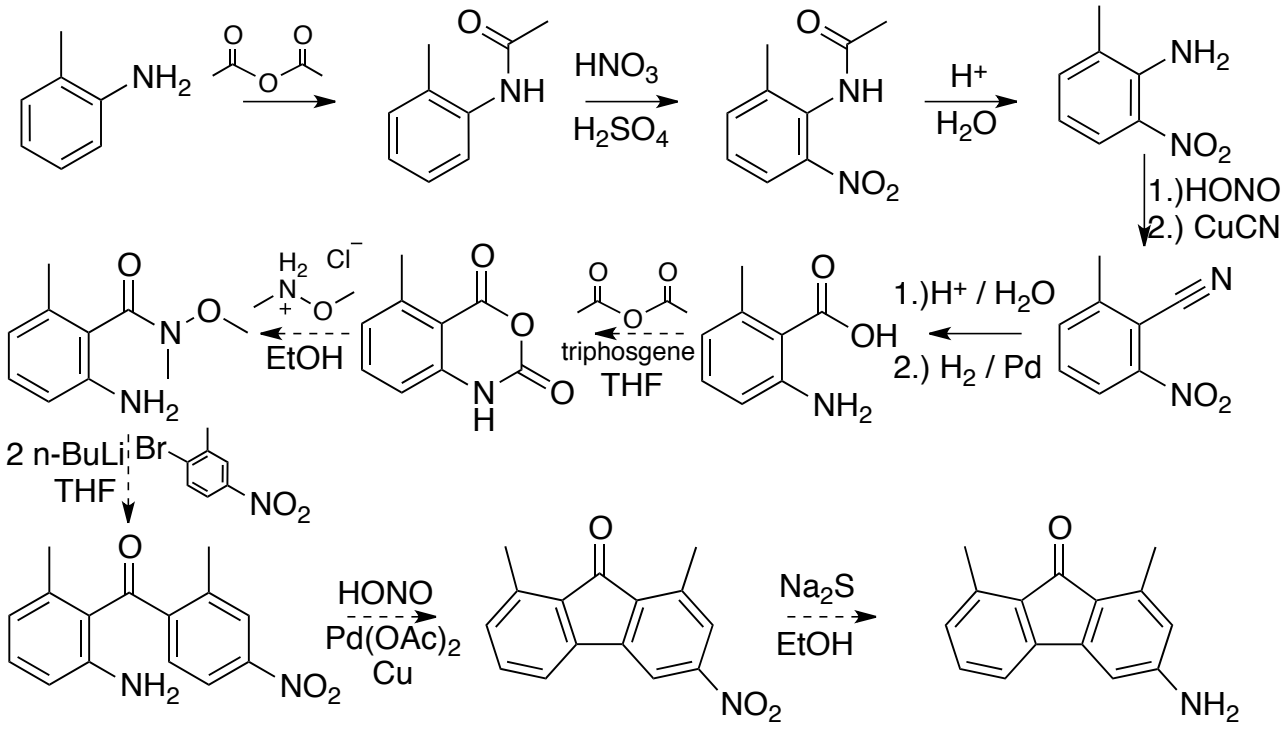

2-methyl-6-nitroaniline was synthesized from *o*-toluidine following the procedure of Howard.[30] Commercially available *o*-toluidine was reacted with acetic anhydride to form *N*-(*o*-tolyl)acetamide. This *N*-(*o*-tolyl)acetamide was then reacted with nitric acid to form a mixture of *N*-acetyl-2-methyl-6-nitroaniline and *N*-acetyl-2-methyl-4-nitroaniline. This mixture was placed in a steam distillation apparatus with HCl to hydrolyze the amides and selectively retrieve 2-methyl-6-nitroaniline. The 2-methyl-6-nitroaniline was then diazotized using nitrous acid and subsequently reacted with copper (I) cyanide in a Sandmeyer reaction to form 2-methyl-6-

nitrobenzonitrile following the procedure of Tsuchiya et al.[31] The 2-methyl-6-nitrobenzonitrile was then hydrolyzed in acid to form 2-methyl-6-nitrobenzoic acid. At this point, the synthesis was abandoned, and the synthesis shown in Figure 15 was adopted to successfully produce compound **3** in a pathway with less than half the number of steps from starting material to final product.

Conclusion

This study determined the effect of steric hindrance of in-plane hydrogen bonds to the carbonyl oxygen of 3-aminofluoren-9-one on the rate and extent of fluorescence quenching in alcohol solvents. 3-aminofluoren-9-one and two derivatives, 3-amino-6,8-dimethylfluoren-9-one and 3-amino-1,8-dimethylfluoren-9-one were successfully synthesized from commercial starting materials. 3-aminofluoren-9-one was synthesized in acceptable overall yield, but the two derivatives would require optimization of the synthetic pathway to be viable for larger scale production. Studies of the fluorescence of these derivatives in binary solvent mixtures of toluene/ethanol and toluene/isopropanol revealed that 3-aminofluoren-9-ones have a slightly lower initial rate of fluorescence quenching when one in-plane hydrogen bond is blocked, and a significantly lower initial rate of fluorescence quenching when both in-plane hydrogen bonds are blocked. This supports the conclusion that the formation of an out-of-plane hydrogen bond to the carbonyl oxygen yields a complex capable of emissive deactivation through fluorescence, whereas the formation of an in-plane hydrogen bond leads to non-radiative deactivation of the singlet excited state of 3-aminofluoren-9-ones. The precise mode of non-radiative decay from the out-of-plane H-bonded state in 3-amino-1,8-dimethylfluoren-9-one is not fully understood, but it may arise from the formation of a second hydrogen bond to the lone pair in the orbital

along the C–O axis, which may also play a role in the relative unresponsiveness of the quenching rates of these molecules to changes in solvent acidity.

Acknowledgements

This Chemistry Honors Thesis is dedicated to Lisa and Greg Alty for their unselfish devotion to supporting the author in his research endeavors. The author especially thanks his advisor Christopher Abelt for providing guidance when problems seemed insurmountable, and for being encouraging in the pursuit of new ideas. This research would not be possible without the collaboration of Doug Cheek, Emma Walhout, and all the other members of the Abelt research group at the College of William & Mary. The author also acknowledges the American Chemical Society's Petroleum Research Fund for financial support, and the William & Mary Charles Center for their generous support in the form of a Monroe Scholar Research Grant and an Honors Fellowship.

References

[1] Weber, G.; Farris, F.J. Synthesis and spectral properties of a hydrophobic fluorescent probe: 6-propionyl-2-(dimethylamino)naphthalene. *Biochemistry* **1979**, *18* (14), 3075-3078.

[2] Cerezo, F.M.; Rocafort, S.C.; Sierra, P.S.; García-Blanco, F.; Oliva, C.D.; Sierra, J.C. Photophysical study of the probes acrylodan (1-[6-(dimethylamino) naphthalen-2-yl] prop-2-en-1- one), ANS (8-anilinonaphthalene-1-sulfonate) and prodan (1-[6-(dimethylamino) naphthalen-2-yl] propan-1-one) in aqueous mixtures of various alcohols. *Helv. Chim. Acta* **2001**, *84*, 3306–3312.

[3] Yoon, A. H.; Whitworth, L. C.; Wagner, J. D.; Abelt, C. J. PRODAN derivatives as highly sensitive sensors of low solvent acidity. *Molecules* **2014**, *19*, 6415-6427.

[4] Green, A. M.; Abelt, C. J. Dual-sensor fluorescent probes of surfactant-induced unfolding of human serum albumin. *J. Phys. Chem. B* **2015**, *119*, 3912-3919.

[5] Marini, A.; Muñoz-Losa, A.; Biancardi, A.; Mennucci, B. What is solvatochromism? *J. Phys. Chem. B* **2010**, *114*, 17128–17135.

[6] Yatsuhashi, T.; Inoue, H. Molecular mechanism of radiationless deactivation of aminoanthraquinones through intermolecular hydrogen-bonding interaction with alcohols and hydroperoxides. *J. Phys. Chem. A* **1997**, *101*, 8166-8173.

[7] Jones, G., II; Feng, Z.; Bergmark, W. R. Photophysical properties of (dimethylamino)anthraquinones: radiationless transitions in solvent and polyelectrolyte media. *J. Phys. Chem.* **1994**, *98*, 4511.

[8] Yatsuhashi, T.; Nakajima, Y.; Shimada, T.; Tachibana, H.; Inoue, H. Molecular mechanism for the radiationless deactivation of the intramolecular charge-transfer excited singlet state of aminofluorenones through hydrogen bonds with alcohols. *J. Phys. Chem. A* **1998**, *102*, 8657-8663.

[9] Yatsuhashi, T.; Nakajima, Y.; Shimada, T.; Inoue, H. Photophysical properties of intramolecular charge-transfer excited singlet state of aminofluorenone derivatives. *J. Phys. Chem. A* **1998**, *102*, 3018-3024.

[10] Alty, I. G.; Cheek, D. W.; Chen, T.; Smith, D. B.; Walhout, E. Q.; Abelt, C. J. Intramolecular hydrogen-bonding effects on the fluorescence of PRODAN derivatives. *J. Phys. Chem A* **2016**, upcoming.

[11] Bunnett, J. F.; Rauhut, M. M. 2-bromo-3-methylbenzoic acid. *Organic Syntheses* **1963***, 4*, 114.

[12] Sams, A. G.; Larsen, M.; Mikkelsen, G. *Patent No. 39572.* International. **2005**.

[13] Sebti, S.; Hamilton, A. *Patent No. 5965539.* United States of America. **1999**.

[14] Iihama, T.; Fu, J.; Bourguignon, M.; Snieckus, V. Regiospecific syntheses of all isomeric nitrofluorenones and nitrofluorenes by transition metal catalyzed cross-coupling reactions. *Synthesis* **1989***, 3*, 184-188.

[15] Ray, F. E.; Barrick, J. G. 3-Nitrofluorenone. *Journal of the American Chemical Society* **1948***, 70*, 1492-1494.

[16] Lakowicz, J. *Principles of Fluorescence Spectroscopy*; Kluwer Academic/Plenum Publishers: New York, NY, USA, 1999.

[17] Zurawsky, W.P.; Scarlata, S.F. Preferential solvation of 6-propionyl (*N,N*-dimethylamino) naphthalene in binary, polar solvent mixtures. *J. Phys. Chem.* **1992**, *96*, 6012–6016.

[18] Atik, Z. Experimental and predicted volumetric and refractive index properties of ternary mixtures of iodoethane with toluene and alcohols at temperature 298.15 K and pressure 101kPa. *J. Chem. Thermodyn.* **2006**, *38*, 201–208.

[19] Herráez, J.V.; Belda, R. Refractive indices, densities and excess molar volumes of monoalcohols in water. *J. Solution Chem.* **2006**, *35*, 1315–1328.
[20] Rosés, M.; Ràfols, C.; Ortega, J.; Bosch, E. Solute–solvent and solvent–solvent interactions in binary solvent mixtures. Part 1. A comparison of several preferential solvation models for describing ET (30) polarity of bipolar hydrogen bond acceptor-cosolvent mixtures. *J. Chem. Soc., Perkin Trans. 2* **1995**, 1607-1615.
[21] Bosch, E.; Rived, F.; Rosés, M. Solute–solvent and solvent–solvent interactions in binary solvent mixtures. Part 4. preferential solvation of solvatochromic indicators in mixtures of 2-methylpropan-2-ol with hexane, benzene, propan-2-ol, ethanol and methanol. *J. Chem. Soc., Perkin Trans. 2* **1996**, 2177-2184.
[22] Ortega, J.; Ràfols, C.; Bosch, E.; Rosés, M. Solute–solvent and solvent–solvent interactions in binary solvent mixtures. Part 3. The ET(30) polarity of binary mixtures of hydroxylic solvents. *J. Chem. Soc., Perkin Trans. 2* **1996**, 1497-1503.
[23] Bosch, E.; Roses, M.; Herodes, K.; Koppel, I.; Leito, I.; Koppel, I.; Taal, V. Solute-solvent and solvent-solvent interactions in binary solvent mixtures. Part 2. Effect of temperature on the ET (30) polarity parameter of dipolar hydrogen bond acceptor-hydrogen bond donor mixtures. *J. Phys. Org. Chem.* **1996**, *9*, 403-410.
[24] Ràfols, C.; Rosés, M.; Bosch, E. Solute–solvent and solvent–solvent interactions in binary solvent mixtures. Part 5. Preferential solvation of solvatochromic indicators in mixtures of propan-2-ol with hexane, benzene, ethanol and methanol. *J. Chem. Soc., Perkin Trans. 2* **1997**, 243-248.
[25] Rosés, M.; Buhvestov, U.; Ràfols, C.; Rived, F.; Bosch, E. Solute–solvent and solvent–solvent interactions in binary solvent mixtures. Part 6. A quantitative measurement of the enhancement of the water structure in 2-methylpropan-2-ol–water and propan-2-ol–water mixtures by solvatochromic indicators. *J. Chem. Soc., Perkin Trans. 2* **1997**, 1341-1348.
[26] Buhvestov, U.; Rived, F.; Ràfols, C.; Bosch, E.; Rosés, M. Solute–solvent and solvent–solvent interactions in binary solvent mixtures. Part 7. Comparison of the enhancement of the water structure in alcohol–water mixtures measured by solvatochromic indicators. *J. Phys. Org. Chem.* **1998**, *11*, 185-192.
[27] Herodes, K.; Leito, I.; Koppel, I.; Rosés, M. Solute–solvent and solvent–solvent interactions in binary solvent mixtures. Part 8. The ET(30) polarity of binary mixtures of formamides with hydroxylic solvents. *J. Phys. Org. Chem.* **1999**, *12*, 109-115.
[28] Dong, G.; Wang, S.; Miao, Z.; Yao, J.; Zhang, Y.; Guo, Z. et al. New tricks for an old natural product: discovery of highly potent evodiamine derivatives as novel antitumor agents by systemic structure - activity relationship analysis and biological evaluations. *J. Med. Chem.* **2012**, *55*, 7593-7613.
[29] Frye, S.V.; Johnson, M.C.; Valvano, N.L. Synthesis of 2-aminobenzone via rapid halogen-lithium exchange in the presence of a 2-amino-*N*-methoxy-*N*-methylbenzamide. *J. Org. Chem.* **1991**, *56*, 3750-3752.
[30] Howard, J.C. 2-amino-3-nitrotoluene. *Organic Syntheses* **1963**, *4*, 42.
[31] Tsuchiya, N.; Matsumoto, Y.; Saitou, H.; Mizuno. *Patent No. 0010004*. United States of America. **2004**.

Appendix A: Photophysical Characterizations

Figure A1. Fluorescence spectra of 5.1μM solutions of **1** in toluene/ethanol mixtures. Data collected by Chris Abelt.
[EtOH] (mole %): 0, 0.2, 0.4, 0.5, 0.7, 0.9, 1.3, 1.8, 2.2, 2.7, 3.5, 4.4, 5.2, 6.8, 8.4, 10.2, 12.0, 15.4, 21.5, 31.3, 42.2, 52.3, 59.3, 69.5, 75.3, 82.0, 90.1, 92.4, 94.8, 97.3, 100.

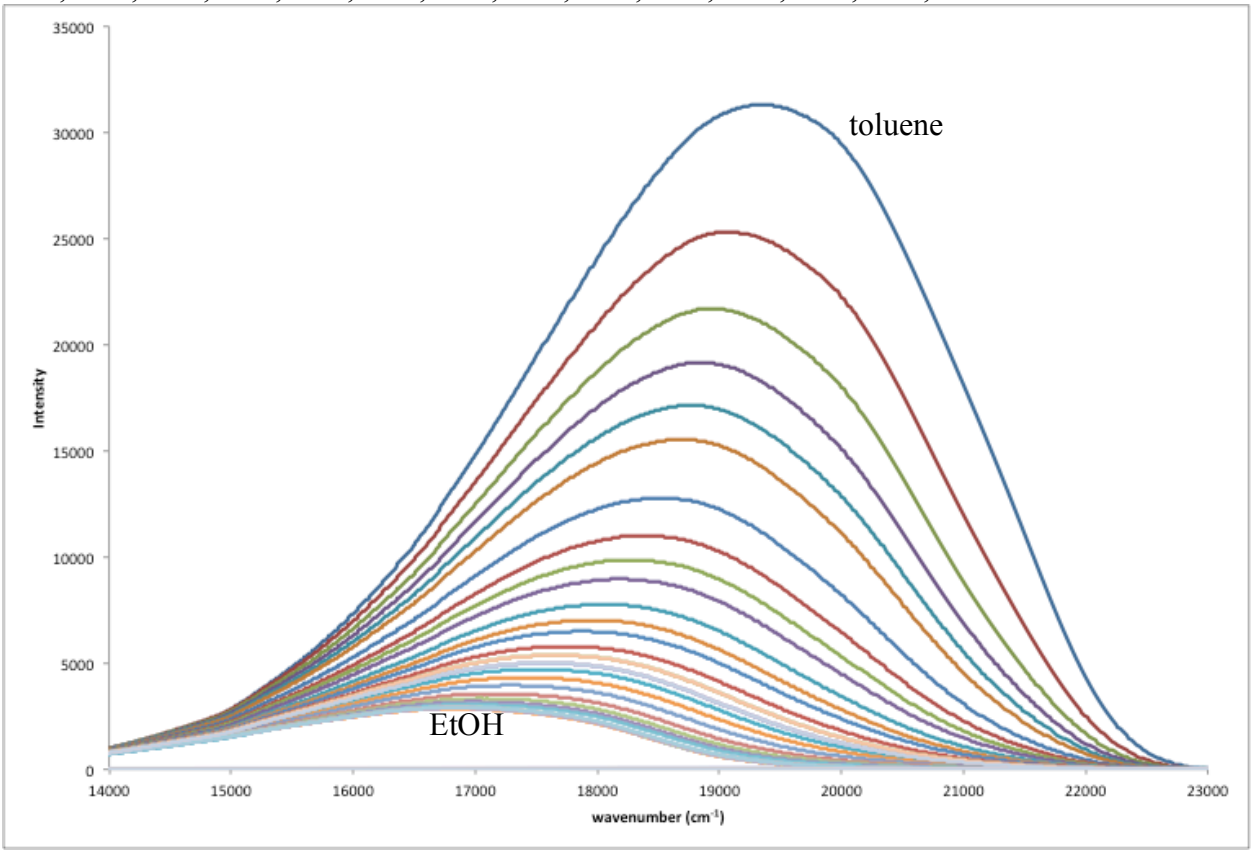

Figure A2. Absorbance spectra of 5.1μM solutions of **1** in toluene/ethanol mixtures. Data collected by Emma Walhout ('17).
[EtOH] (mole %): 0, 5.2, 10.2, 20.1, 40.6, 59.3, 80.2, 90.1, 94.8, 100.

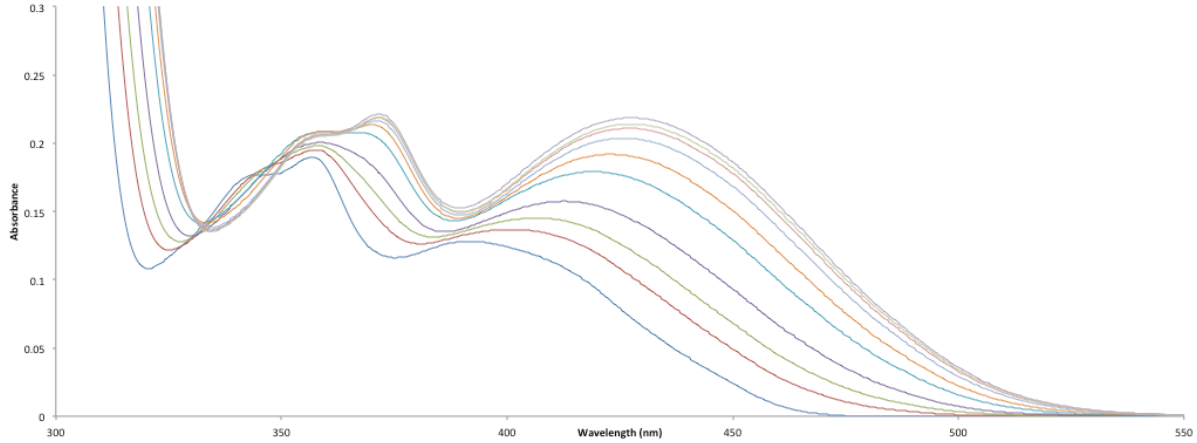

Figure A3. Fluorescence spectra of 5.1μM solutions of **1** in toluene/isopropanol mixtures. Data collected by Chris Abelt.
[*i*PrOH] (mole %): 0, 0.1, 0.3, 0.4, 0.6, 0.7, 1.0, 1.4, 1.7, 2.0, 2.7, 3.4, 4.0, 5.3, 6.5, 8.0, 9.5, 12.2, 17.3, 25.8, 35.8, 45.5, 52.7, 63.5, 69.9, 77.7, 87.4, 90.3, 93.3, 96.5, 100.

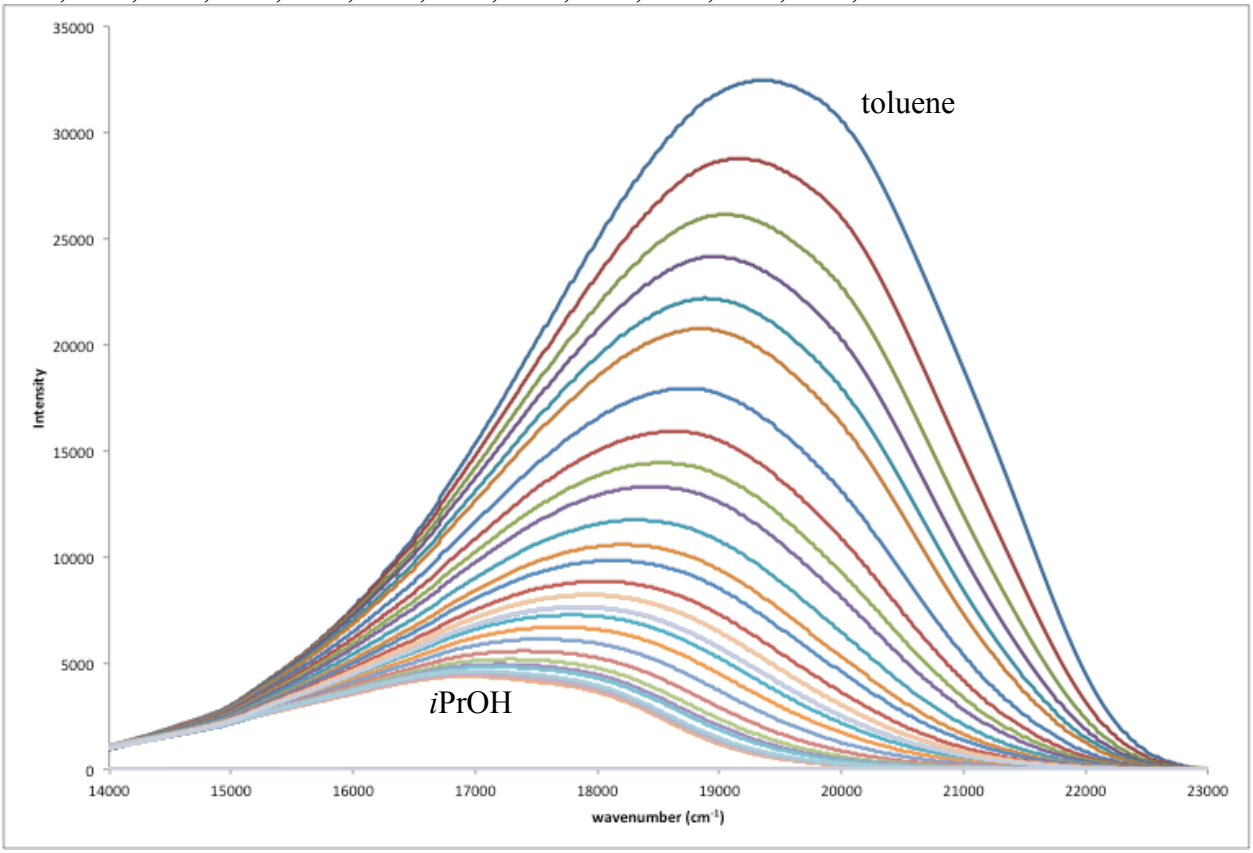

Figure A4. Absorbance spectra of 5.1μM solutions of **1** in toluene/isopropanol mixtures. Data collected by Chris Abelt.
[*i*PrOH] (mole %): 0, 5.0, 10.0, 20.0, 40.1, 52.7, 63.5, 79.9, 90.3, 100.

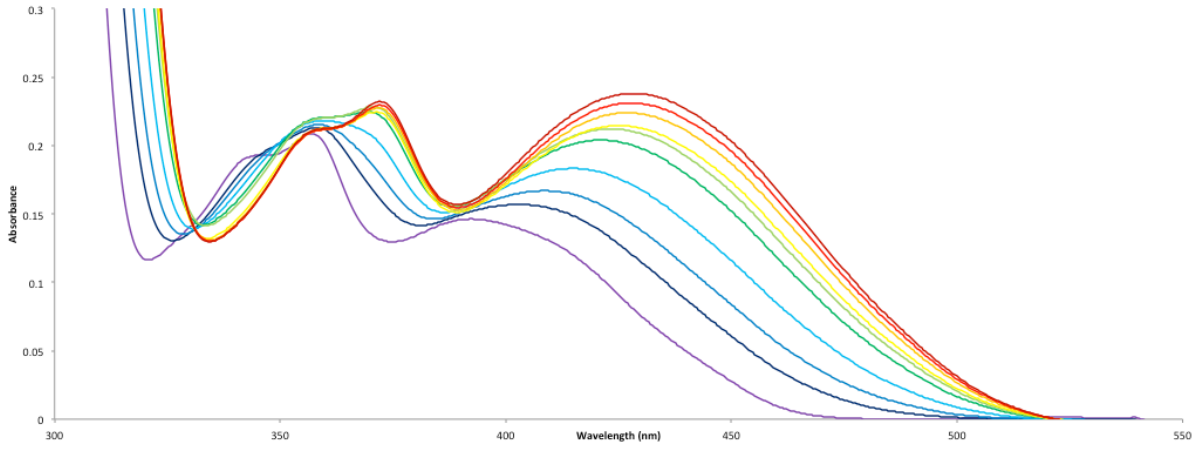

Figure A5. Fluorescence spectra of 4.5μM solutions of **2** in toluene/ethanol mixtures. Data collected by Chris Abelt.
[EtOH] (mole %): 0, 0.1, 0.2, 0.3, 0.4, 0.5, 0.5, 0.6, 0.7, 0.9, 1.3, 1.8, 2.7, 4.4, 8.4, 15.4, 21.5, 31.3, 42.2, 52.3, 59.3, 69.5, 75.3, 82.0, 90.1, 100.

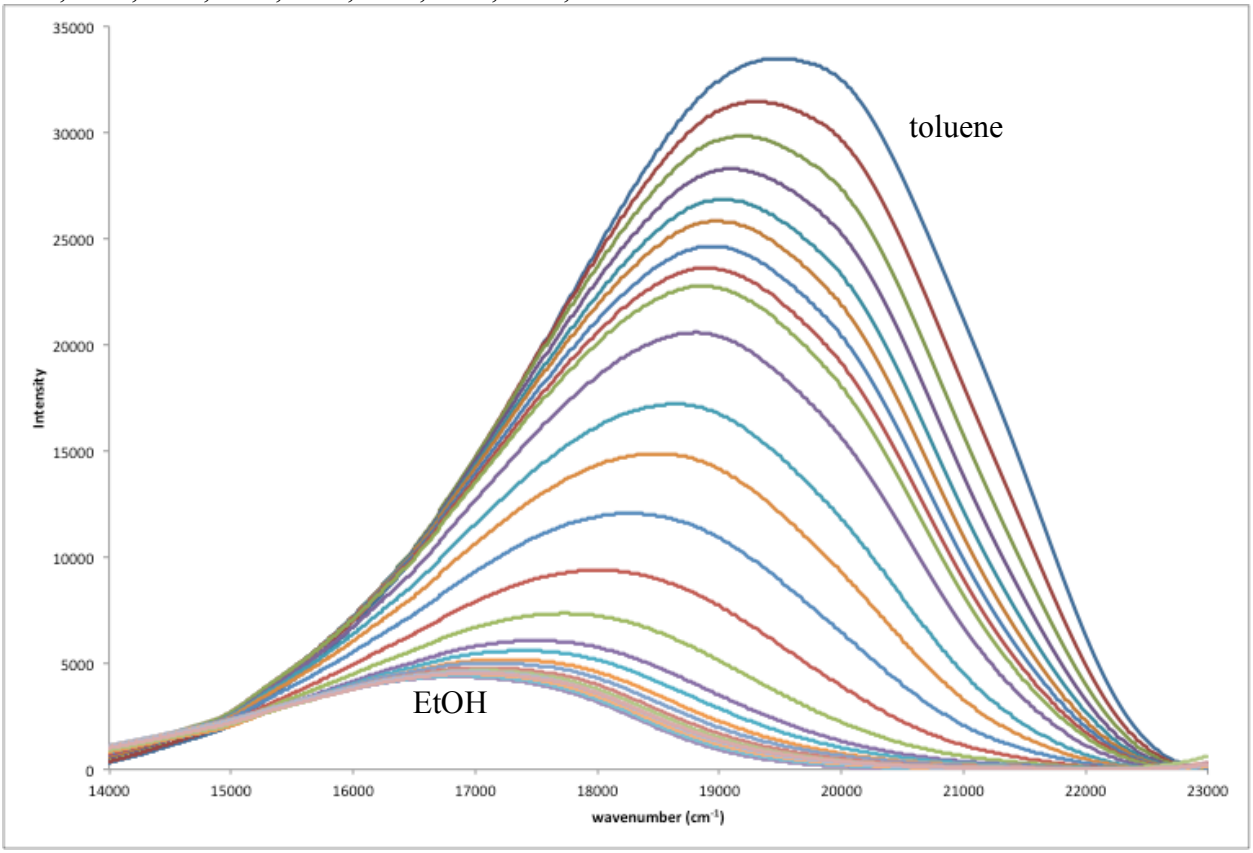

Figure A6. Absorbance spectra of 4.5μM solutions of **2** in toluene/ethanol mixtures. Data collected by Chris Abelt.
[EtOH] (mole %): 0, 5.2, 10.2, 20.1, 40.6, 59.3, 80.2, 90.1, 94.8, 100.

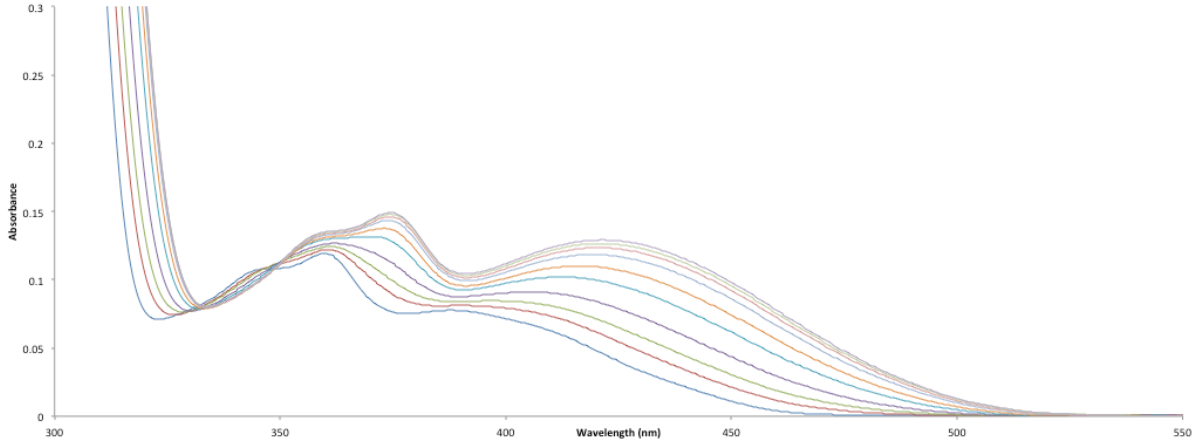

Figure A7. Fluorescence spectra of 4.5μM solutions of **2** in toluene/isopropanol mixtures. Data collected by Doug Cheek ('14, MS '15).
[*i*PrOH] (mole %): 0, 0.1, 0.3, 0.4, 0.6, 0.7, 1.0, 1.4, 1.7, 2.0, 2.7, 3.4, 4.0, 5.3, 6.5, 8.0, 9.5, 12.2, 17.3, 25.8, 35.8, 45.5, 52.7, 63.5, 69.9, 77.7, 87.4, 90.3, 93.3, 96.5, 100.

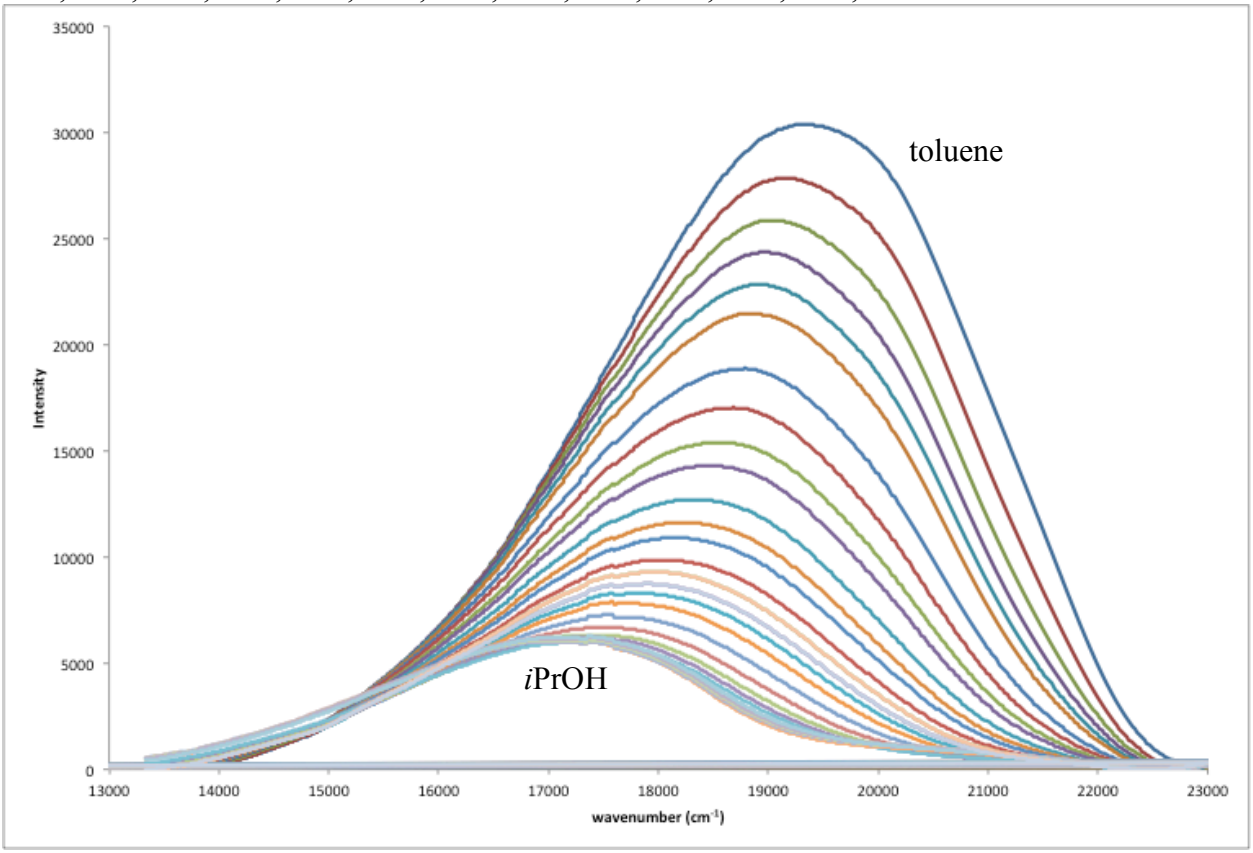

Figure A8. Absorbance spectra of 4.5μM solutions of **2** in toluene/isopropanol mixtures. Data collected by Chris Abelt.
[*i*PrOH] (mole %): 0, 5.0, 10.0, 20.0, 40.1, 52.7, 63.5, 79.9, 90.3, 94.9, 100.

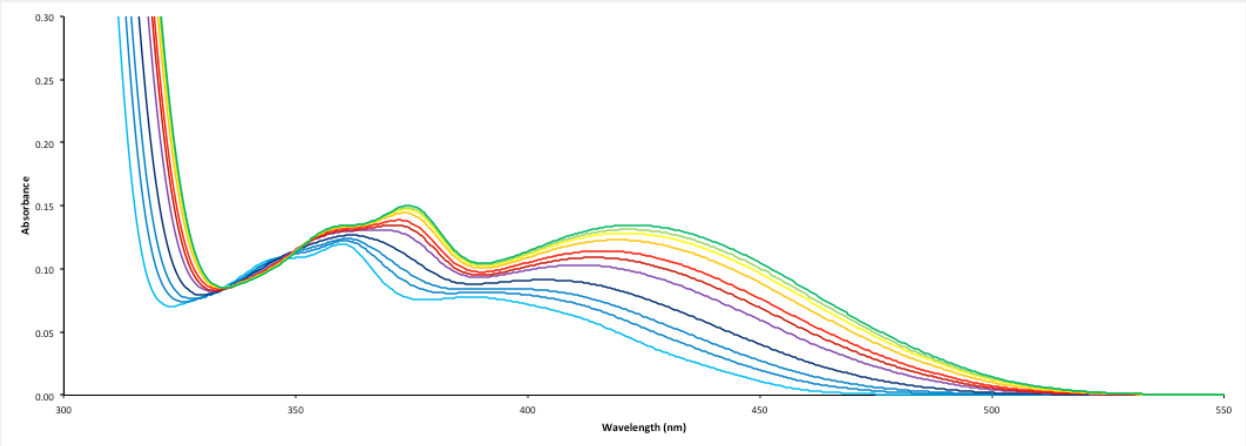

Figure A9. Fluorescence spectra of 2.2μM solutions of **3** in toluene/ethanol mixtures. Data collected by Chris Abelt.
[EtOH] (mole %): 0, 0.1, 0.2, 0.3, 0.4, 0.5, 0.5, 0.6, 0.7, 0.9, 1.3, 1.8, 2.7, 4.4, 8.4, 15.4, 21.5, 31.3, 42.2, 52.3, 59.3, 69.5, 75.3, 82.0, 90.1, 100.

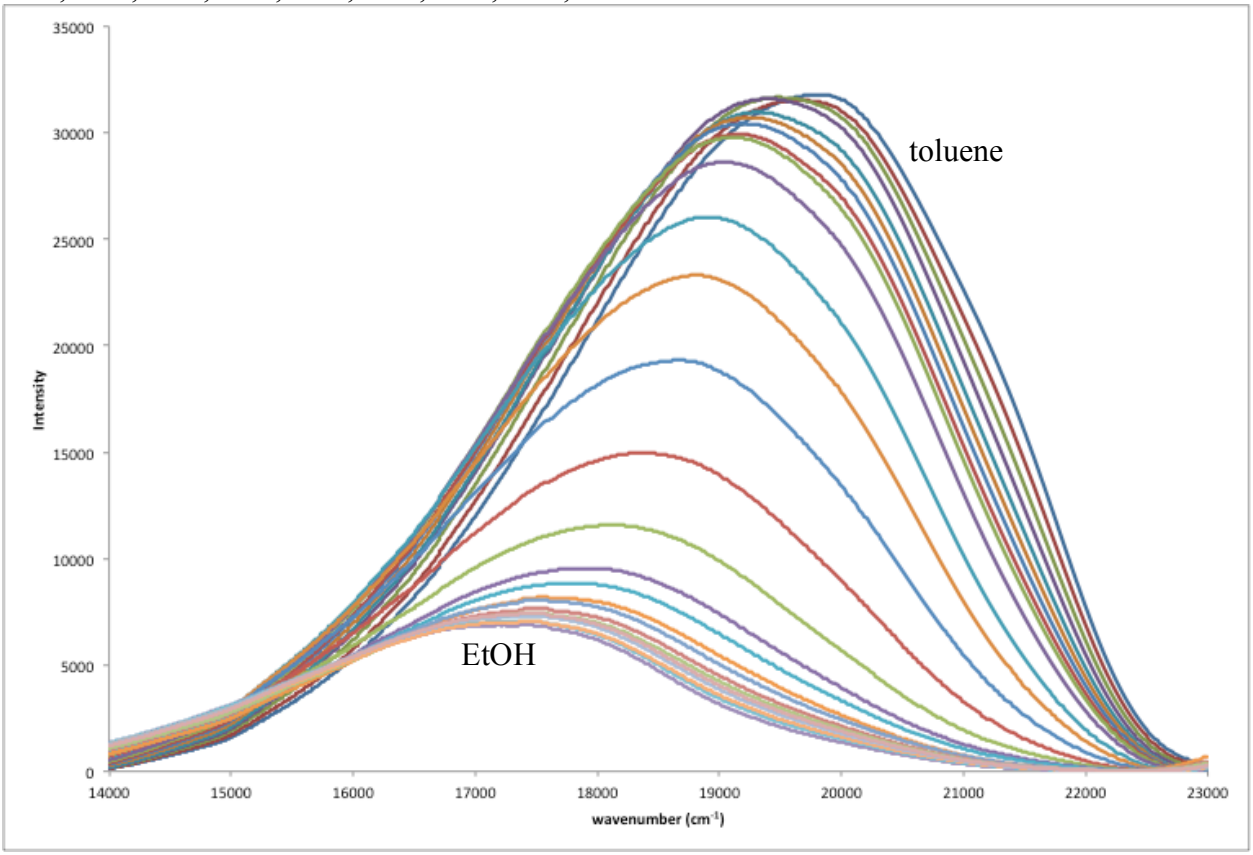

Figure A10. Absorbance spectra of 2.2μM solutions of **3** in toluene/ethanol mixtures. Data collected by Chris Abelt.
[EtOH] (mole %): 0, 5.2, 10.2, 20.1, 40.6, 59.3, 80.2, 90.1, 94.8, 100.

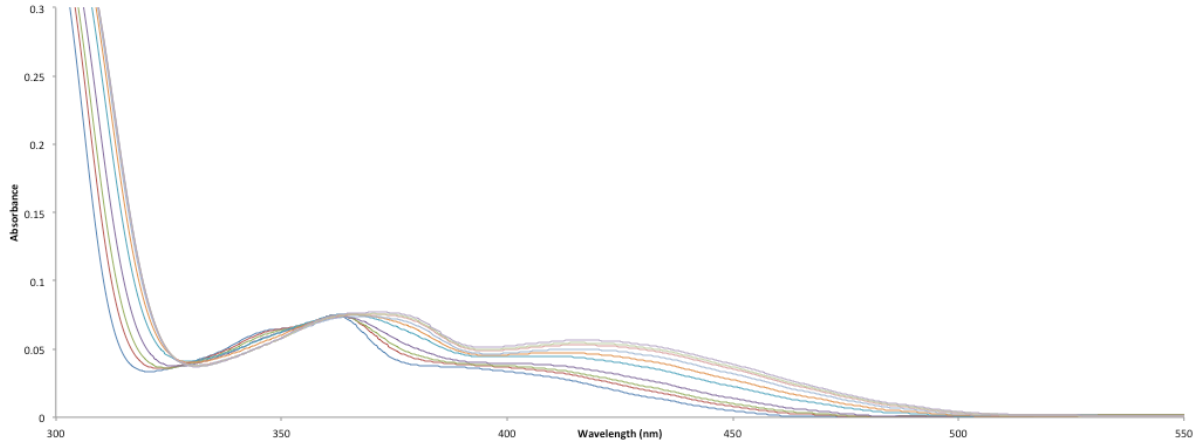

Figure A11. Fluorescence spectra of 2.2μM solutions of **3** in toluene/isopropanol mixtures. Data collected by Chris Abelt.
[*i*PrOH] (mole %): 0, 0.1, 0.1, 0.2, 0.3, 0.3, 0.4, 0.5, 0.6, 0.7, 1.0, 1.4, 2.0, 3.4, 6.5, 12.2, 17.3, 25.8, 35.8, 45.5, 52.7, 63.5, 69.9, 77.7, 87.4, 100.

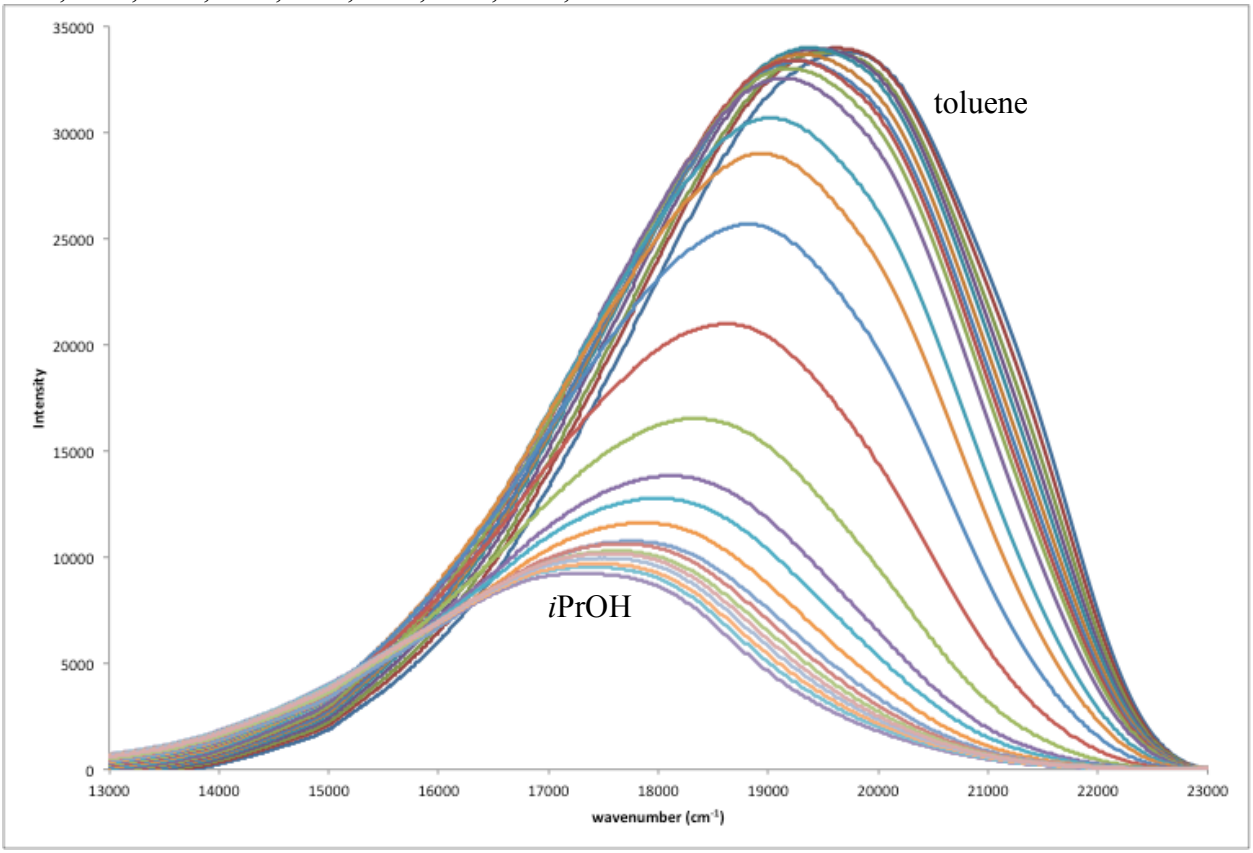

Figure A12. Absorbance spectra of 2.2μM solutions of **3** in toluene/isopropanol mixtures. Data collected by Chris Abelt.
[*i*PrOH] (mole %): 0, 5.0, 10.0, 20.0, 40.1, 52.7, 63.5, 79.9, 90.3, 100.

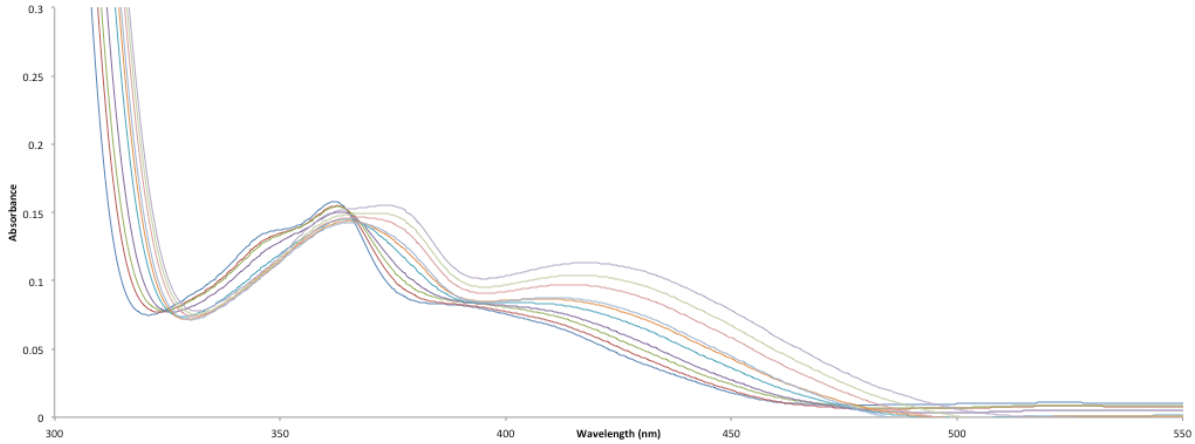

Figure A13. Stern-Volmer plot for **1** in toluene/ethanol mixtures.

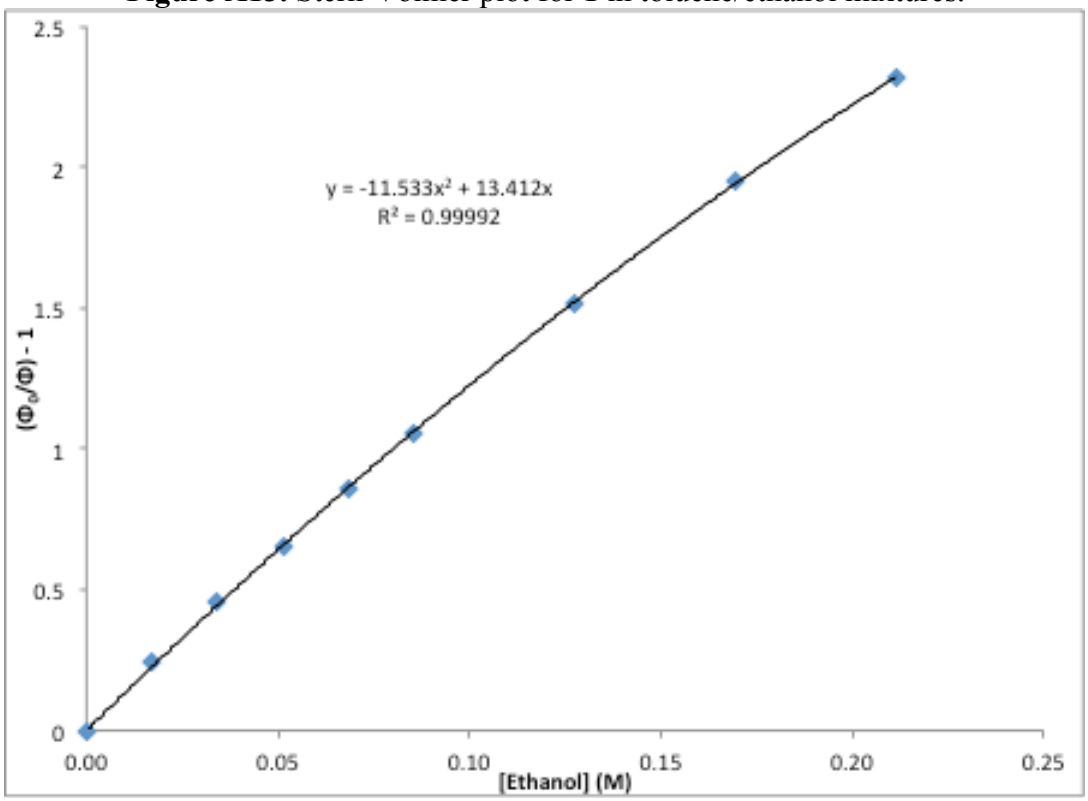

Figure A14. Preferential solvation plot for **1** in toluene/ethanol mixtures.

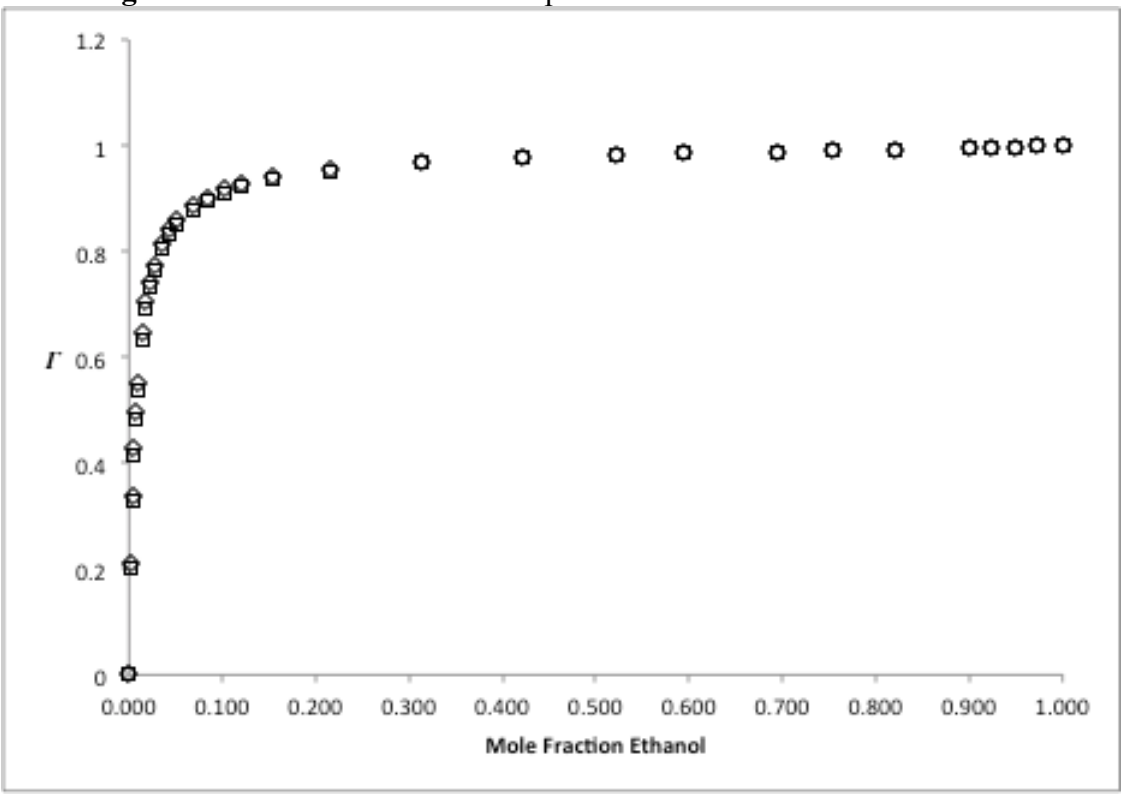

Figure A15. Stern-Volmer plot for **1** in toluene/*i*PrOH mixtures.

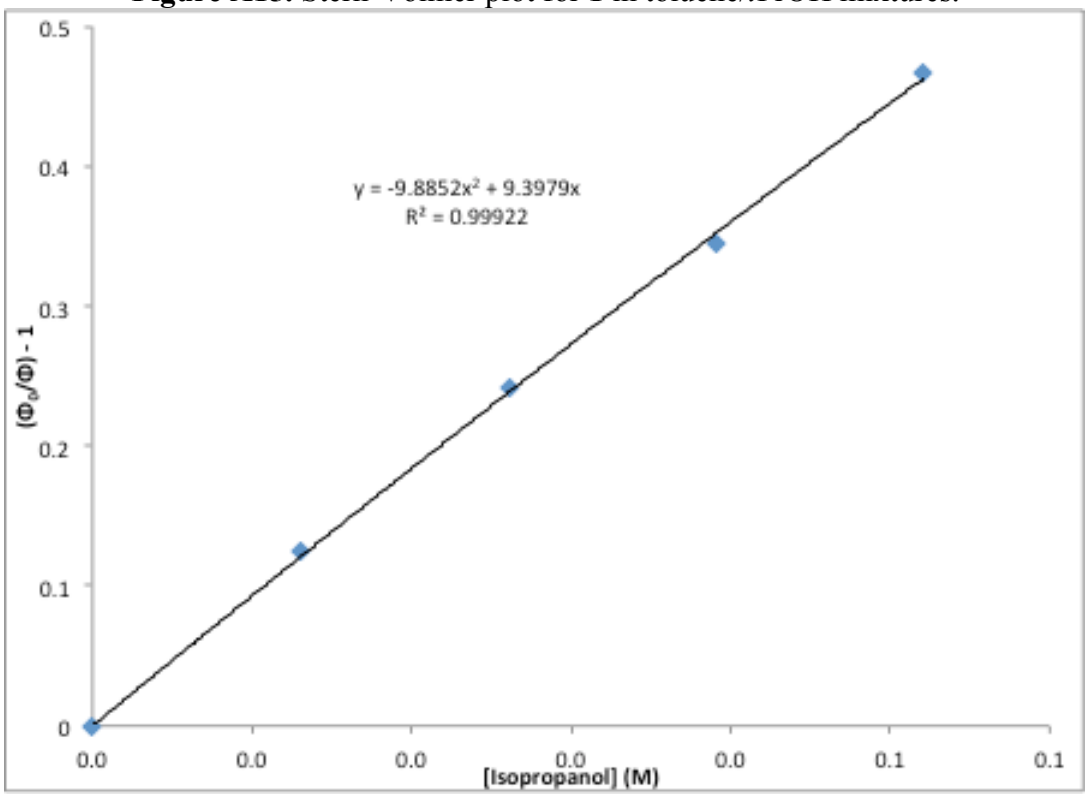

Figure A16. Preferential solvation plot for **1** in toluene/*i*PrOH mixtures.

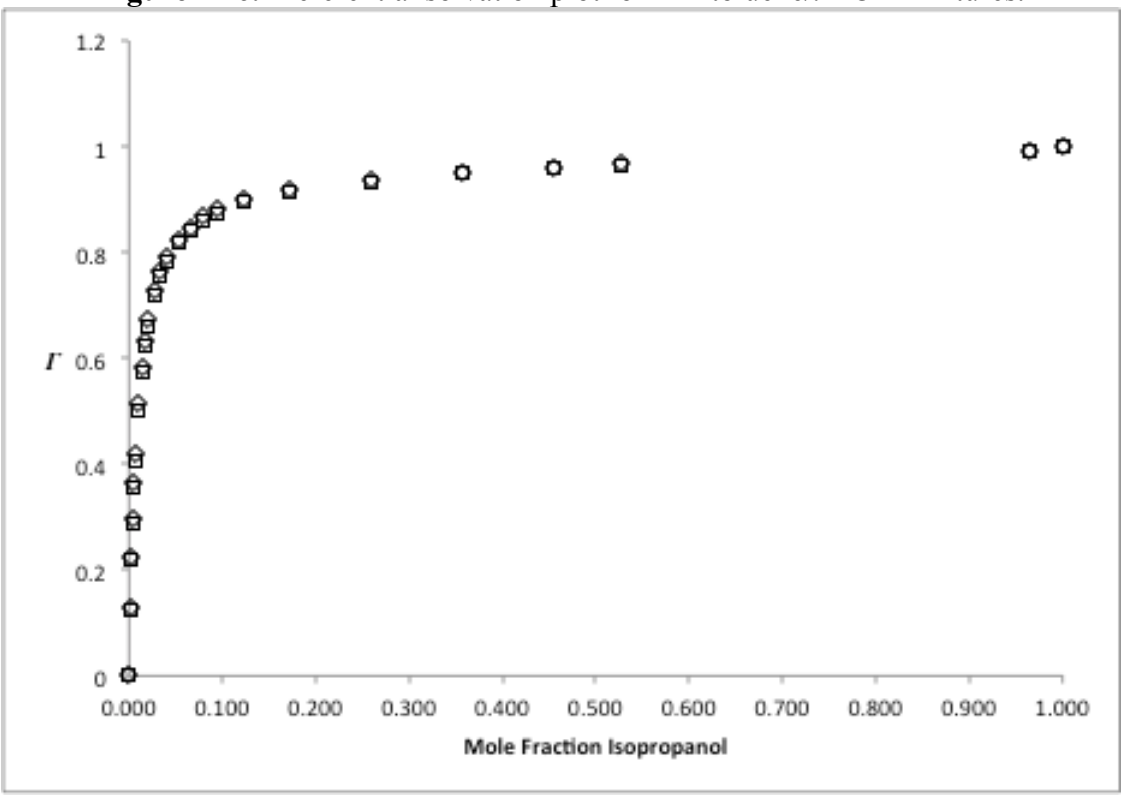

Figure A17. Stern-Volmer plot for **2** in toluene/EtOH mixtures.

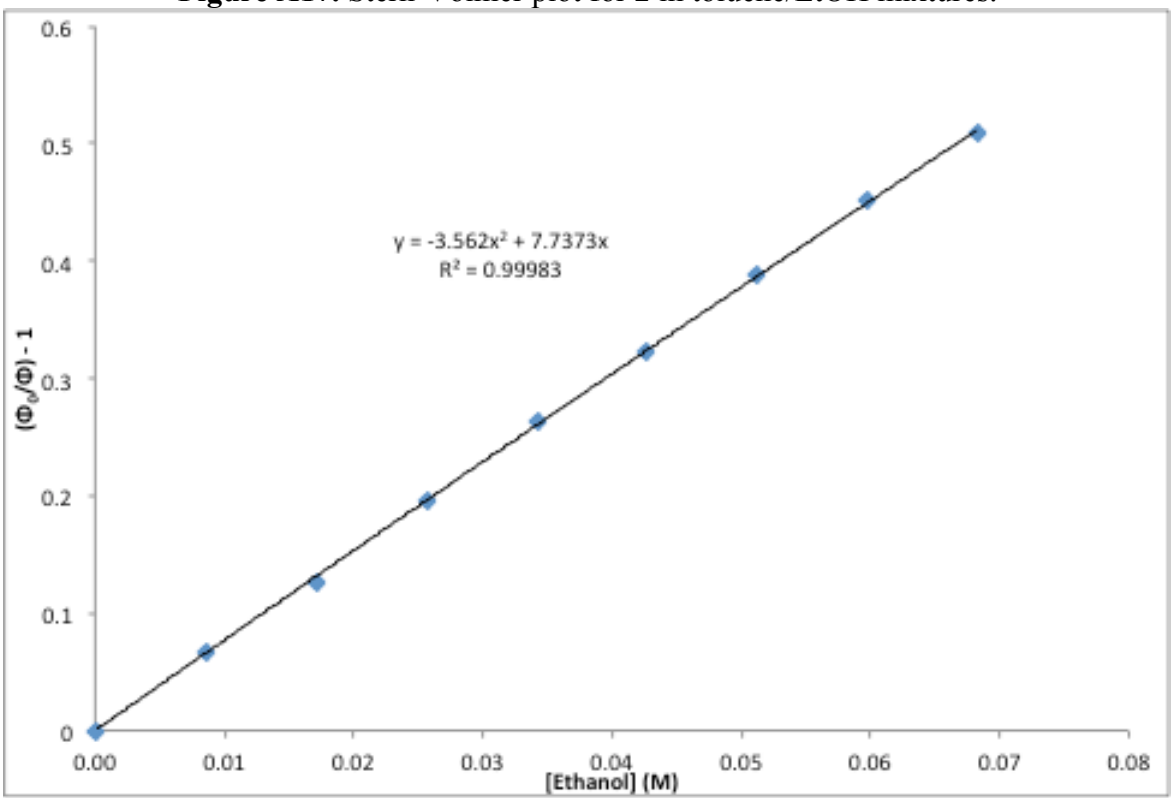

Figure A18. Preferential solvation plot for **2** in toluene/EtOH mixtures.

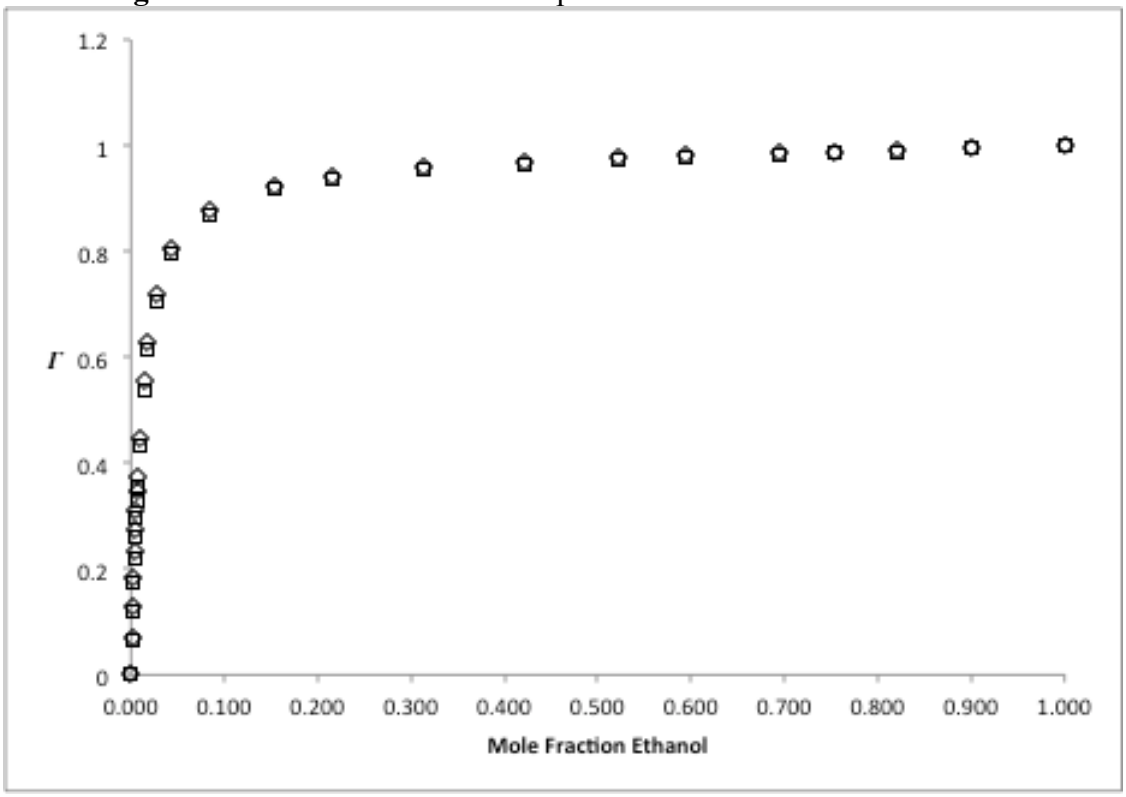

Figure A19. Stern-Volmer plot for **2** in toluene/*i*PrOH mixtures.

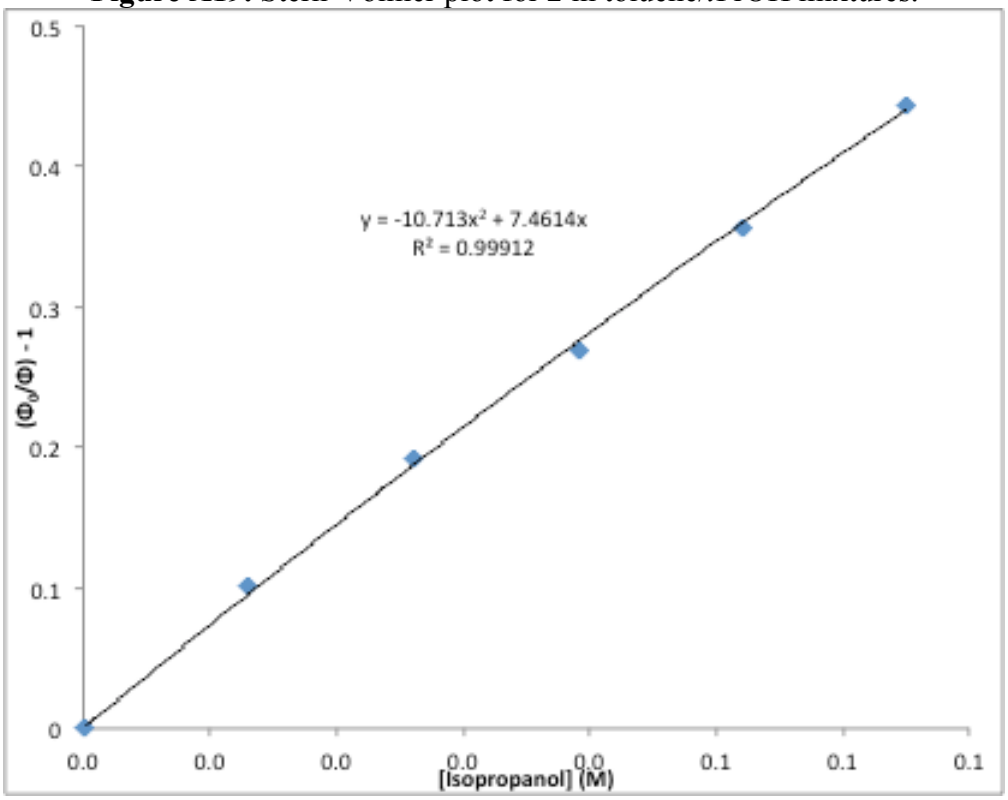

Figure A20. Preferential solvation plot for **2** in toluene/*i*PrOH mixtures.

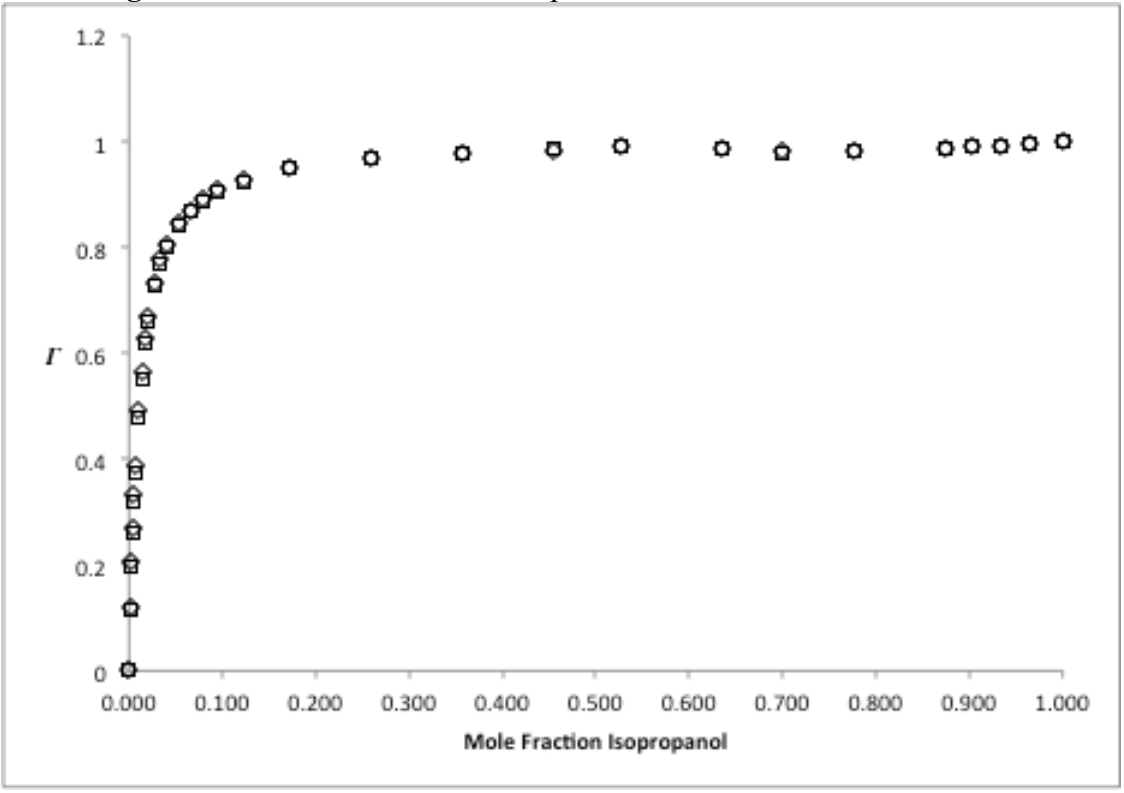

Figure A21. Stern-Volmer plot for **3** in toluene/EtOH mixtures.

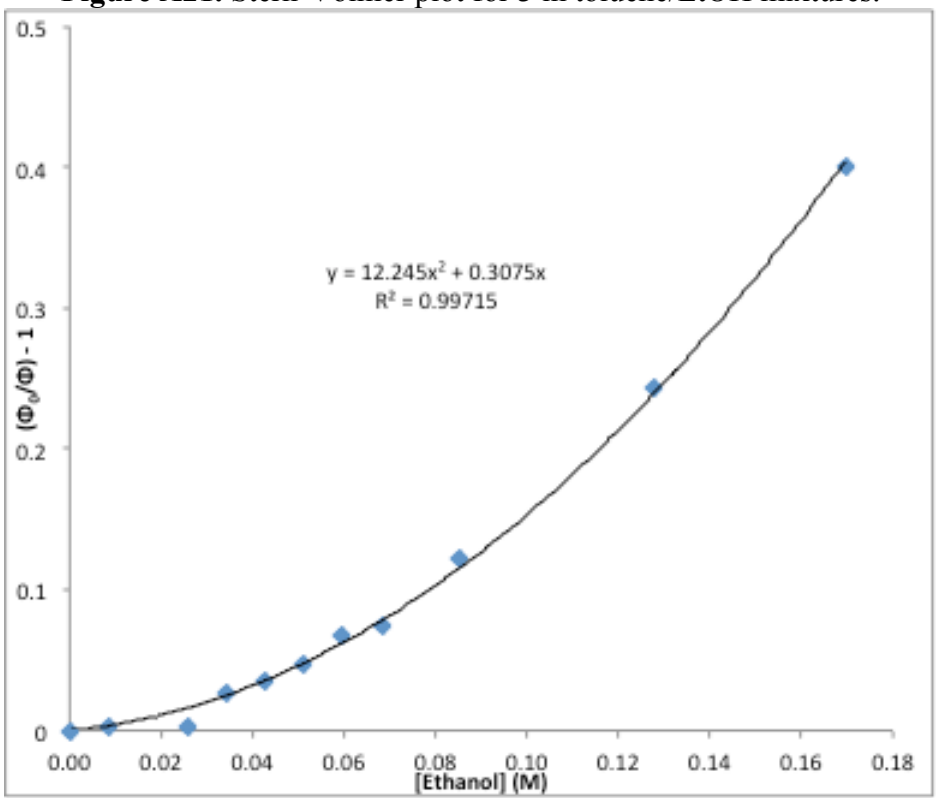

Figure A22. Preferential solvation plot for **3** in toluene/EtOH mixtures.

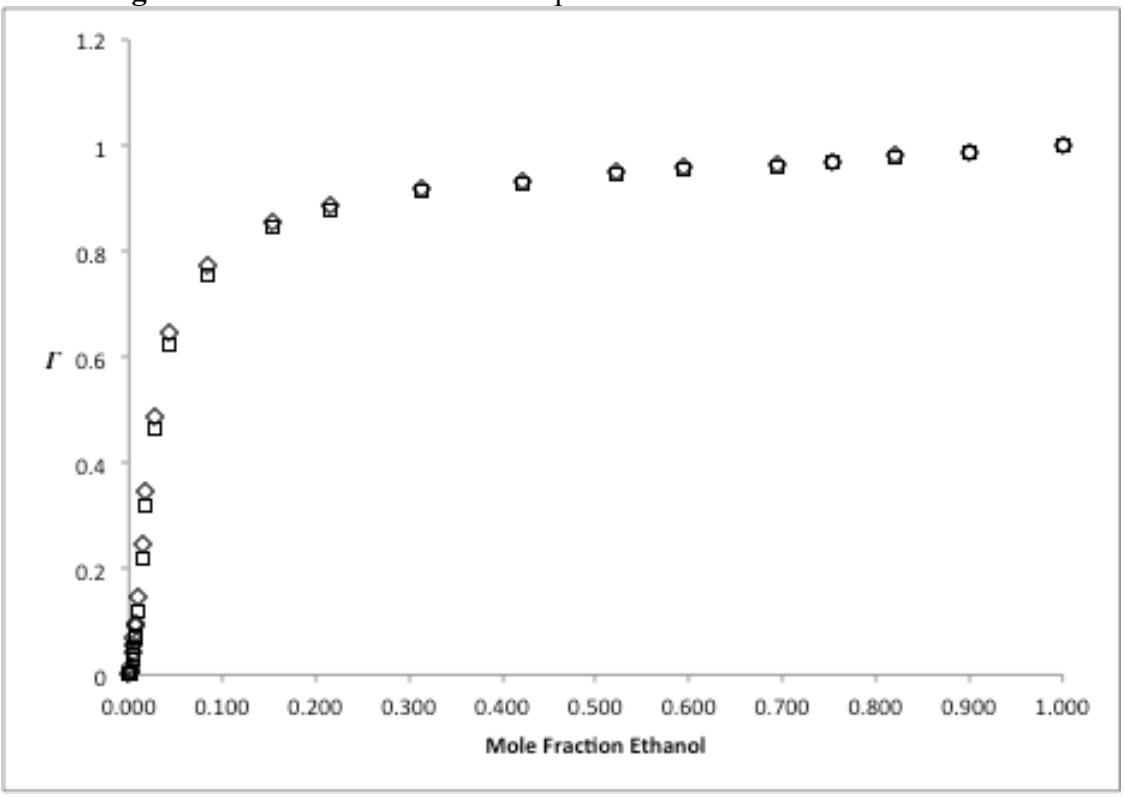

Figure A23. Stern-Volmer plot for **3** in toluene/*i*PrOH mixtures.

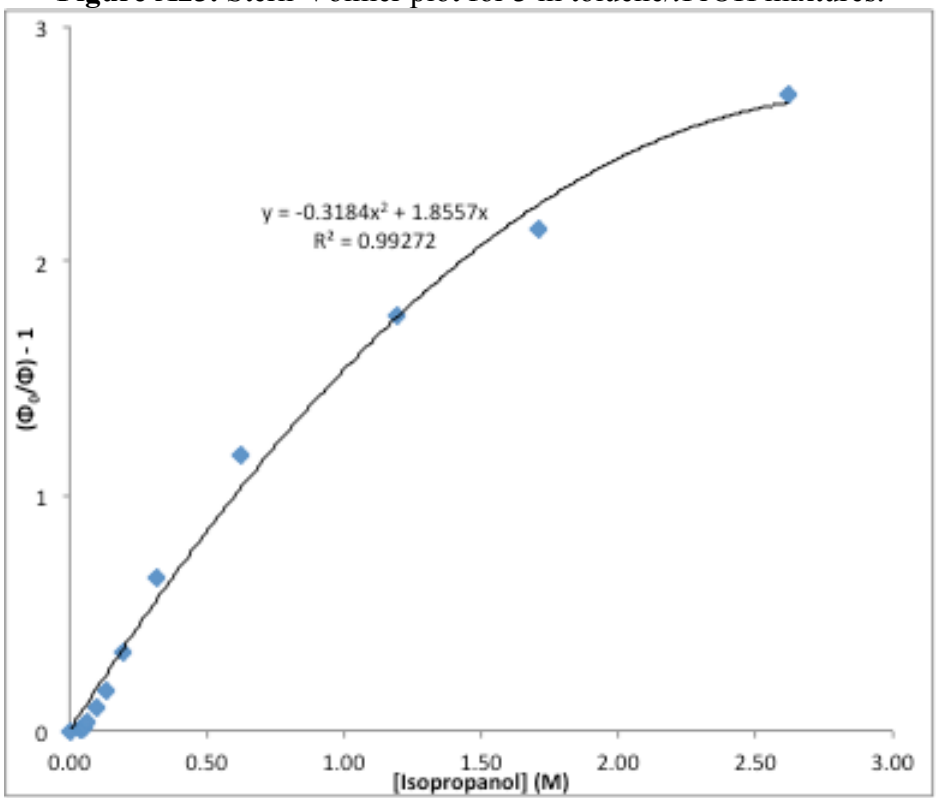

Figure A24. Preferential solvation plot for **3** in toluene/*i*PrOH mixtures.

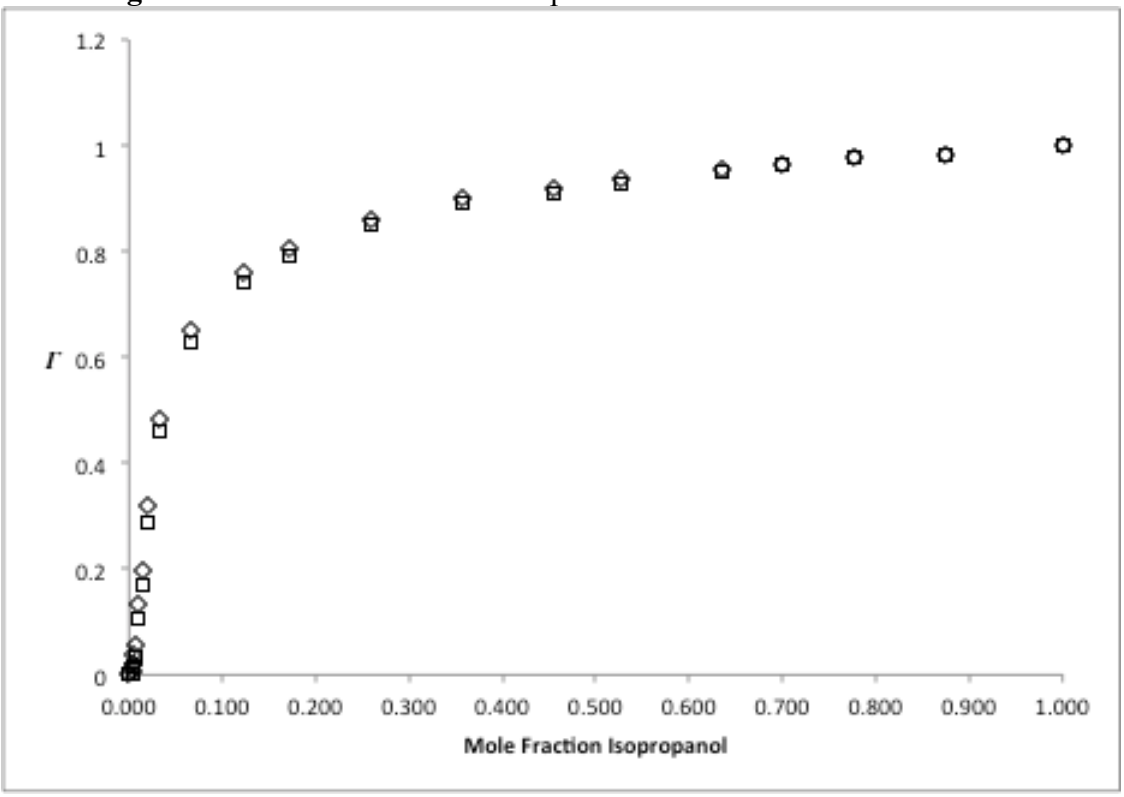

Table A1. Example of spreadsheet used to calculate mole fractions of each solvent in binary solvent mixtures for absorbance data collection, showing volumes of aliquots added for each individual trial.

solvent1=	Toluene
solvent2=	ethanol

	Density (g/m3)	MW (g/mol)
Toluene	0.87	92.14
ethanol	0.79	46.07

Sample	volume #1	volume#2	moles #1	moles #2	fract#2	fract#1
1	2000.00	0.00	0.0188	0.0000	0.000	1.00
2	2000.00	60.00	0.0188	0.0010	0.052	0.95
3	2000.00	125.00	0.0188	0.0021	0.102	0.90
4	2000.00	275.00	0.0188	0.0047	0.201	0.80
5	2000.00	750.00	0.0188	0.0128	0.406	0.59
6	2000.00	1600.00	0.0188	0.0274	0.593	0.41
7	0.00	2000.00	0.0000	0.0343	1.000	0.00
8	200.00	2000.00	0.0019	0.0343	0.948	0.05
9	400.00	2000.00	0.0038	0.0343	0.901	0.10
10	900.00	2000.00	0.0084	0.0343	0.802	0.20

Table A2. Example of spreadsheet used to calculate mole fractions of each solvent in binary solvent mixtures for fluorescence data collection, showing volumes of aliquots added for each individual trial.

solvent1= Toluene
solvent2= ethanol

	Density (g/m3)	MW (g/mol)
Toluene	0.87	92.14
ethanol	0.79	46.07

Sample	volume #1	volume#2	moles #1	moles #2	fract#2	fract#1
1	2000.00	0.00	0.0188	0.0000	0.000	1.00
2	2000.00	2.00	0.0188	0.0000	0.002	1.00
3	2000.00	4.00	0.0188	0.0001	0.004	1.00
4	2000.00	6.00	0.0188	0.0001	0.005	0.99
5	2000.00	8.00	0.0188	0.0001	0.007	0.99
6	2000.00	10.00	0.0188	0.0002	0.009	0.99
7	2000.00	15.00	0.0188	0.0003	0.013	0.99
8	2000.00	20.00	0.0188	0.0003	0.018	0.98
9	2000.00	25.00	0.0188	0.0004	0.022	0.98
10	2000.00	30.00	0.0188	0.0005	0.027	0.97
11	2000.00	40.00	0.0188	0.0007	0.035	0.96
12	2000.00	50.00	0.0188	0.0009	0.044	0.96
13	2000.00	60.00	0.0188	0.0010	0.052	0.95
14	2000.00	80.00	0.0188	0.0014	0.068	0.93
15	2000.00	100.00	0.0188	0.0017	0.084	0.92
16	2000.00	125.00	0.0188	0.0021	0.102	0.90
17	2000.00	150.00	0.0188	0.0026	0.120	0.88
18	2000.00	200.00	0.0188	0.0034	0.154	0.85
19	2000.00	300.00	0.0188	0.0051	0.215	0.79
20	2000.00	500.00	0.0188	0.0086	0.313	0.69
21	2000.00	800.00	0.0188	0.0137	0.422	0.58
22	2000.00	1200.00	0.0188	0.0206	0.523	0.48
23	2000.00	1600.00	0.0188	0.0274	0.593	0.41
24	0.00	2000.00	0.0000	0.0343	1.000	0.00
25	100.00	2000.00	0.0009	0.0343	0.973	0.03
26	200.00	2000.00	0.0019	0.0343	0.948	0.05
27	300.00	2000.00	0.0028	0.0343	0.924	0.08
28	400.00	2000.00	0.0038	0.0343	0.901	0.10
29	800.00	2000.00	0.0075	0.0343	0.820	0.18
30	1200.00	2000.00	0.0113	0.0343	0.753	0.25
31	1600.00	2000.00	0.0150	0.0343	0.695	0.30

Appendix B: Experimental

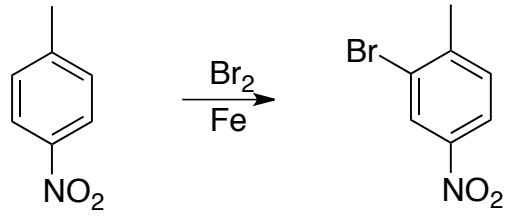

4-nitrotoluene 2-bromo-4-nitrotoluene

1a. 2-BROMO-4-NITROTOLUENE

To a 100mL two-neck round-bottomed flask fitted with a water-jacketed condenser and a 25mL addition funnel were added 0.20g Fe powder and 13.7g 4-nitrotoluene. The suspension was heated with stirring to 80˚C in a resistively heated silicon oil bath, then 6.1mL bromine was slowly added from the addition funnel over the course of 10 min. The flask was allowed to stir for 1.5 h at 80˚C, after which the reaction mixture was poured into 150mL 10%NaOH (w/w) and the solids were collected by vacuum filtration. These solids were dissolved in 150mL CH_2Cl_2 and transferred to a separatory funnel. The organic solution was washed with two 50mL portions of 10% HCl (v/v), then with a 50mL portion of 5%NaOH (w/w). The organic layer was collected, dried over $MgSO_4$, filtered into a round-bottomed flask, and the solvent was removed *in vacuo*. The crude cream-colored product was then recrystallized from hot EtOH to yield pale yellow crystals of 2-bromo-4-nitrotoluene (14.23g; 65.63%).

^{1}H NMR (400MHz, $CDCl_3$): δ = 8.43 (s, 1 H), 8.09 (d, 2 H), 7.41 (d, 2 H), 2.72 (s, 3 H).

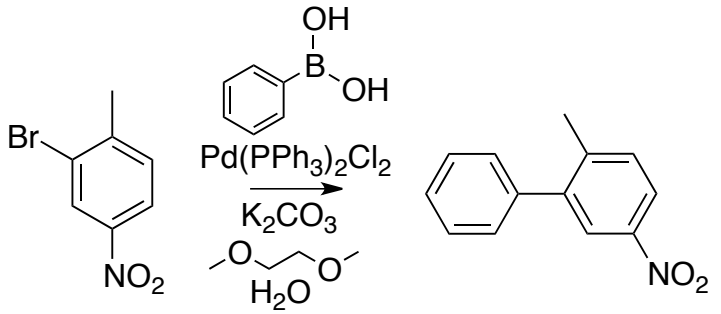

2-bromo-4-nitrotoluene 4-nitro-2-phenyltoluene

1b. 4-NITRO-2-PHENYLTOLUENE

To a 250mL round-bottomed flask were added 20mL dI H_2O and 25mL ethylene glycol dimethyl ether under nitrogen atmosphere. The flask was stirred and de-gassed for 5 min, after which were added 10.40g K_2CO_3, 3.15g phenylboronic acid, 0.83g $Pd(PPh_3)_2Cl_2$, and 5.08g 2-bromo-4-nitrotoluene. A water-jacketed condenser was affixed to the flask and the reaction mixture was heated to reflux with stirring for 18 h on a resistively heated silicon oil bath (T=120˚C). Following this, 100mL dI H_2O was added to the reaction mixture, which was then poured into a separatory funnel and extracted with three 50mL portions of ethyl acetate. The combined organic extracts were dried over Na_2CO_3, filtered, and the solvent was removed *in vacuo*. The product oil was triturated with dI H_2O and the resulting crystals were recrystallized from hot MeOH (30mL), collected by vacuum filtration, and washed with dI H_2O to yield gray-brown crystals of 4-nitro-2-phenyltoluene (4.53g; 90.44%).

^{1}H NMR (400MHz, $CDCl_3$): δ = 8.13 (s, 1 H), 8.11 (d, 1 H), 7.38–7.51 (m, 4 H), 7.32 (d, 2 H), 2.37 (s, 3 H).

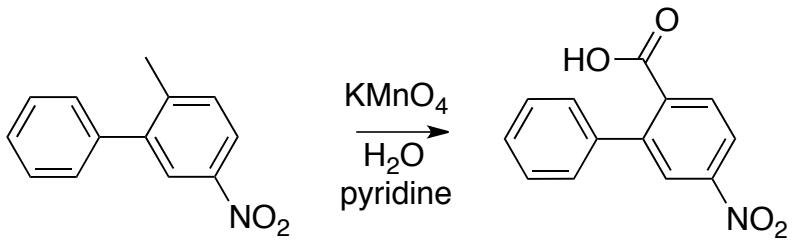

4-nitro-2-phenyltoluene 4-nitro-2-phenylbenzoic acid

1c. 4-NITRO-2-PHENYLBENZOIC ACID

To a 250mL round-bottomed flask were added 33mL pyridine and 66mL dI H_2O. 7.05g 4-nitro-2-phenyloluene was added with stirring and the mixture was heated to 80˚C. 31.35g $KMnO_4$ was then added in portions, following which the temperature was raised to 135˚C for 2 h. The reaction mixture was then filtered and acidified with 100mL 6M HCl. The resulting precipitate was collected by vacuum filtration. This crude product was then dissolved in 200mL CH_2Cl_2 and washed with two 100mL portions of 10%NaOH. The combined aqueous layers were then acidified with conc. HCl to cloudiness. The suspension was then cooled and the precipitate was collected by vacuum filtration and washed with ice-cold dI H_2O to yield yellow-white crystals of 4-nitro-2-phenylbenzoic acid (4.26g; 52.97%).

^{1}H NMR (400MHz, $CDCl_3$): δ = 8.28 (d, 1 H), 8.27 (s, 1 H), 8.07 (d, 1 H), 7.40-7.45 (m, 3 H), 7.35 (d, 2 H).

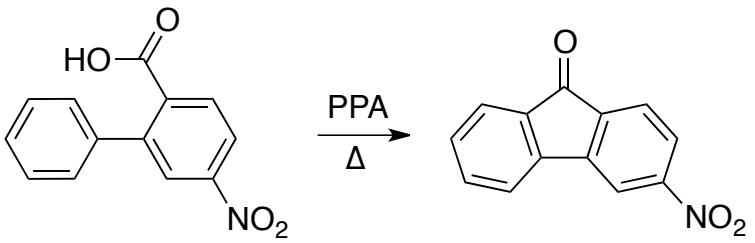

4-nitro-2-phenylbenzoic acid 3-nitrofluoren-9-one

1d. 3-NITROFLUOREN-9-ONE

To a round-bottomed flask were added 4.26g 4-nitro-2-phenylbenzoic acid and 64.33g polyphosphoric acid under nitrogen atmosphere. The flask was heated to 160˚C with stirring for 5 h. The flask was then allowed to cool to below 100˚C, after which 200mL dI H_2O was added. The flask was allowed to stir for 30 min without heating and then cooled in an ice bath. The solid product was then collected by vacuum filtration to yield yellow crystals of 3-nitrofluoren-9-one (3.79g; 96.08%).

^{1}H NMR (400MHz, $CDCl_3$): δ = 8.35 (d, 1 H), 8.20 (d, 1 H), 7.82 (d, 1 H), 7.75 (d, 1 H), 7.67 (d, 1 H), 7.62 (t, 1 H), 7.43 (t, 1 H)

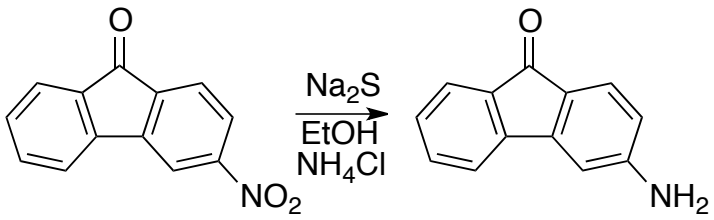

3-nitrofluoren-9-one 3-aminofluoren-9-one

1. 3-AMINOFLUOREN-9-ONE

To a round-bottomed flask were added 1.00g 3-nitro-9-fluorenone, 100mL EtOH, and 2.00g NH_4Cl with stirring. The flask was then heated to 120˚C and 5.00g Na_2S were added in portions over a 2 h period. After addition of Na_2S was complete, the flask was allowed to reflux for an additional hour. The flask was then removed from heat and 100mL dI H_2O was added. The solution was extracted with three 75mL portions of Et_2O and the combined organic layers were extracted with two 150mL portions of 10% HCl, neutralized with NaOH solution, and allowed to crystallize. The solids were collected by vacuum filtration to yield yellow crystals of 3-aminofluoren-9-one (**1**) (0.47g; 54.23%).

^{1}H NMR (400MHz, $CDCl_3$): δ = 7.61 (d, 1 H), 7.51 (d, 1 H), 7.42 (t, 1 H), 7.41 (d, 1 H), 7.29 (t, 1 H), 6.77 (s, 1 H), 6.45 (d, 1 H), 4.28 (s, 2 H, NH_2)

^{13}C NMR (100MHz, $CDCl_3$): δ = 192.260, 152.861, 147.367, 143.209, 135.947, 133.594, 129.102, 126.750, 124.632, 123.547, 119.768, 113.341, 106.284

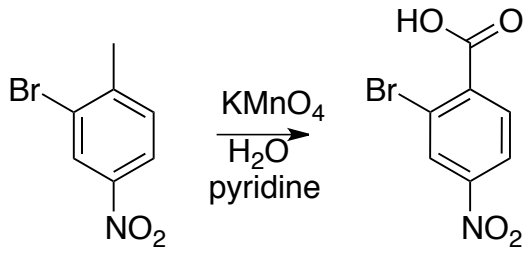

2-bromo-4-nitrotoluene 2-bromo-4-nitrobenzoic acid

2b. 2-BROMO-4-NITROBENZOIC ACID

To a round-bottomed flask were added 5.00g 2-bromo-4-nitrotoluene, 23mL pyridine, and 46mL dI H_2O with stirring. The mixture was then heated to 60˚C and 18.29g $KMnO_4$ was added in portions with stirring. After $KMnO_4$ addition was complete, the flask was fitted with a water-jacketed condenser and the temperature was increased to 115˚C. The reaction mixture was allowed to reflux overnight, after which the contents of the flask were filtered into a separatory funnel and acidified with 5mL conc. HCl. The mixture was extracted with three 50mL portions of EtOAc, dried with Na_2SO_4, filtered, and the solvent was removed *in vacuo* to yield orange-brown crystals of 2-bromo-4-nitrobenzoic acid (3.04g; 53.38%).

^{1}H NMR (400MHz, $CDCl_3$): δ = 8.50 (s, 1 H), 8.20 (d, 1 H), 7.97 (d, 1 H)

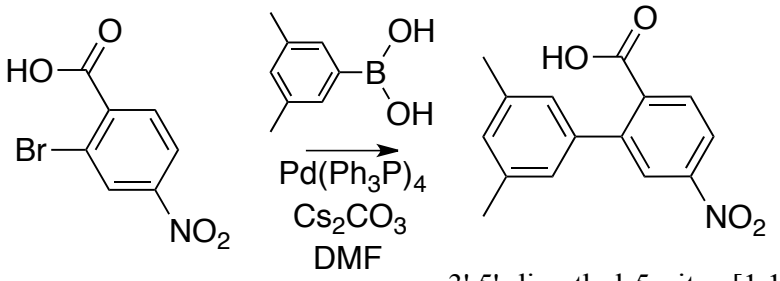

2-bromo-4-nitrobenzoic acid

3',5'-dimethyl-5-nitro-[1,1'-biphenyl]-2-carboxylic acid

2c. 3',5'-DIMETHYL-5-NITRO-[1,1'-BIPHENYL]-2-CARBOXYLIC ACID

To a 50mL round-bottomed flask were added 0.50g 2-bromo-4-nitrobenzoic acid, 0.34g 3,5-dimethylphenylboronic acid, and 25mL *N*,*N*-dimethylformamide, followed by 1.66g Cs_2CO_3 and 0.12g $Pd(PPh_3)_4$. The reaction mixture was heated to 100˚C and allowed to stir overnight, after which the mixture was poured into 50mL 10% HCl in a 250mL separatory funnel. This solution was extracted with three 50mL portions of Et_2O. The combined organic extracts were dried over $MgSO_4$, filtered, and the solvent was removed *in vacuo* to yield a brown oil. This oil was purified by silica gel column chromatography (10%EtOAc in hexanes) to yield yellow crystals of 3',5'-dimethyl-5-nitro-[1,1'-biphenyl]-2-carboxylic acid (0.17g, 30.9%).

^{1}H NMR (400MHz, $CDCl_3$): δ = 8.25 (s, 1 H), 8.24 (d, 1 H), 8.02 (d, 1 H), 7.07 (s, 1 H), 6.98 (s, 2 H), 2.37 (s, 6 H)

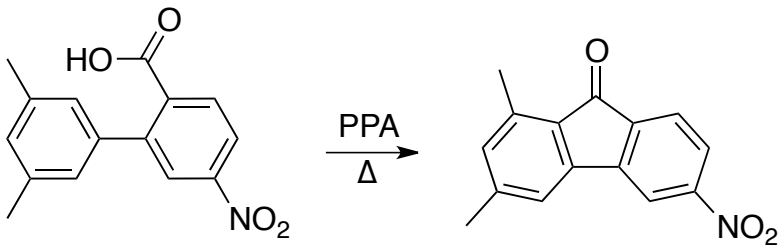

3',5'-dimethyl-5-nitro-[1,1'-biphenyl]-2-carboxylic acid

1,3-dimethyl-6-nitrofluoren-9-one

2d. 1,3-DIMETHYL-6-NITROFLUOREN-9-ONE

To a 50mL round-bottomed flask were added 1.45g 3',5'-dimethyl-5-nitro-[1,1'-biphenyl]-2-carboxylic acid and 19.6g polyphosphoric acid under nitrogen atmosphere. The flask was heated to 160˚C with stirring for 5 h. The flask was then allowed to cool to below 100˚C, after which 70mL dI H_2O was added. The flask was allowed to stir for 30 min without heating and then cooled in an ice bath. The solid product was then collected by vacuum filtration to yield dark yellow sludge, which sublimed at 175˚C to yield yellow crystals of 1,3-dimethyl-6-nitrofluoren-9-one (0.55g; 40.6%).

^{1}H NMR (400MHz, $CDCl_3$): δ = 8.25 (s, 1 H), 8.18 (d, 1 H), 7.68 (d, 1 H), 7.31 (s, 1 H), 6.99 (s, 1 H), 2.60 (s, 3 H), 2.41 (s, 3 H).

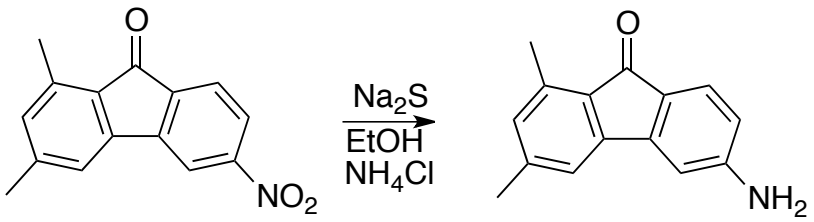

1,3-dimethyl-6-nitrofluoren-9-one 3-amino-6,8-dimethylfluoren-9-one

2. 3-AMINO-6,8-DIMETHYLFLUOREN-9-ONE

To a 50mL round-bottomed flask were added 0.55g sublimed 1,3-dimethyl-6-nitrofluoren-9-one, 1.10g NH_4Cl, and 55mL EtOH with stirring. The flask was then heated to 120˚C and 2.75g Na_2S was added in portions over a 2 h period. After addition of Na_2S was complete, the flask was allowed to reflux for an additional hour. The flask was then removed from heat and 50mL dI H_2O was added. The solution was extracted with three 50mL portions of Et_2O and the combined organic layers were extracted with three 50mL portions of 10% HCl, neutralized with 25% NaOH solution, and allowed to crystallize in an ice bath. The solids were collected by vacuum filtration and sublimed at 200˚C to yield bright yellow crystals of 3-aminofluoren-9-one (**2**) (0.09g; 20%).

^{1}H NMR (400MHz, $CDCl_3$ / 5% DMSO): δ = 7.44 (d, 1 H), 7.09 (s, 1 H), 6.83 (s, 1 H), 6.75 (s, 1 H), 6.43 (d, 1 H), 4.18 (s, 2 H, NH_2), 2.57 (s, 3 H), 2.36 (s, 3 H).

^{13}C NMR (100MHz, $CDCl_3$ / 5% DMSO): δ = 209.340, 152.381, 146.515, 143.670, 138.396, 132.317, 125.958, 125.843, 118.430, 117.285, 113.232, 105.894, 104.915, 21.799, 17.466

MS: HRMS (ESI): calcd. for $C_{15}H_{13}NONa^+$ $[M+Na]^+$ 246.08894; found 246.08905

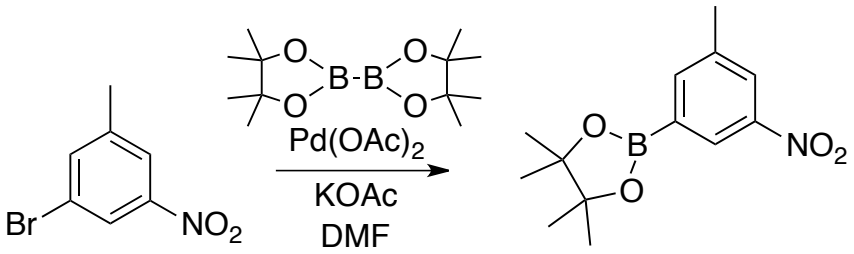

3-bromo-5-nitrotoluene

4,4,5,5-tetramethyl-2-(3-methyl-5-nitrophenyl)-1,3,2-dioxaborolane

3a. 4,4,5,5-TETRAMETHYL-2-(3-METHYL-5-NITROPHENYL)-1,3,2-DIOXABOROLANE

To a 50mL round-bottomed flask were added 1.17g 3-bromo-5-nitrotoluene, 1.38g bis-(pinacolato)diboron, 1.59g KOAc, and 25mL DMF with stirring. The flask was then degassed under vacuum for 15 min after which 0.061g $Pd(OAc)_2$ was added and the mixture was heated to 90˚C with stirring for 2 h under nitrogen atmosphere. The mixture was allowed to cool, then it was poured into 150mL CH_2Cl_2 and washed 6x with 100mL H_2O. The combined organic extracts were dried over $MgSO_4$, filtered, and the solvent was removed *in vacuo* to yield a dark brown oil. This oil was purified by silica gel column chromatography (12%EtOAc in hexanes) to yield pale yellow powdery crystals of 4,4,5,5-tetramethyl-2-(3-methyl-5-nitrophenyl)-1,3,2-dioxaborolane (0.62g, 43.5%).

^{1}H NMR (400MHz, $CDCl_3$): δ = 8.43 (s, 1 H), 8.11 (s, 1 H), 7.92 (s, 1 H), 2.46 (s, 3 H), 1.35 (s, 12 H).

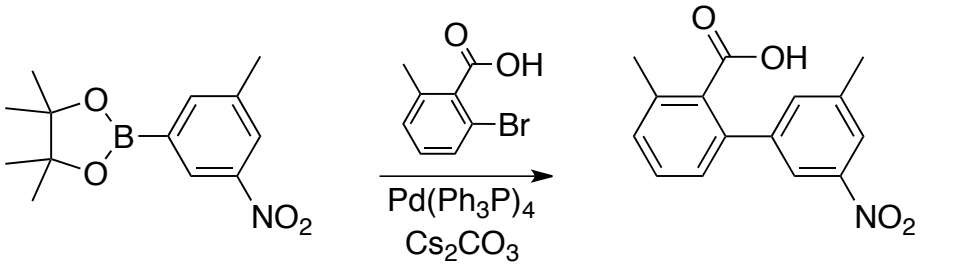

4,4,5,5-tetramethyl-2-(3-methyl-5-nitrophenyl)-1,3,2-dioxaborolane

3,3'-dimethyl-5'-nitro-[1,1'-biphenyl]-2-carboxylic acid

3b. 3,3'-DIMETHYL-5'-NITRO-[1,1'-BIPHENYL]-2-CARBOXYLIC ACID

To a 50mL round-bottomed flask were added 0.46g commercially available 2-bromo-6-methylbenzoic acid, 0.60g 4,4,5,5-tetramethyl-2-(3-methyl-5-nitrophenyl)-1,3,2-dioxaborolane, and 25mL DMF. The flask was then degassed under vacuum for 15 min after which were added 1.66g $CsCO_3$ and 0.12g $Pd(PPh_3)_4$ and the mixture was heated to 100˚C with stirring for 24 h under nitrogen atmosphere. The reaction was then poured into 50mL 10% HCl and extracted 3x with 50mL Et_2O. The combined organic extracts were dried with $MgSO_4$, filtered, and the solvent was removed *in vacuo* to yield a cloudy light brown oil. This oil was purified by silica gel column chromatography (20% EtOAc in hexanes) to yield orange crystals of 3,3'-dimethyl-5'-nitro-[1,1'-biphenyl]-2-carboxylic acid (0.30g, 51.7%).

^{1}H NMR (400MHz, $CDCl_3$): δ = 8.07 (s, 1 H), 8.01 (s, 1 H), 7.52 (s, 1 H), 7.41 (t, 1 H), 7.29 (d, 1 H), 7.20 (d, 1 H), 2.46 (s, 6 H).

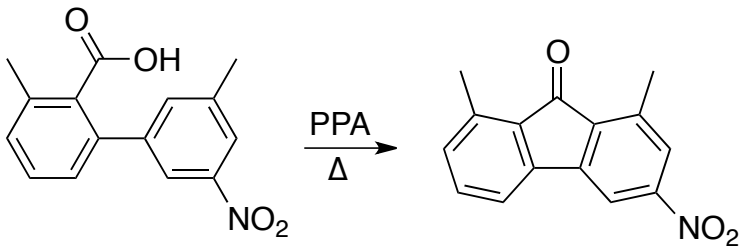

3,3'-dimethyl-5'-nitro-[1,1'-biphenyl]-2-carboxylic acid

1,8-dimethyl-3-nitrofluoren-9-one

3c. 1,8-DIMETHYL-3-NITROFLUOREN-9-ONE

To a 50mL round-bottomed flask were added 0.43g 3,3'-dimethyl-5'-nitro-[1,1'-biphenyl]-2-carboxylic acid and 5.82g polyphosphoric acid under nitrogen atmosphere. The flask was heated to 150˚C with stirring for 5 h. The flask was then allowed to cool to below 100˚C, after which 30mL dI H_2O was added. The flask was allowed to stir for 30 min without heating and then the mixture was poured into150mL dI H_2O and extracted with three 50mL portions of CH_2Cl_2. The combined organic extracts were dried with $MgSO_4$, filtered, and the solvent was removed *in vacuo* to yield yellow crystals of 1,8-dimethyl-3-nitrofluoren-9-one (0.16g; 39.9%).

^{1}H NMR (400MHz, $CDCl_3$): δ = 8.15 (s, 1 H), 7.95 (s, 1 H), 7.47 (d, 1 H), 7.44 (t, 1 H), 7.16 (d, 1 H), 2.76 (s, 3 H), 2.64 (s, 3 H).

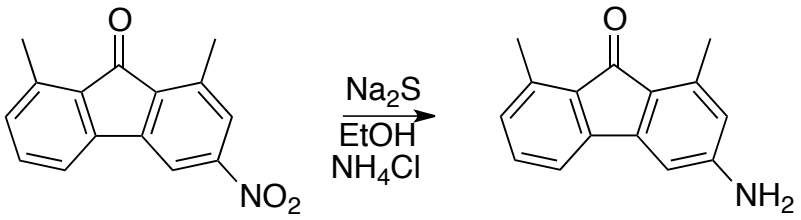

1,8-dimethyl-3-nitrofluoren-9-one 3-amino-1,8-dimethylfluoren-9-one

3. 3-AMINO-1,8-DIMETHYLFLUOREN-9-ONE

To a 50mL round-bottomed flask were added 0.16g 1,8-dimethyl-3-nitrofluoren-9-one, 0.32g NH_4Cl, and 16mL EtOH with stirring. The flask was then heated to 120˚C and 0.80g Na_2S was added in portions over a 2 h period. After addition of Na_2S was complete, the flask was allowed to reflux for an additional hour. The flask was then removed from heat and 15mL dI H_2O was added to the flask. The solution was extracted with three 25mL portions of Et_2O and the combined organic layers were dried with $MgSO_4$, filtered, and concentrated to a final volume of 20mL, after which they were extracted with three 20mL portions of 10% HCl (v/v), neutralized with 25% NaOH (w/v) solution, and extracted with three 50mL portions of CH_2Cl_2. The combined organic extracts were dried with $MgSO_4$, filtered, and the solvent was removed *in vacuo* to yield yellow crystals of 3-amino-1,8-dimethylfluoren-9-one (**3**) (0.03g; 21.3%).

^{1}H NMR (400MHz, $CDCl_3$ / 5% DMSO): δ = 7.27 (t, 1 H), 7.27 (d, 1 H), 7.02 (d, 1 H), 6.63 (s, 1 H), 6.22 (s, 1 H), 4.13 (s, 2 H, NH_2), 2.62 (s, 3 H), 2.54 (s, 3 H).

^{13}C NMR (100MHz, $CDCl_3$ / 5% DMSO): δ = 226.179, 157.093, 152.761, 146.940, 143.047, 141.165, 137.538, 132.439, 132.363, 131.634, 117.034, 114.978, 103.974, 17.974, 17.364

MS: Sent for analysis, results pending.

Appendix C: NMR Spectra

Figure C1. ^{1}H NMR spectrum of **1a**.

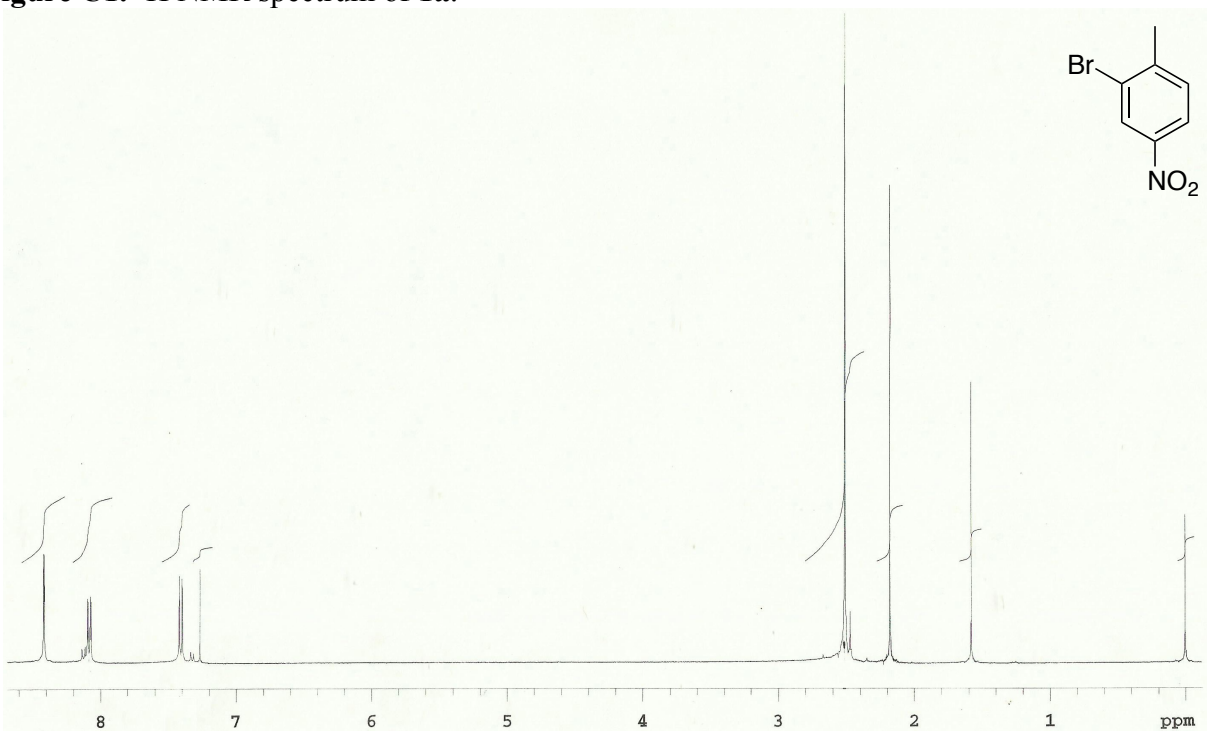

Figure C2. ^{1}H NMR spectrum of **1b**.

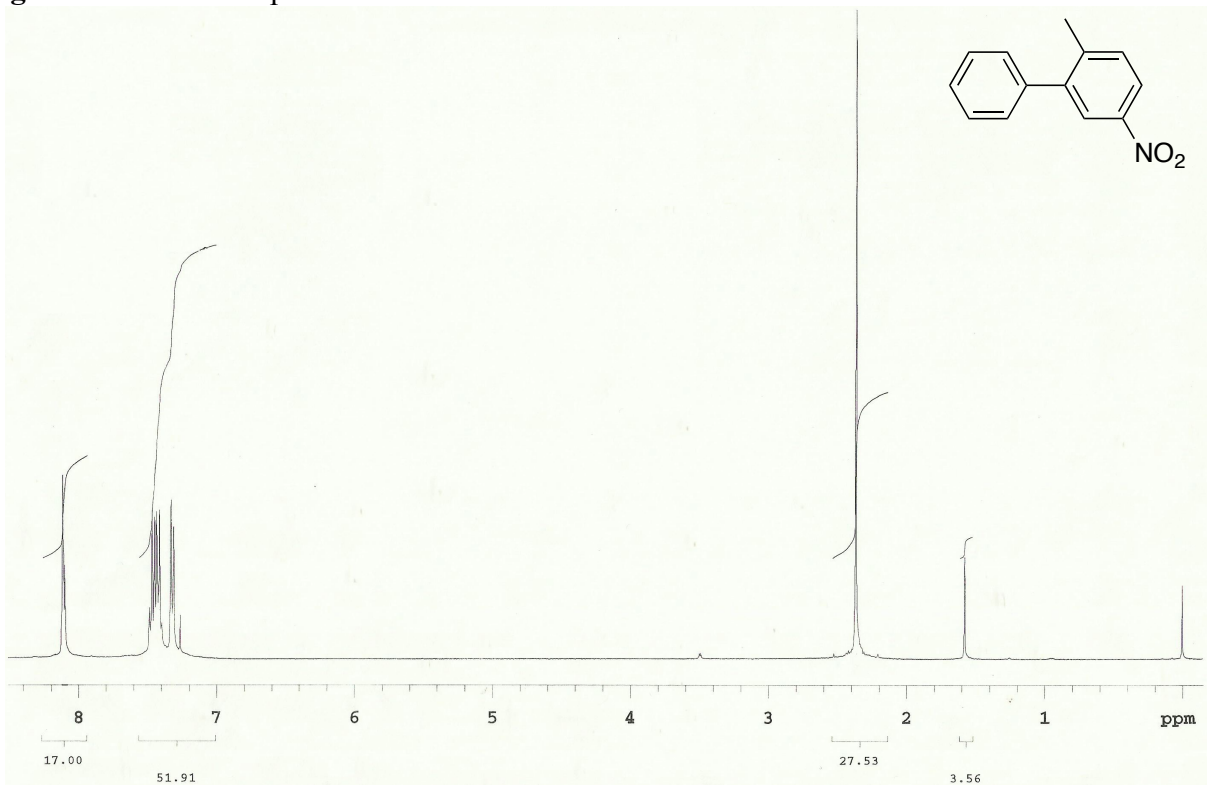

Figure C3. ^{1}H NMR spectrum of **1c**.

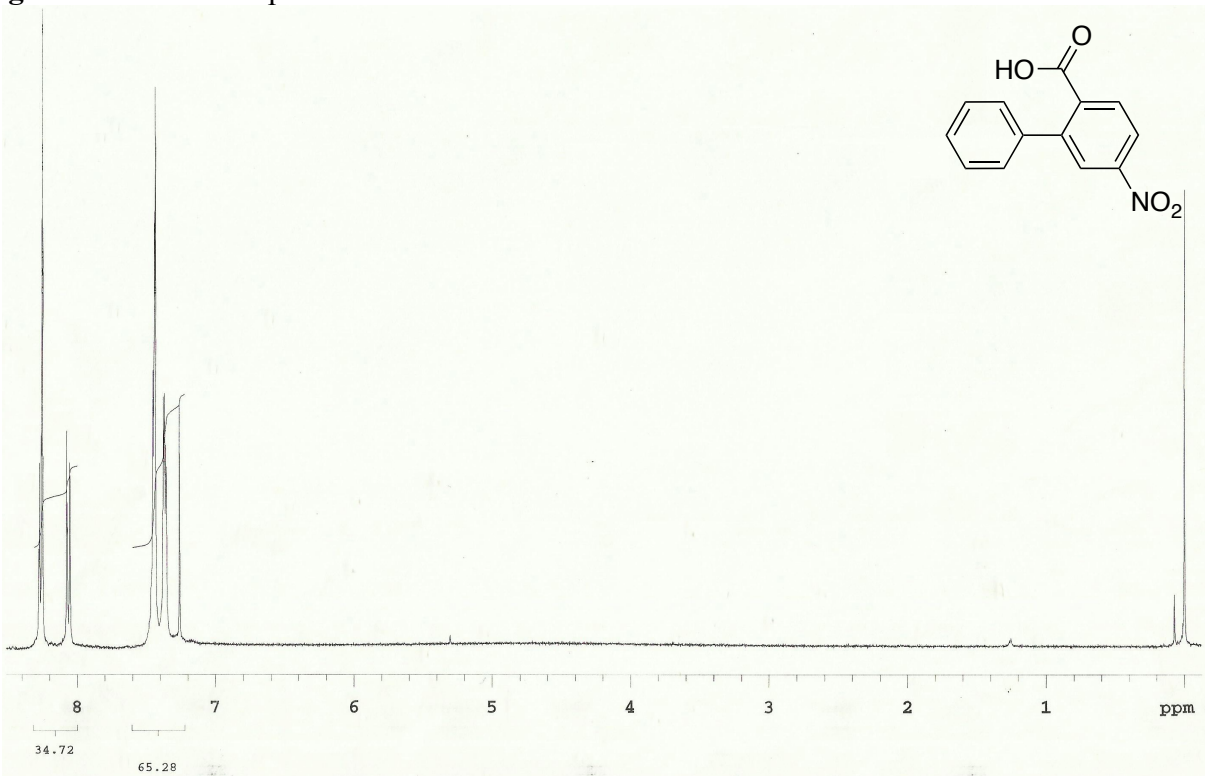

Figure C4. ^{1}H NMR spectrum of **1d**.

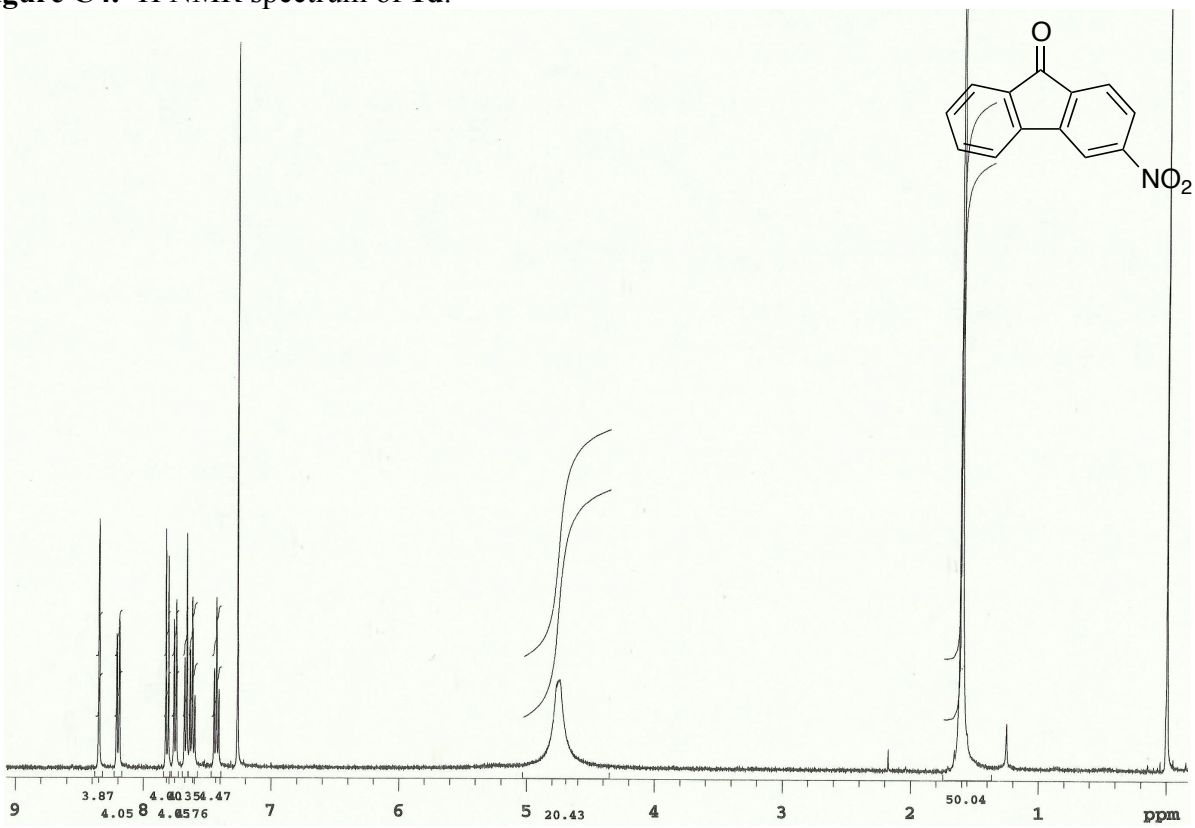

Figure C5. ^{1}H NMR spectrum of **1**.

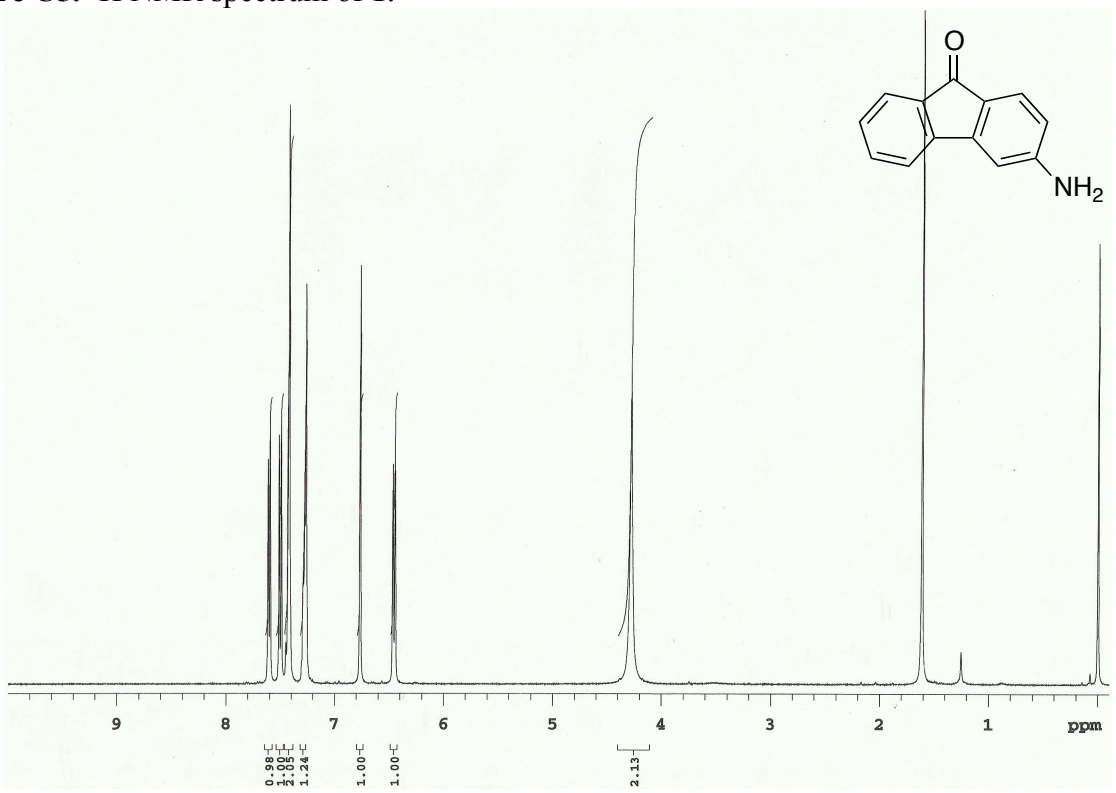

Figure C6. ^{13}C NMR spectrum of **1**.

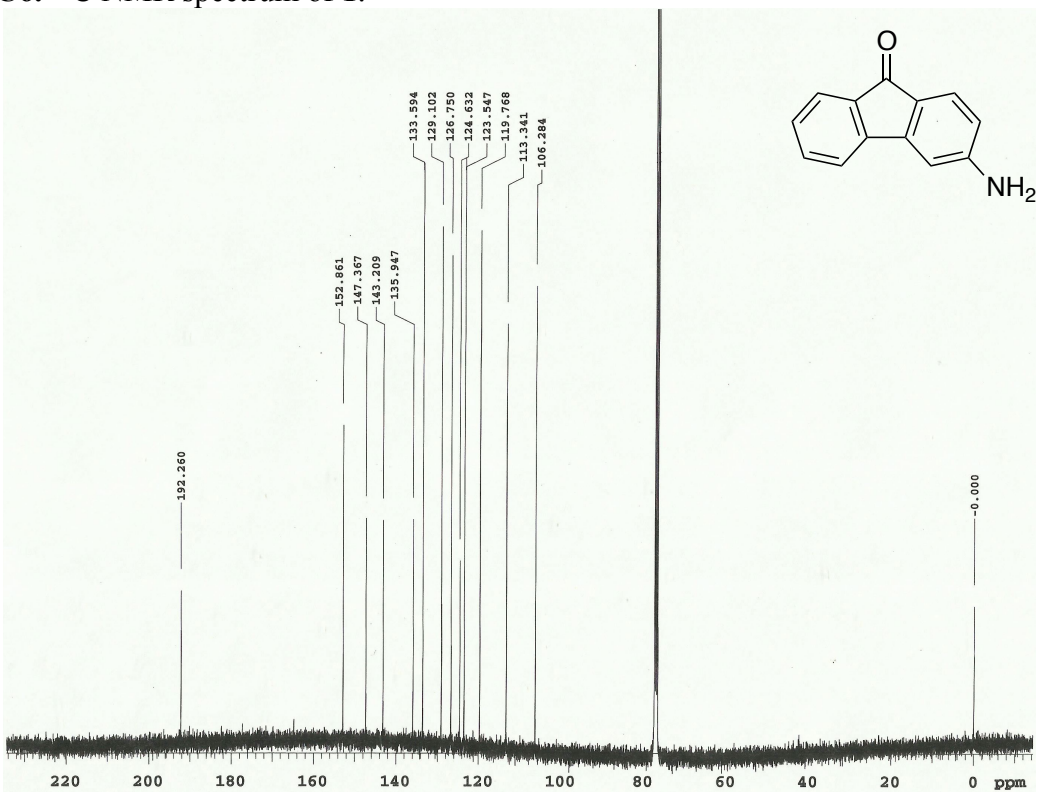

Figure C7. ^{1}H NMR spectrum of **2b**.

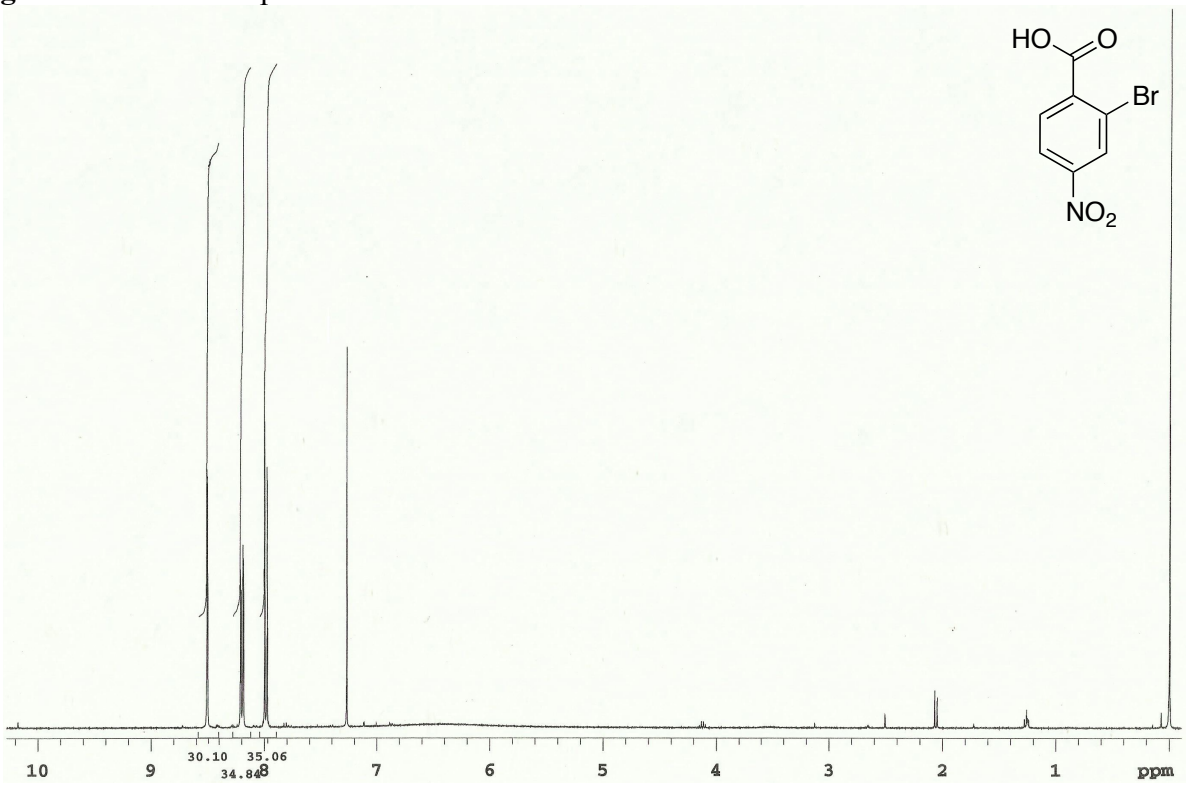

Figure C8. ^{1}H NMR spectrum of **2c**.

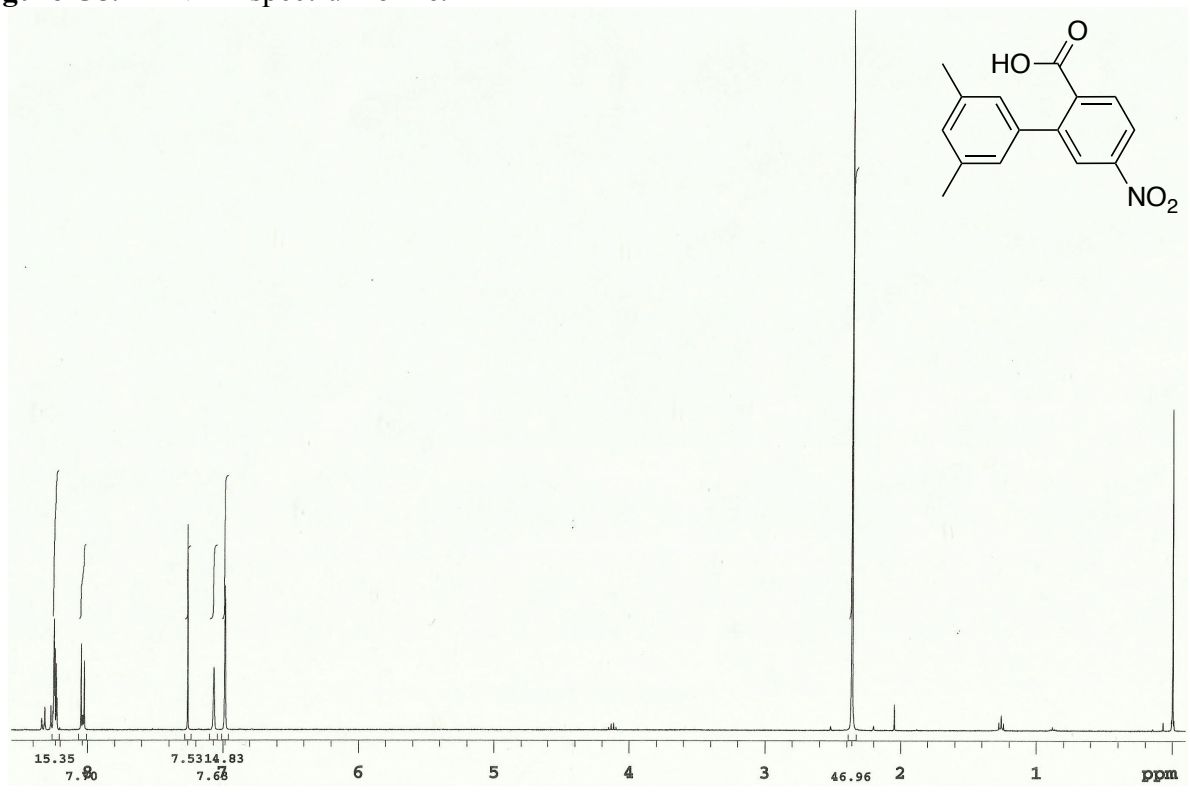

Figure C9. ^{1}H NMR spectrum of **2d**.

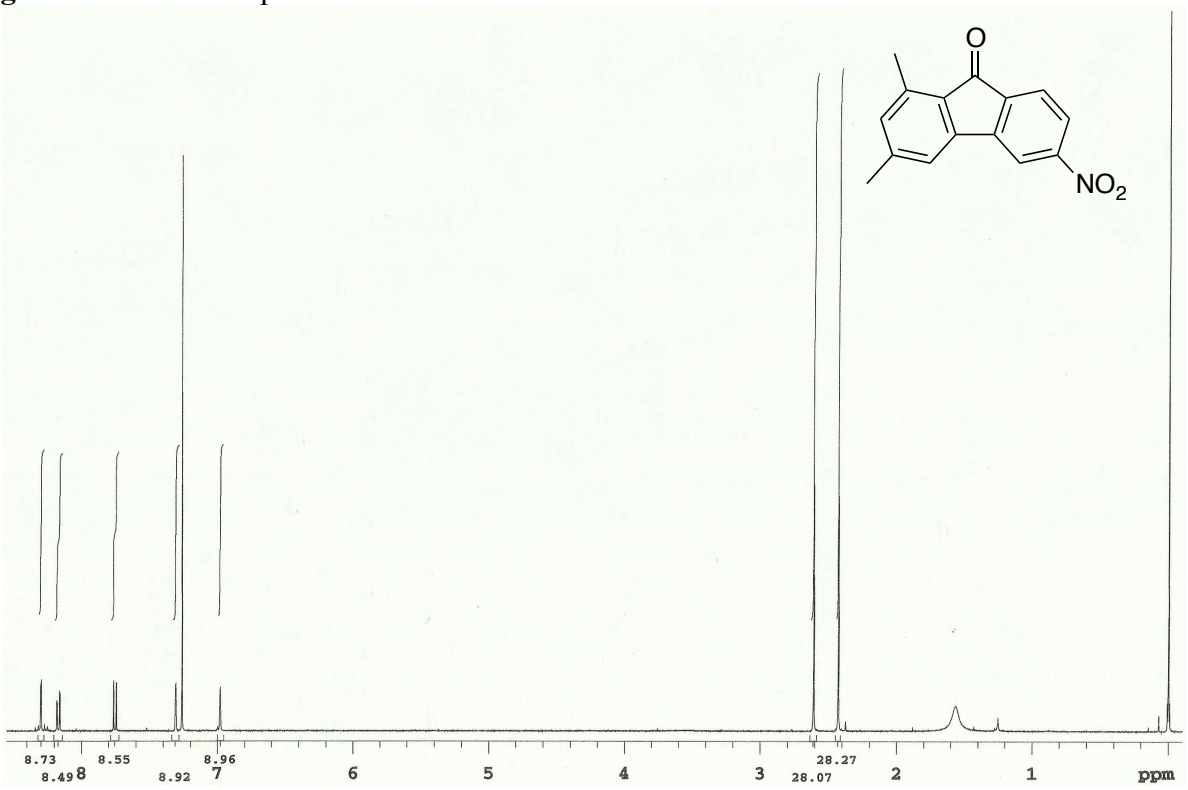

Figure C10. ^{1}H NMR spectrum of **2**.

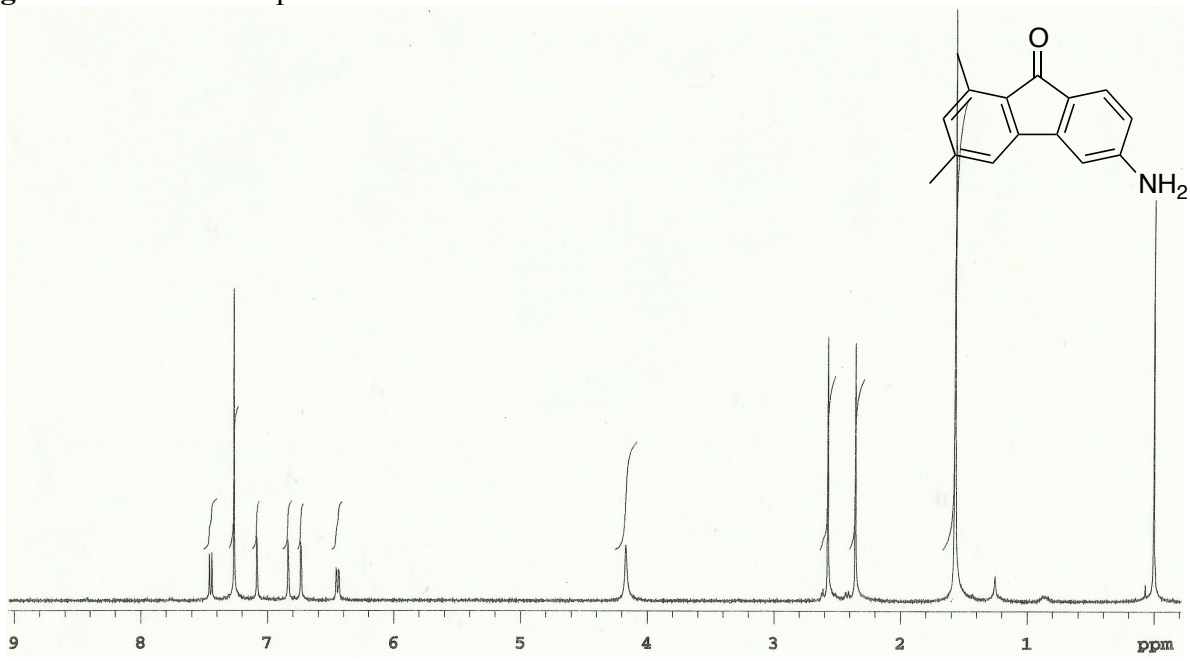

Figure C11. ^{13}C NMR spectrum of **2**.

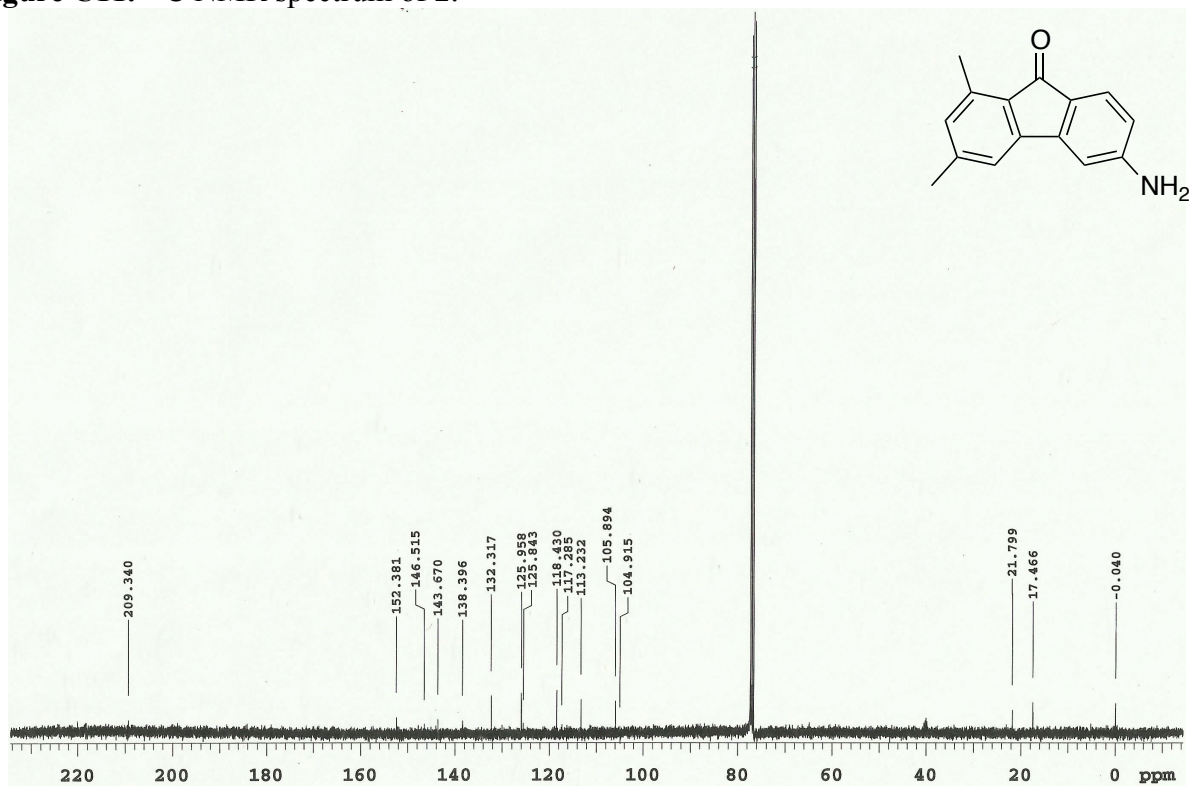

Figure C12. ^{1}H NMR spectrum of **3a**.

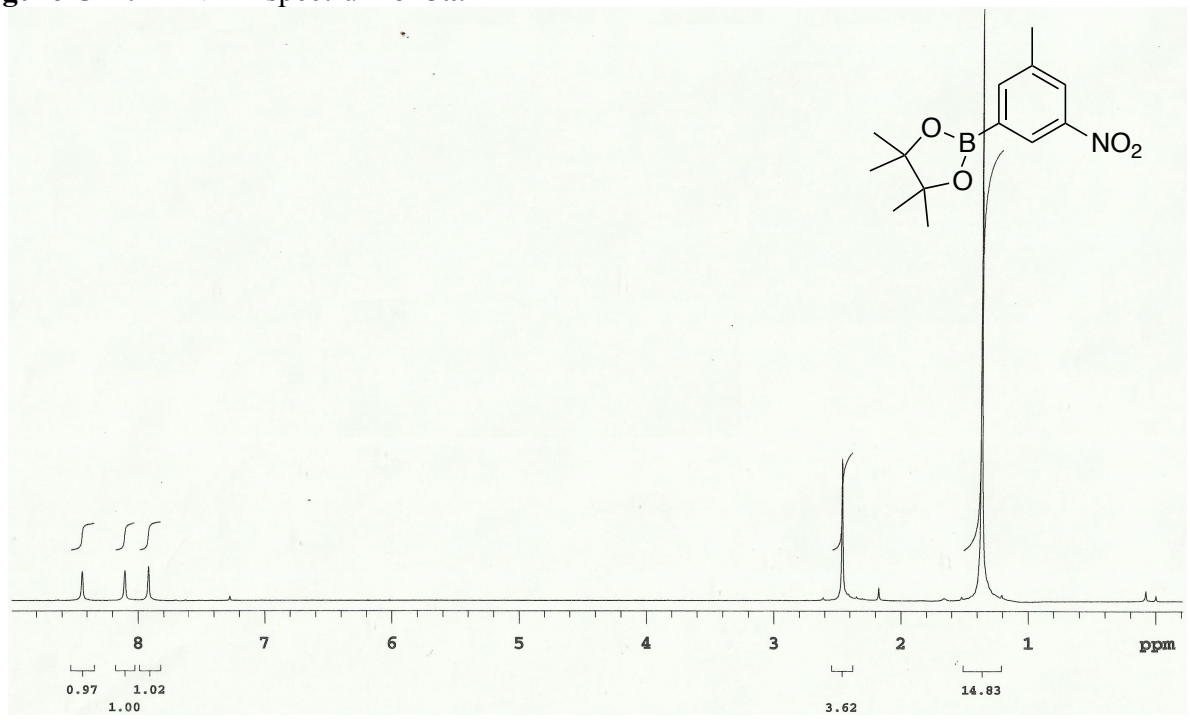

Figure C13. ^{1}H NMR spectrum of **3b**.

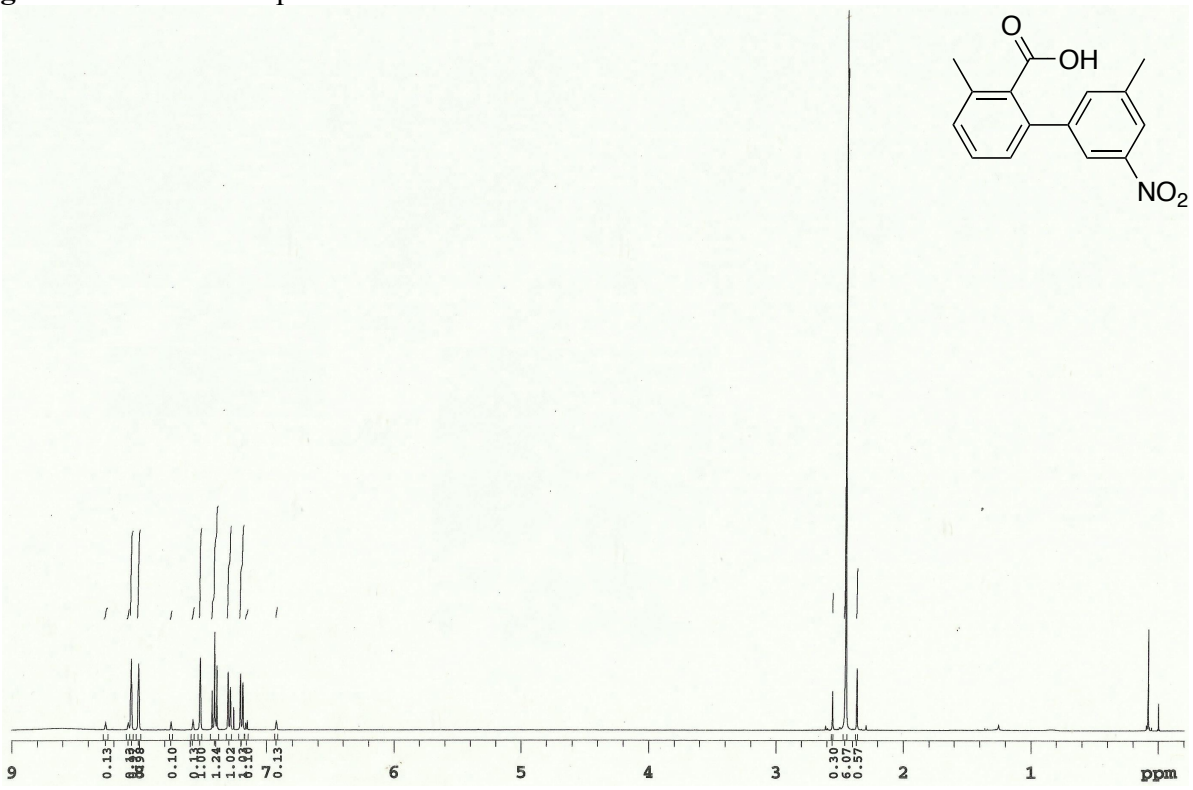

Figure C14. ^{1}H NMR spectrum of **3c**.

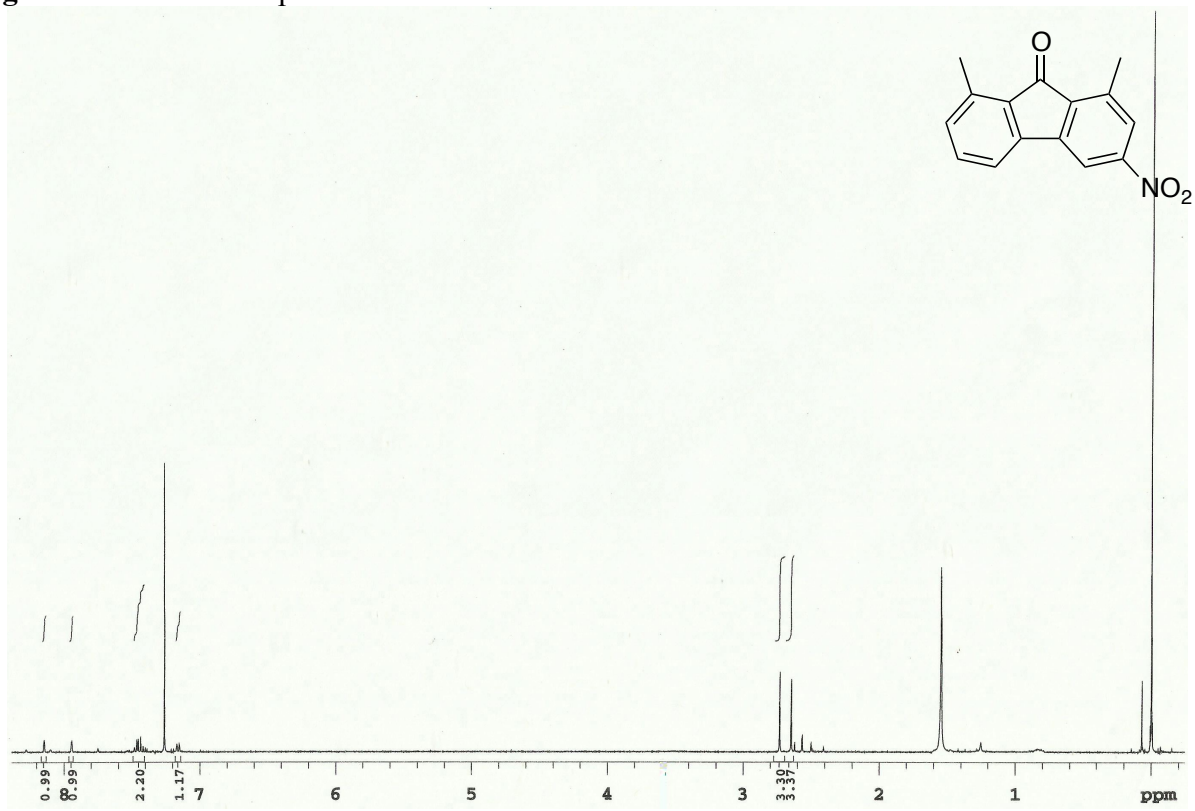

Figure C15. ^{1}H NMR spectrum of **3**.

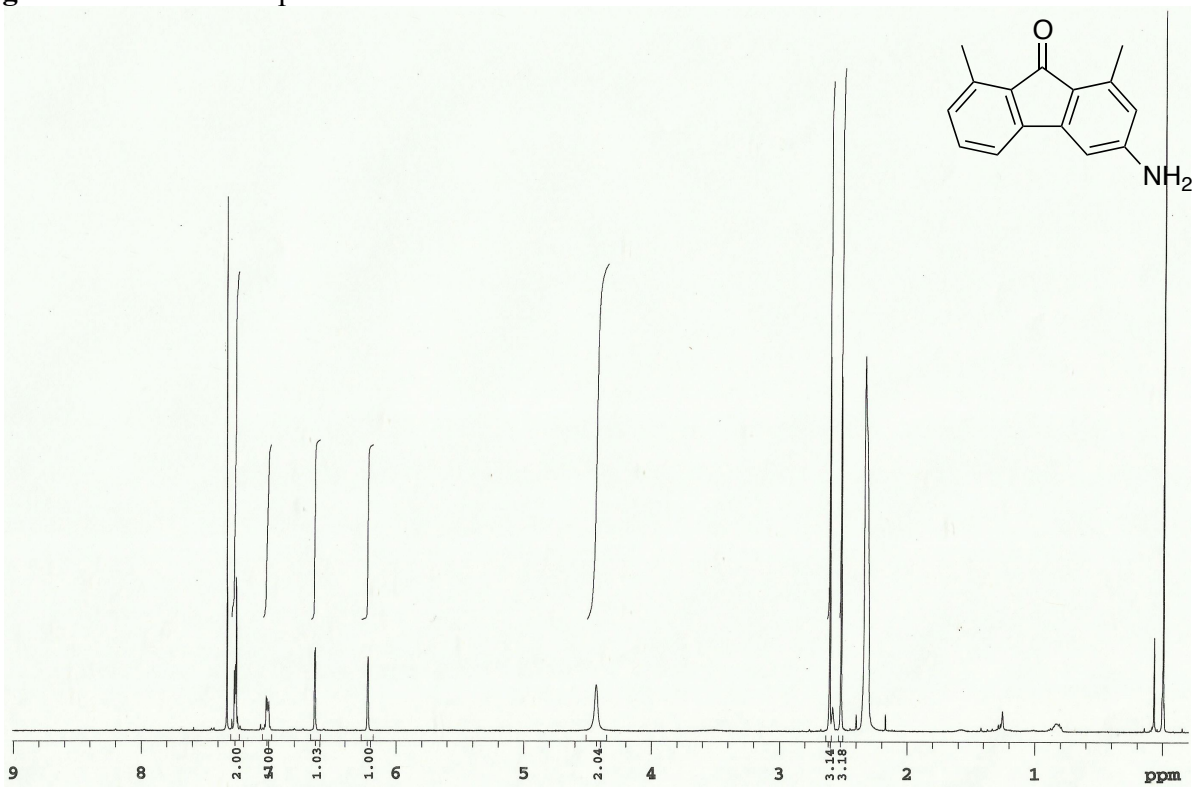

Figure C16. ^{13}C NMR spectrum of **3**.